

EVOLUTION OF ENRICHED MANTLE
FROM DERIVATIVE
BASALT, PERIDOTITE AND DIAMOND INCLUSION GEOCHEMISTRY

by

STEPHEN HILARY RICHARDSON

B. Sc. (Hons), University of Cape Town
(1977)

Submitted in partial fulfillment of the requirements for the

degree of

DOCTOR OF PHILOSOPHY

at the

MASSACHUSETTS INSTITUTE OF TECHNOLOGY

January 1984

© Massachusetts Institute of Technology 1984

Signature of Author _____

Center for Geoalchemy, Department of Earth, Atmospheric,
and Planetary Sciences
January 10, 1984

Certified by _____

Stanley R. Hart
Thesis Supervisor

Accepted by _____

Theodore R. Madden
Chairman, Department Committee on Graduate Students

MASSACHUSETTS INSTITUTE
OF TECHNOLOGY

ADD 2 6 1004 1 1001001

EVOLUTION OF ENRICHED MANTLE
FROM DERIVATIVE
BASALT, PERIDOTITE AND DIAMOND INCLUSION GEOCHEMISTRY

by

STEPHEN HILARY RICHARDSON

Submitted to the Department of Earth, Atmospheric, and Planetary Sciences on January 10, 1984 in partial fulfillment of the requirements for the degree of Doctor of Philosophy

ABSTRACT

The existence of enriched mantle may be inferred from the geochemistry of derivative basalts. In particular, the Nd and Sr isotopic signature of 70 Ma old tholeiitic basalts from the crest of the Walvis Ridge in the southeast Atlantic Ocean suggests derivation from an ancient incompatible element enriched mantle source. Trace element and Nd, Sr and Pb isotopic correlations described by ridge crest and flank basalts allow inferences on the nature and timing (>800 Ma) of this enrichment.

Direct evidence of the existence of ancient enriched mantle is provided by garnet peridotite xenoliths from southern African kimberlites. Deformed and coarse garnet lherzolites from Thaba Putsoa, northern Lesotho, and Bultfontein, Kimberley area, variously display inter-mineral Nd and Sr isotopic equilibrium or inverse disequilibrium at the time of sampling by kimberlite (90 Ma). They evidently do not retain any internal age information beyond that of emplacement. However, their time-integrated chemical histories are revealed by emplacement age isotopic signatures. Deformed garnet lherzolites (with more fertile major element compositions) from Thaba Putsoa (craton margin) have trace element and isotopic signatures resembling depleted (high Sm/Nd, low Rb/Sr) MORB type sources such as those conventionally associated with the convecting asthenosphere. In contrast, the common coarse garnet peridotites (with residual major element compositions) from the Kimberley area (craton interior) bear isotopic signatures indicative of enriched (low Sm/Nd, high Rb/Sr) sources stabilized in the sub-continental lithosphere for at least 1 Ga.

Even more durable enriched mantle is apparent in the Nd and Sr isotopic signatures of syngenetic inclusions in diamonds from southern African kimberlites. Sub-calcic garnets encapsulated by diamonds from relatively young (90 Ma) Kimberley cluster and Finsch kimberlites, yield ancient Sm-Nd and Rb-Sr model ages of 3.2 to 3.3 Ga. The chemistry and distribution of these and associated sub-calcic garnets from kimberlite heavy mineral concentrate, indicate diamonds formed following enrichment of residual Archean mantle such as that remaining after widespread extraction of 3.5 Ga komatiitic lavas. Diamonds are clearly xenocrysts in the kimberlite magma. Furthermore, diamond-bearing kimberlite compositions may themselves reflect variable incorporation of enriched sub-calcic garnet and diamond host assemblages residing in Archean craton root zones.

Thesis supervisor: Stanley R. Hart, Professor of Geology and Geochemistry

ACKNOWLEDGEMENTS

The study presented in Chapter 1 was spawned by the author's participation in the Walvis Ridge transect, Deep Sea Drilling Project Leg 74, during June-July 1980. Captain Clarke and the marine and drilling crews aboard R/V Glomar Challenger are thanked for a classic cruise. The cooperation and camaraderie of co-chief scientists T C Moore and P D Rabinowitz, the shipboard scientific party and DSDP support staff contributed to a great learning experience. The geochemical study of basalts sampled by the author on the high seas was initiated at the University of Cape Town in collaboration with A J Erlank, A R Duncan and D L Reid. Major and trace element data were determined by XRF techniques familiar to the author from previous exhilarating exposure in the Department of Geochemistry at UCT. A comprehensive report of the major and trace element and Nd and Sr isotope data, with the above persons as coauthors, was submitted to DSDP in January 1982 and is due to be published in the Initial Reports of the DSDP, volume 74. Chapter 1 represents a derivative account, featuring Nd, Sr and Pb isotope data and a distillation of the trace element data, essentially identical to that published with the same coauthors in *Earth & Planetary Science Letters* 59 (1982) 327-342.

The peridotite nodules from southern African kimberlites featured in Chapter 2, come from the collections (*sensu lato*) of A J Erlank (Bultfontein), N Shimizu (Thaba Putsoa) and S R Shee (Finsch). Selection of nodules for time-and-effort-intensive mineral separate preparation was based on previous diverse results of these and numerous other workers in the field (literal and figurative) who are collectively acknowledged. An early account of the isotope data, with A J Erlank and N Shimizu as coauthors, was presented at the 3rd International Kimberlite Conference at Clermont-Ferrand, with financial assistance from CNRS. This was followed by an opportunity to stalk the Bultfontein dumps in the company of A J Erlank, F Waters and J Robey on a field trip to Kimberley in 1982. The assistance and hospitality of the staff of the De Beers Geology Department is appreciated.

The most technically challenging and perhaps the most exciting part of this thesis is covered in Chapter 3. This project arose from the confluence of J J Gurney's studies of the link between sub-calcic garnets and diamonds and the author's isotopic studies of garnets from peridotite nodules, as suggested and orchestrated by A J Erlank. Here again the author is heavily indebted to De Beers Consolidated Mines for provision of durable raw materials. J B Hawthorne, Consulting Geologist (Diamonds), and J Hartley, A van Niekerk and V Anderson, the indefatigable sorters of the Diamond Sorting Office in Kimberley, are particularly acknowledged for making the project possible. J W Harris commissioned and checked the massive diamond sorting operation. J J Gurney identified sub-calcic garnets from heavy mineral concentrate by EMP analysis and shared his ideas on their derivation. A pared down version of Chapter 3, with J J Gurney, A J Erlank and J W Harris as coauthors, is being submitted to Nature.

Successful completion of this opus inevitably and inexorably depended on the resources, support and friendship of Stan Hart and crew at the Center for Geoalchemy. All power to Capt Stan who has entertained each new proposition with enthusiasm and encouragement. His polymathic appreciation of all things great and small has served as the ultimate inspiration for these endeavors. Honorary privileges to Tony Erlank, a prime source of raw and processed materials as well as insight and motivation. In many ways, he has served as a mentor and second southern hemispheric supervisor. Nobu Shimizu provided seminal previews of the chemical complexity of the mantle sample and ample empathy on this and related issues. Ken Burrhus is credited with innovative machine design and, in partnership with Stan Hart, paternity of NIMA-B, a mass spectrometer that delivers. Ken was perennially accessible and willingly applied his engineering expertise to everything from diamond manipulation to foreign exchange. These and numerous other individuals, at home and abroad, contributed to the development and maintenance of existing lab facilities and chemical techniques utilized in the course of analysis. On the production side, Donna Hall generously took responsibility for graphics between many lives while Gile Beye graciously covered unmarked bases. Angela Hurshman handled text processing with finesse and sympathetic appreciation of the thesis writing syndrome.

Financial assistance from the Harry Crossley Foundation, the Myer Levinson Fund of the University of Cape Town and NSF grants EAR78-03342 and EAR83-08809 (supporting SRH's isotope laboratory) is gratefully acknowledged.

This thesis is dedicated to my mother Natalie, and the memory of my father Edward John Richardson (1925-1982) who flew in WWII and lived ... to let me tell this tale.

TABLE OF CONTENTS

| | |
|------------------------------------------------------------------------------------------------------------------------------------------------------------------|----|
| Abstract | 2 |
| Acknowledgements | 3 |
| Introduction | 8 |
| Chapter 1 Correlated Nd, Sr and Pb isotope variation in Walvis Ridge basalts and implications for the evolution of their enriched mantle source | 9 |
| 1.1 Introduction | 10 |
| 1.2 Geological setting | 11 |
| 1.3 Petrography | 14 |
| 1.4 Analytical techniques | 14 |
| 1.5 Results | 15 |
| 1.5.1 Major and trace element variation | 15 |
| 1.5.2 Nd and Sr isotope variation | 22 |
| 1.5.3 Pb isotope variation | 29 |
| 1.6 Discussion | 34 |
| 1.6.1 Relation to oceanic basalt trace element and isotopic systematics | 34 |
| 1.6.2 Mantle source evolution | 38 |
| 1.6.2.1 Crustal contamination of melts from homogeneous mantle | 38 |
| 1.6.2.2 Mixing of melts from heterogeneous mantle | 39 |
| 1.6.2.3 Melting of mantle with small scale heterogeneity | 46 |
| 1.7 Conclusions | 51 |
| Chapter 2 Evolution of depleted and enriched sub-continental mantle inferred from the Nd and Sr isotopic systematics of garnet peridotites from kimberlite | 53 |
| 2.1 Introduction | 54 |
| 2.2 Peridotite lithology and chemistry | 58 |
| 2.2.1 Petrography | 58 |

| | | |
|----------------------------------------------------------------------------------------------------------------------------------------------------------------|------------------------------------------------|-----|
| 2.2.2 | Major and trace element chemistry | 59 |
| 2.2.3 | Previous Sr, Nd and Pb isotopic studies | 60 |
| 2.3 | Analytical techniques | 64 |
| 2.4 | Host kimberlites | 67 |
| 2.5 | Xenolith whole rocks | 75 |
| 2.6 | Thaba Putsoa peridotites | 79 |
| 2.7 | Bultfontein peridotites | 88 |
| 2.7.1 | Deformed garnet lherzolites | 89 |
| 2.7.2 | Coarse garnet lherzolites | 97 |
| 2.7.3 | Coarse harzburgites | 107 |
| 2.8 | Finsch peridotites | 109 |
| 2.9 | Conclusions | 111 |
| Chapter 3 Origin of diamonds in old enriched mantle: Sm-Nd and Rb-Sr age constraints from sub-calcic garnets in diamonds and host kimberlite concentrate | | 113 |
| 3.1 | Introduction | 114 |
| 3.2 | Sub-calcic garnets in diamonds | 119 |
| 3.3 | Sub-calcic garnets from kimberlite concentrate | 123 |
| 3.4 | Analytical techniques | 125 |
| 3.5 | Sm-Nd and Rb-Sr isotopic systematics | 130 |
| 3.6 | Model age constraints on diamond formation | 139 |
| 3.7 | Nature of enriched precursor | 147 |
| 3.8 | Implications for kimberlite compositions | 148 |
| 3.9 | Conclusions | 150 |
| References | | 151 |
| Appendix Precise calibration of mixed Sm-Nd spike solutions for determination of Sm/Nd and Nd isotope ratios on totally spiked samples. | | 163 |
| Biographical note | | 191 |

INTRODUCTION

This thesis consists of three semi-autonomous chapters covering three quasi-independent projects pursued by the author at MIT since formal certification of fitness for thesis research. In view of the author's heritage, all inevitably have a rich mellow southern African flavor. The overall theme is the origin and evolution of enriched mantle and its consequent availability for incorporation in mantle-derived magmas. The most likely place for long-term storage of durable enriched mantle appears to be the sub-continental lithosphere. The geochemistry of Cretaceous Walvis Ridge basalts suggests derivation from Precambrian enriched mantle marginally associated with the African portion of the Gondwanaland supercontinent. Direct evidence of even more durable enriched mantle comes from geochemical studies of garnet peridotite xenoliths and sub-calcic garnets in concentrate and diamonds, sampled by Cretaceous kimberlites erupted through the Archean Kaapvaal craton in southern Africa.

The applicability of present results to sub-continental mantle in general is necessarily speculative. In this context, the semblance of a large-scale mantle isotopic anomaly in the southern hemisphere (Dupre & Allegre, 1983; Hart, 1984) should be noted. Documentation and interpretation of such an anomaly may prove to be a central theme of chemical geodynamics (Allegre, 1982) in years ahead.

CHAPTER 1

CORRELATED Nd, Sr AND Pb ISOTOPE VARIATION IN WALVIS RIDGE BASALTS
AND IMPLICATIONS FOR
THE EVOLUTION OF THEIR ENRICHED MANTLE SOURCE

1.1 Introduction

Ever since Wilson (1963) proposed that the Walvis Ridge might represent a mantle plume trace, it has been suspected that this feature was igneous in origin. Basalts with alkaline affinities were subsequently dredged from the vicinity of the ridge (Hekinian, 1972; Humphris & Thompson, 1982). This served to strengthen the association with the volcanic islands of Tristan da Cunha and Gough which lie on an approximate southwest extrapolation of the ridge. Among models advanced for the formation of this and other aseismic ridges (Dingle & Simpson, 1976), the hotspot or mantle plume hypothesis stands out as having attracted the most support (Morgan, 1971, 1972; Goslin & Sibuet, 1975; Burke & Wilson, 1976; Detrick & Watts, 1979). Until recently, however, an oceanic crustal origin for the Walvis Ridge could not be presumed because of the divergence between overall ridge orientation and adjacent crustal flow lines. In an alternative proposal (van der Linden, 1980), the ridge originated as a fragment of continental crust, which split from the main continental mass during early rifting of the South Atlantic.

On the basis of detailed bathymetry and magnetic anomaly identification (Rabinowitz & LaBrecque, 1979; Rabinowitz & Simpson, 1979), Rabinowitz (1984) has suggested that NNW-SSE oriented segments of the Walvis Ridge originated at the paleo mid-ocean ridge, followed by successive ridge jumps. On the IPOD Leg 74 Walvis Ridge transect, basement rocks in the form of tholeiitic basalt flows and pillows were recovered by drilling (Moore et al, 1983). Their deviant trace element and Nd, Sr and Pb isotope geochemistry (relative to average MORB)

detailed below, provides direct evidence for a compositionally distinct mantle source. An appropriately sized source must be envisaged for the large volumes of basalt which presumably constitute the bulk of the Walvis Ridge. The presence of chemically modified upper mantle beneath the Walvis Ridge has previously been suggested by Chave (1979) on the basis of regional Rayleigh wave dispersion characteristics. Circumstantial evidence thus favors a laterally extensive source at shallow upper mantle depths rather than a diametrically restricted plume source originating in the lower mantle.

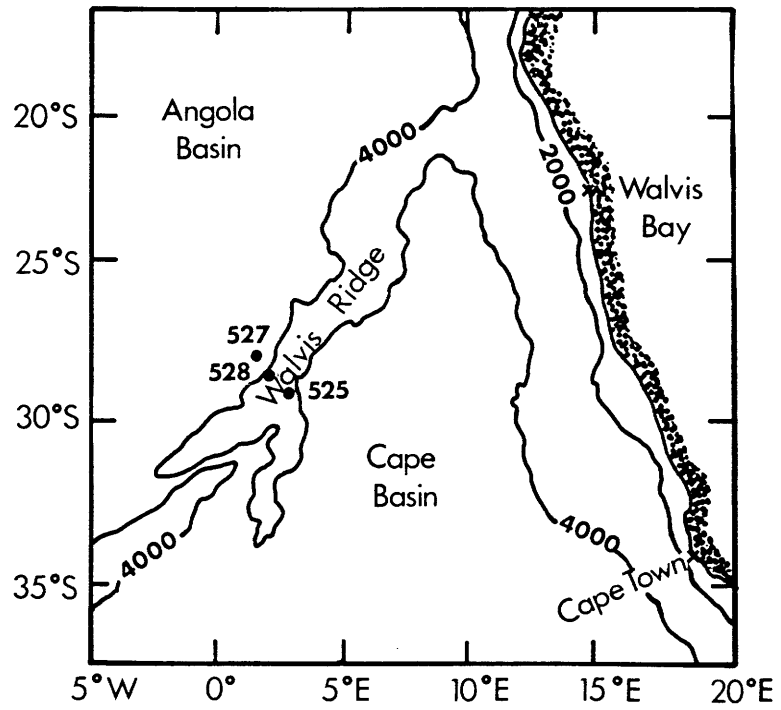
1.2 Geological Setting

The IPOD Leg 74 Walvis Ridge transect was located on a NNW-SSE trending block of the ridge at 28-29°S and 3°E (Moore et al, 1983). This orientation is perpendicular to adjacent crustal flow lines and thus approximates that of the paleo ridge axis. Basement was encountered at sites 525, 528 and 527, respectively situated on the crest and mid and lower NW flank of the ridge (Figure 1-1). At all three sites the basement complex consists of basalt flows with thin glassy upper chilled margins and minor intercalated volcanoclastic and biogenic sediments (Figure 1-2).

A distinctive pillow basalt sequence occurring at the crestal site 525 confirms the submarine extrusive origin of the ridge volcanics. On the basis of both magnetostratigraphy (magnetic anomaly 31 to 32 time) and biostratigraphy of intercalated and overlying sediments (Maestrichtian to Campanian time) the age of basement rocks in this segment of the ridge is approximately 69-71 Ma (Moore et al, 1983). In detail, the deeper sites are progressively slightly younger than the crestal site. Within each hole the biostratigraphy of intercalated

FIGURE 1-1

Sketch map of the south east Atlantic showing the location of IPOD Leg 74 Walvis Ridge transect sites where basement was intersected (adapted from Moore et al, 1983): 525 ($29^{\circ}04.24'S$, $02^{\circ}59.12'E$); 528 ($28^{\circ}31.49'S$, $02^{\circ}19.44'E$); 527 ($28^{\circ}02.49'S$, $01^{\circ}45.80'E$).



sediments indicates episodic eruption of flows over intervals of up to a million years.

1.3 Petrography

Glassy margins, grain size variation, macroscopic petrography and sediment breaks serve to define the cooling units enumerated in Figure 1-2 (Richardson et al, 1984). Apart from occasional lone plagioclase phenocrysts observable in the drill core, basalts from the crestal site 525 are all essentially aphyric. Basalts from the two flank sites 528 and 527 vary from aphyric to highly plagioclase phyric. Plagioclase phenocrysts in the later range up to 10 x 15 mm in size and 25 vol % in abundance and are strongly zoned (An_{90} - An_{60} ; Richardson et al, 1984). Sparse olivine and augite phenocrysts also occur, but the olivine is altered to clays. Groundmasses consist predominantly of subophitic intergrowths of plagioclase and augite, with subordinate titanomagnetite. In hole 525A, glass is present in the groundmass matrix of the upper part of unit 5 and dominates in glassy pillow margins of unit 4. Recognizable glassy chilled margins in the other two holes are completely altered. Except for the highly altered top 20 meters of hole 525A and aphyric basalts of holes 528 and 527 the overall degree of alteration is slight to moderate with development of clay minerals in the groundmass and the occurrence of calcite (\pm pyrite) in veins.

1.4 Analytical Techniques

Surface alteration and vein materials were avoided during careful shipboard sampling of cores. Shore-based whole rock sample preparation comprised sawn surface removal by abrasion with silicon carbide, ultrasonic cleaning in acetone and distilled water, coarse crushing in a steel jaw crusher and grinding in agate vessels. Acid

leaching of basalt samples to remove matrix alteration phases was not attempted because the poor selectivity of this technique makes it appropriate only to rocks of close to zero isotopic age correction. Instead, small ultrapure separates of fresh isotropic glass (30 mg) from one pillow margin (525A-59-4, 35) and plagioclase (7 mg) from one highly plagioclase phyric basalt (527-41-4, 10) were prepared by hand-picking.

Powders were analyzed for major and selected trace elements, using X-ray fluorescence (XRF) spectrometric techniques summarized in le Roex et al (1981). Single dissolutions of whole rock powders and grain separates were used for measuring combined Sr and Nd isotopic compositions and Rb, Sr, Sm and Nd concentrations by isotope dilution (ID) mass spectrometry. Separate dissolutions of whole rock powders were used for Pb isotopic compositions. Chemical and mass spectrometric techniques for determination of Rb and Sr concentrations and $^{87}\text{Sr}/^{86}\text{Sr}$ ratios are as described in Hart and Brooks (1977); for Sm and Nd concentrations and $^{143}\text{Nd}/^{144}\text{Nd}$ ratios as adapted from the techniques of Cerrae & Testa (1963) and Richard et al (1976) and summarized in Zindler et al (1979); for Pb isotopic compositions as adapted from the techniques of Strelow & Toerien (1966) and Manhès et al (1978) for use in this lab (W J Pegram, pers comm, 1981). Procedural blanks are all insignificant. Standard values used in normalization of isotope ratios for mass discrimination and systematic instrumental bias are given in Table 1-1.

1.5 Results

1.5.1 Major and Trace Element Variation

Major and trace element data, determined by XRF, for a set of samples covering the range of variability within and between basalt units (Figure 1-2) are reported elsewhere (Richardson et al, 1984). In addition,

FIGURE 1-2

Schematic representation of basalt lithology in IPOD Leg 74 holes 525A, 528 and 527, respectively situated on the crest, mid flank and lower flank of the Walvis Ridge. Appearing from left to right under each hole number are depth below the top of basement (meters; same scale for all three holes), drill core numbers and recovery (solid vertical bars), sample locations (dashes), intercalated sediment horizons (shading), cooling unit numbers and basalt type and morphology (from Richardson et al, 1984).

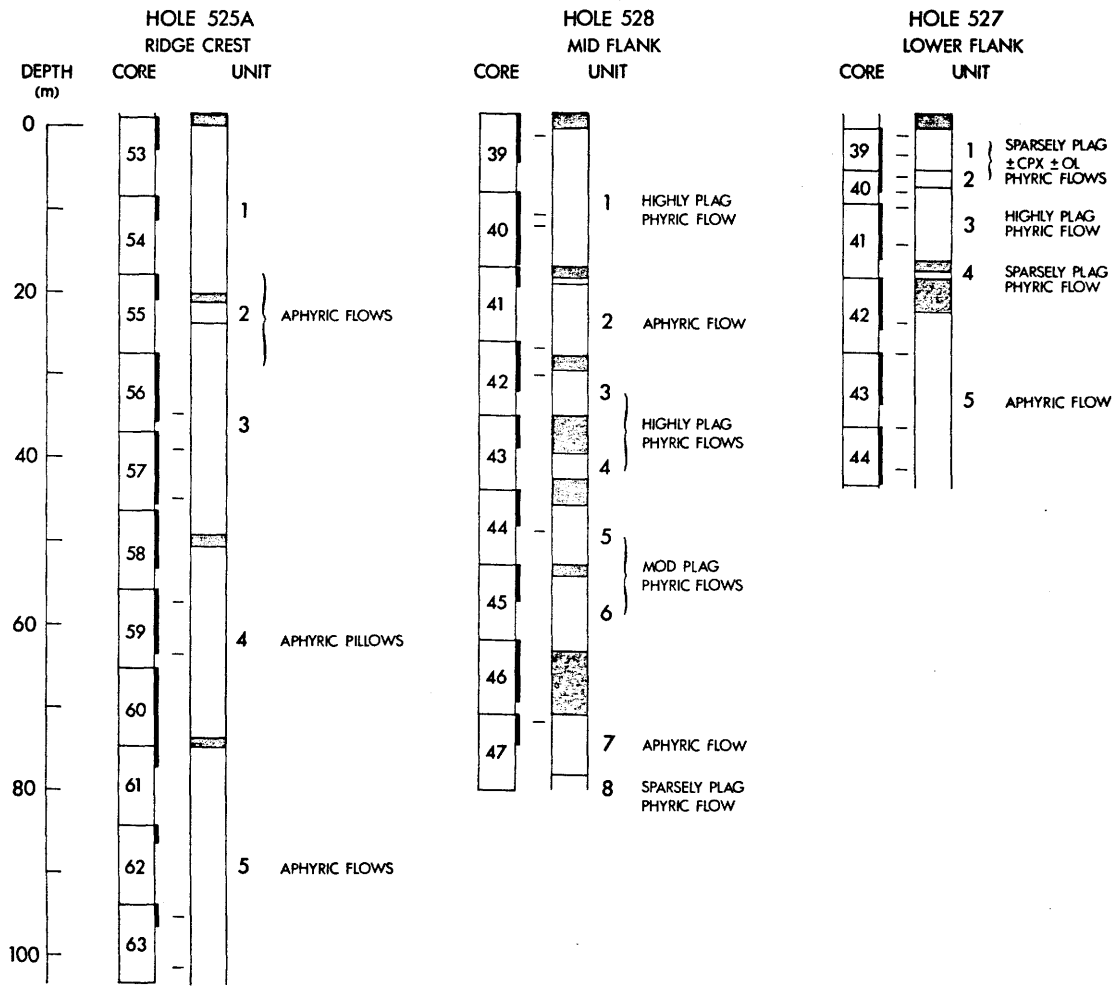


TABLE 1-1 Rb, Sr, Sm and Nd concentrations¹ and Sr, Nd and Pb isotopic compositions² of basalts from holes 525A, 528, and 527 on the Leg 74 Walvis Ridge transect.

| | Rb | Sr | ⁸⁷ Rb/ ⁸⁶ Sr | ⁸⁷ Sr/ ⁸⁶ Sr _p | ⁸⁷ / ⁸⁶ Sr _i | Sm | Nd | ¹⁴⁷ Sm/ ¹⁴⁴ Nd | ¹⁴³ Nd/ ¹⁴⁴ Nd _p | ¹⁴³ / ¹⁴⁴ Nd _i | 206/204 _{Pb} | 207/204 _{Pb} | 208/204 _{Pb} |
|---------------|-------|-----|------------------------------------|-------------------------------------------------|-----------------------------------------------|--------|-------|--------------------------------------|---------------------------------------------------|-------------------------------------------------|-----------------------|-----------------------|-----------------------|
| 525A- | | | | | | | | | | | | | |
| 57-1,119-124 | 2.29 | 437 | 0.0152 | 0.70498±5 | 0.70496 | 6.74 | 29.8 | 0.1367 | 0.512461±21 | 0.512398 | 17.648 | 15.472 | 38.120 |
| 59-4,35-39 | 18.3 | 367 | 0.1443 | 0.70500±5 | 0.70486 | 7.03 | 31.1 | 0.1369 | 0.512466±23 | 0.512403 | 17.641 | 15.477 | 38.149 |
| 59-4,35-39 GL | 18.8 | 375 | 0.1451 | 0.70486±3 | 0.70472 | 7.29 | 32.5 | 0.1356 | 0.512456±17 | 0.512394 | | | |
| 63-1,86-91 | 12.5 | 488 | 0.0742 | 0.70512±3 | 0.70505 | 9.53 | 44.9 | 0.1283 | 0.512376±17 | 0.512317 | 17.650 | 15.483 | 38.227 |
| 63-2,63-68 | 7.22 | 495 | 0.0422 | 0.70511±3 | 0.70507 | 9.65 | 45.7 | 0.1277 | 0.512379±16 | 0.512321 | 17.535 | 15.471 | 38.138 |
| 528- | | | | | | | | | | | | | |
| 42-1,40-45 | 38.1 | 293 | 0.3764 | 0.70498±2 | 0.70461 | 6.80 | 33.8 | 0.1217 | 0.512555±17 | 0.512499 | 18.029 | 15.491 | 38.820 |
| 42-2,145-150 | 6.03 | 224 | 0.0779 | 0.70423±3 | 0.70415 | 2.50 | 9.23 | 0.1637 | 0.512699±35 | 0.512624 | 18.180 | 15.508 | 38.629 |
| 47-3,23-28 | 19.9 | 310 | 0.1858 | 0.70444±3 | 0.70426 | 5.65 | 24.1 | 0.1420 | 0.512682±22 | 0.512617 | 18.070 | 15.494 | 38.632 |
| 527- | | | | | | | | | | | | | |
| 41-4,10-15 | 1.72 | 146 | 0.0341 | 0.70417±3 | 0.70414 | 2.80 | 9.40 | 0.1800 | 0.512694±13 | 0.512612 | 18.315 | 15.524 | 38.774 |
| 41-4,10-15 PL | 0.067 | 180 | 0.0011 | 0.70391±3 | 0.70391 | 0.0539 | 0.176 | 0.1848 | | | | | |
| 44-1,52-57 | 19.2 | 313 | 0.1776 | 0.70455±3 | 0.70437 | 6.40 | 28.3 | 0.1376 | 0.512566±16 | 0.512503 | 18.160 | 15.507 | 38.760 |

¹Concentrations in ppm (µg/g) by isotope dilution, with precision for Sr, Nd and Sm ~0.3% and for Rb~1%. All blanks insignificant.

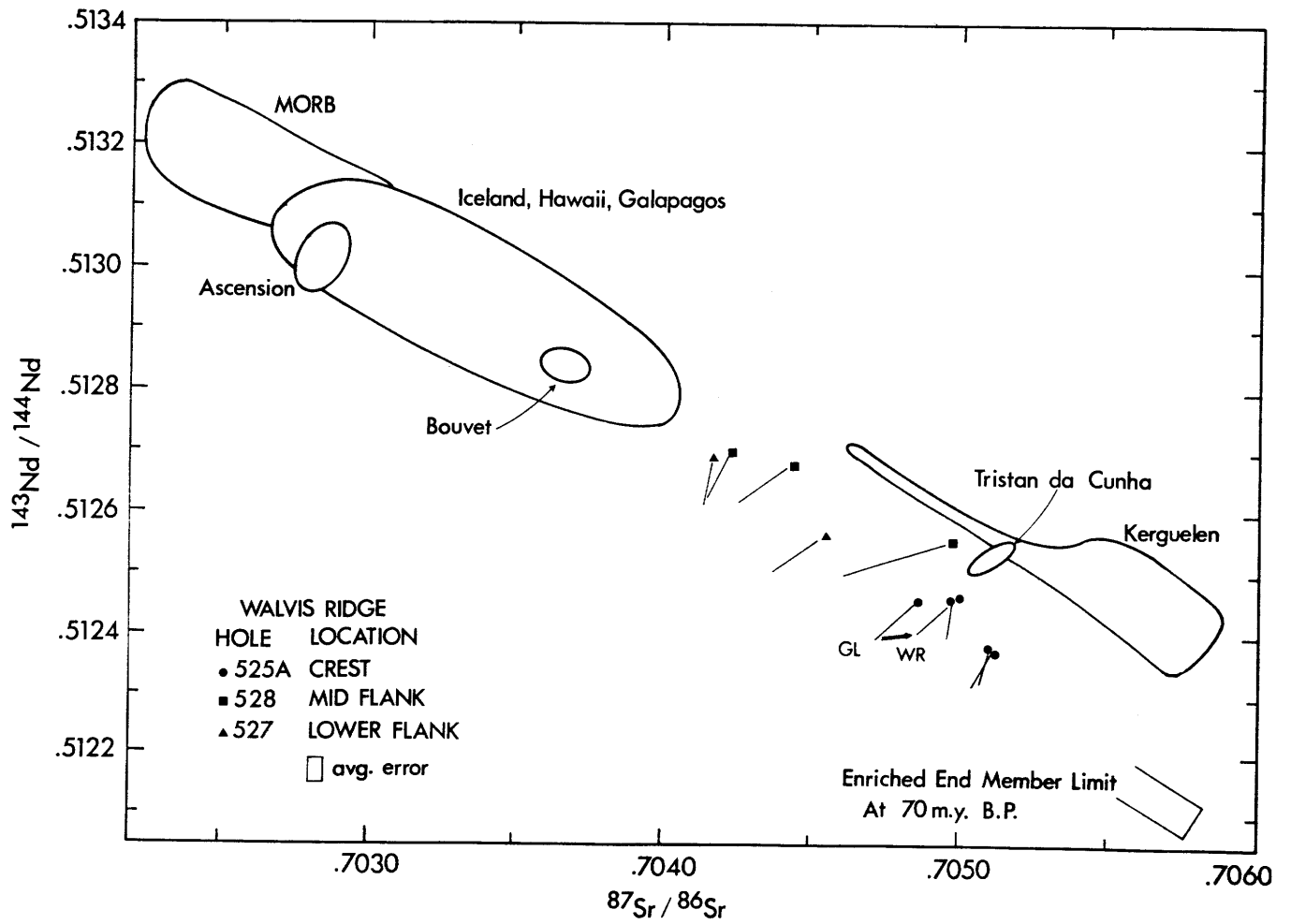
²⁸⁷Sr/⁸⁶Sr ratios normalized to 0.70800 for E & A SrCO₃ using ⁸⁶Sr/⁸⁸Sr = 0.1194. ¹⁴³Nd/¹⁴⁴Nd ratios normalized to 0.51264 for BCR-1 using ¹⁴⁶Nd/¹⁴⁴Nd = 0.7219. In-run precision given by errors (2σ_{mean}) corresponding to least significant digits. Initial ratios calculated for an age of 70 Ma using λ_{Rb} = 1.42 × 10⁻¹¹a⁻¹ and λ_{Sm} = 6.54 × 10⁻¹²a⁻¹. Pb isotope ratios are normalized for mass discrimination using that obtained for NBS SRM 981. Reproducibility is better than 0.05% • AMU⁻¹. In-run precision is on average an order of magnitude better and not reported.

concentrations of Rb, Sr, Nd and Sm determined by ID, for a subset of samples appear in Table 1-1. Basalts from the ridge crest site 525 are mildly quartz normative tholeiites whereas those from the two flank sites are all mildly olivine normative tholeiites. In order of increasing relative variation, major element abundances (normalized to 100% volatile free, with all Fe as FeO and designated FeO*) range from 49-53% for SiO₂, 14-20% for Al₂O₃, 9-13% for FeO*, 2.4-3.6% for Na₂O, 4-7% for MgO, 6-13% for CaO, 1-3% for TiO₂, 0.1-0.5% for P₂O₅ and 0.2-2.4% for K₂O. The relative magnitude of intra-unit variation is generally a small fraction of the total variation between units. Overall, positive correlations exist between SiO₂, TiO₂, P₂O₅ and K₂O, notwithstanding alteration-related loss of K₂O for a few samples from the crest hole 525A, suggested by their scatter off the correlations involving K₂O (Richardson et al, 1984). Ti, P and K are incompatible (strongly partitioned into melt) and the relevant correlations have approximate unit slopes. This indicates crude consistency of Ti/P, Ti/K and K/P ratios in the source materials of these basalts. For Al₂O₃, CaO, MgO and FeO* (major components of phenocryst plagioclase, clinopyroxene and olivine) no clear trends are apparent. Small scale variation within individual units is attributable to crystal-liquid sorting.

Nb and Ba are the most incompatible of the trace elements reported in Richardson et al (1984) and show concentration ranges of 6-53 ppm and 72-626 ppm respectively; the range observed for Zr is slightly less (62-360 ppm). Nd ranges from 9 to 46 ppm and Sm from 3 to 10 ppm (Table 1-1). Incompatible element abundances as well as light rare earth enrichment increase dramatically from minima in the highly plagioclase phyric basalts of the flank holes 527 and 528 to maxima in the aphyric

FIGURE 1-3

Nd-Sr isotope correlation diagram showing the Walvis Ridge basalt trend parallel to an extension of the oceanic mantle array defined by fields for MORB and some recent ocean island volcanics. Aphyric basalts from the ridge crest lie at the lower right end of this trend and highly phyrlic basalts from the flank at its upper left end. Lines indicate isotopic evolution of individual basalts over the 70 Ma since formation of this segment of the ridge. Whole rock initial $^{87}\text{Sr}/^{86}\text{Sr}$ ratios suffered variable increases due to exchange with seawater as exemplified by the vector between those of a fresh glass and corresponding whole rock (525A-59-4, 35-39). The enriched end member limit derived by interpretation of the initial ratio-reciprocal concentration trends as mixing lines (Figure 1-4) is shown at lower right. Data sources: Richard et al, 1976 (MORB, Iceland); DePaolo and Wasserburg, 1976 (MORB, Hawaii); O'Nions et al, 1977 (MORB, Hawaii, Iceland, Ascension, Bouvet, Tristan da Cunha); White and Hofmann, 1978 (Galapagos); Dosso and Murthy, 1980 (Kerguelen). All Nd data normalized to $^{146}\text{Nd}/^{144}\text{Nd} = 0.7219$ (O'Nions et al, 1977) and $^{143}\text{Nd}/^{144}\text{Nd} = 0.51264$ for BCR-1 (Dosso & Murthy, 1980; Wasserburg et al, 1981).



basalts of the ridge crest hole 525A. Speculation that the basalts from the three holes may be related in part by crystal fractionation is not supported by inter-element ratios such as Zr/Nb and Zr/Y which indicate that the hole 525A basalts form a separate group (Figure 1-10). Present understanding of the partitioning behavior of Zr and Nb during crystal fractionation processes (le Roex et al, 1981) does not support the derivation of the more evolved hole 525A basalts (Zr/Nb = 10-12) from the hole 528 and 527 basalts (Zr/Nb = 5 - 10) by such processes.

While the effects of alteration are imperceptible for Zr, Nb, Y, Nd and Sm, they are readily apparent in K-Rb relationships (Richardson et al, 1984). Rb ranges from 2 to 38 ppm, giving a range of K/Rb ratios from 410 to 1770. Substantial variation in K/Rb within individual units from crest hole 525A is evident. The samples with high K/Rb are the same ones that appear to have lost K, suggesting even greater losses of Rb. Conversely, at least one of the 525A samples (525A-59-4, 35) with low K/Rb (480) has retained close to magmatic K and Rb contents as confirmed by data for a corresponding fresh glass separate. Sr ranges from 146 to 495 ppm but alteration related Rb variation translates into large scatter in Rb/Sr ratios (Table 1-1).

1.5.2 Nd and Sr Isotope Variation

Combined Nd and Sr isotope ratios and Sm, Nd, Rb and Sr concentrations of representative whole rocks and glass and plagioclase separates are listed in Table 1-1. Whole rock samples are from separate cooling units except for the pair of samples from unit 5 in hole 525A. Initial ratios have been calculated for an average age of 70 Ma (see Geological Setting). Present day and initial ratios are plotted on a Nd-Sr isotope correlation diagram in Figure 1-3 along with fields of

published data for MORB and several ocean islands (Richard et al, 1976; DePaolo & Wasserburg, 1976b; O'Nions et al, 1977; White & Hofmann, 1978; Dosso & Murthy, 1980; Cohen et al, 1980). Vectors joining initial and present day ratios indicate isotopic evolution in these basalts over the 70 Ma since their formation. Except for the basalts with high Rb/Sr ratios (eg 528-42-1, 40-45) the isotopic evolution of their sources over the equivalent short time period will not have been substantially different.

Values for the fresh glass separate and the corresponding whole rock (525A-59-4, 35-39) are also plotted in Figure 1-3. Their $^{147}\text{Sm}/^{144}\text{Nd}$, $^{143}\text{Nd}/^{144}\text{Nd}$ and $^{87}\text{Rb}/^{86}\text{Sr}$ ratios are essentially identical. However, their $^{87}\text{Sr}/^{86}\text{Sr}$ ratios (present or initial) differ by 2 parts in 10^4 . This serves to illustrate the extent of alteration of some whole rock $^{87}\text{Sr}/^{86}\text{Sr}$ ratios. The set of basalts in Table 1-1 was chosen to represent the maximum range in major and trace element chemistry previously identified (Richardson et al, 1984) and thus included samples such as the aphyric basalts 528-42-1, 40 and 528-47-3, 23 which are petrographically moderately altered. Assuming unchanged $^{143}\text{Nd}/^{144}\text{Nd}$ ratios, these appear to have suffered the largest alteration induced increases in $^{87}\text{Sr}/^{86}\text{Sr}$ relative to the overall trend.

The initial $^{87}\text{Sr}/^{86}\text{Sr}$ ratio of the plagioclase (0.70391) from the highly plagioclase phyric basalt (527-41-4, 10-15) is lower than that of the whole rock (0.70414) by 3 parts in 10^4 . This can be attributed either to alteration of the whole rock groundmass or to a xenocrystal origin for the plagioclase. The plagioclase Sm/Nd ratio is also higher than that expected from calculations of partitioning between plagioclase and the whole rock liquid. However, the plagioclase (with a modal

FIGURE 1-4

Variation between initial isotope ratio (at 70 Ma) and reciprocal concentration for basalts from holes 525A, 528 and 527 on the Walvis Ridge transect. As discussed in the text, Nd and Sr concentrations have been variously affected by differentiation and dilution due to crystal-liquid sorting while initial $^{87}\text{Sr}/^{86}\text{Sr}$ ratios have been variously increased by exchange with seawater. Lines show extrapolations to intercepts of 0.5121 at $1/\text{Nd} = 0$ and 0.7058 at $1/\text{Sr} = 0$ (infinite enrichment) in one direction and typical MORB compositions in the other. If these are interpreted as simple binary mixing lines, the intercept composition represents the limit of the enriched end member. This hypothetical composition falls on an extension of the Nd-Sr array in Figure 1-3. MORB data sources: Schilling, 1971; Hart, 1976; references in Figure 1-3.

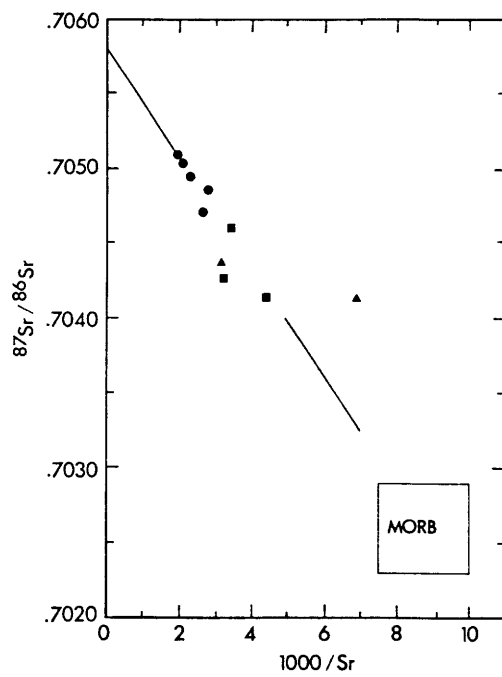
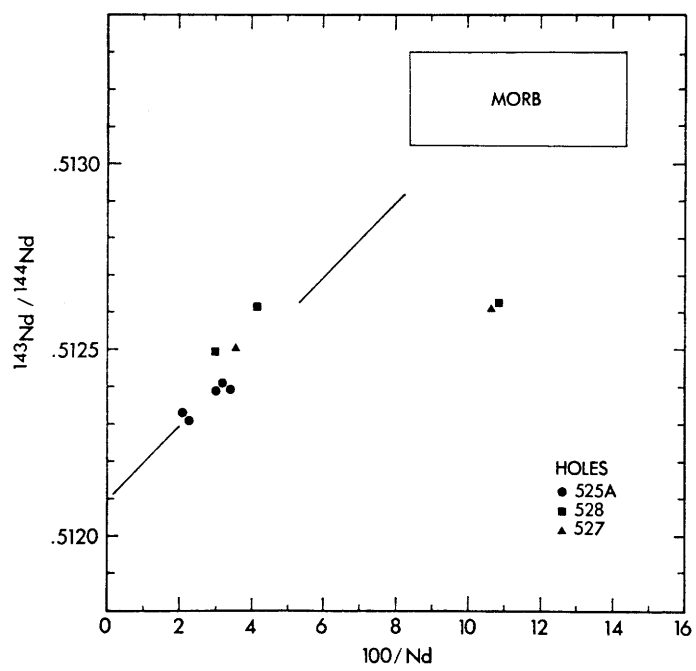
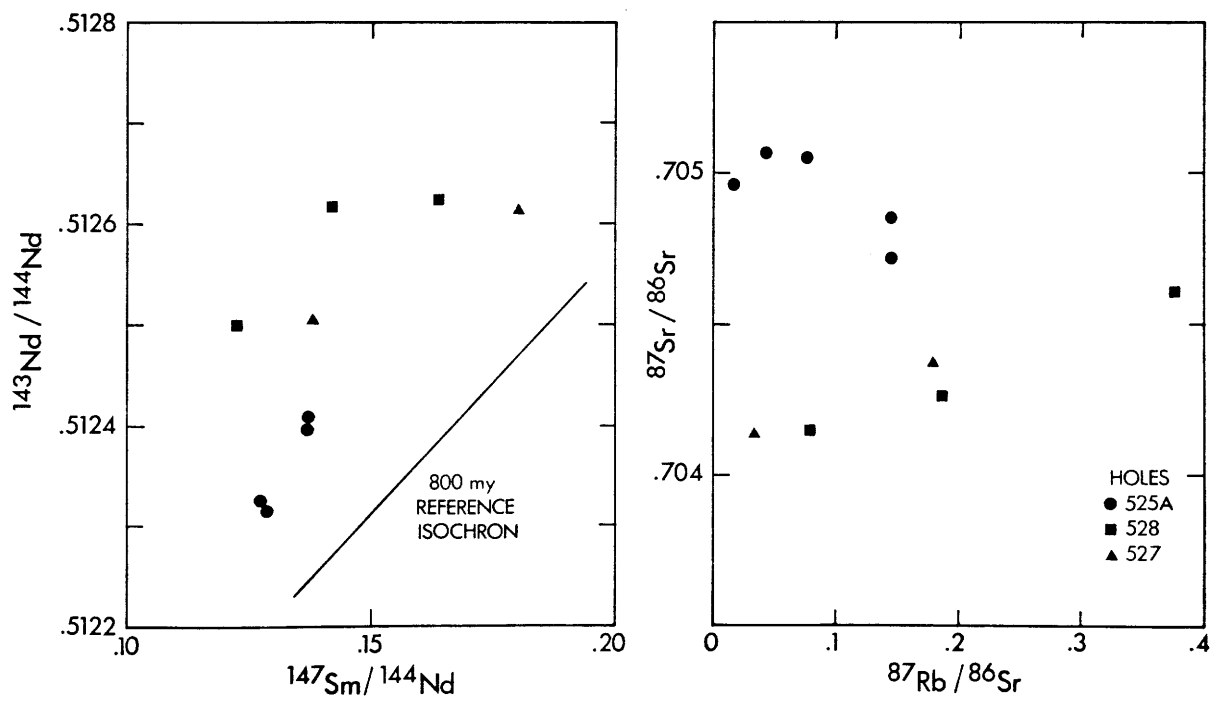


FIGURE 1-5

Sm-Nd and Rb-Sr isochron diagrams showing variation between initial isotope ratio (at 70 Ma) and parent-daughter ratio. As discussed in the text, ratios have been variously affected by differentiation and alteration. An 800 Ma Sm-Nd isochron slope is shown for reference.



abundance of up to 25%) contributes less than 0.5% of the Sm and Nd budget of the whole rock (Table 1-1). If it is in fact xenocrystal, it will have diluted Sm and Nd concentrations while leaving the Sm/Nd ratio essentially unchanged. In addition, the plagioclase $^{87}\text{Sr}/^{86}\text{Sr}$ ratio is sufficiently close to the whole rock value and removed from MORB values to rule out derivation from a MORB liquid.

Systematic negative covariation of $^{143}\text{Nd}/^{144}\text{Nd}$ and $^{87}\text{Sr}/^{86}\text{Sr}$ ratios is apparent in Figure 1-3 notwithstanding second order alteration effects. Basalts from the ridge crest hole 525A individually and collectively have the lowest $^{143}\text{Nd}/^{144}\text{Nd}$ (0.51238) and highest $^{87}\text{Sr}/^{86}\text{Sr}$ (0.70512) ratios. Highly plagioclase phyric basalts from the midflank hole 528 and lower flank hole 527 have the highest $^{143}\text{Nd}/^{144}\text{Nd}$ (0.51270) and the lowest $^{87}\text{Sr}/^{86}\text{Sr}$ (0.70417) ratios. Aphyric basalts from both flank sites have isotope ratios intermediate between the above extremes.

Whole rock $^{143}\text{Nd}/^{144}\text{Nd}$ and $^{87}\text{Sr}/^{86}\text{Sr}$ ratios are respectively negatively and positively correlated with Nd (9-46 ppm) and Sr (146-495 ppm) concentrations. This is shown graphically in Figure 1-4 where initial ratios are plotted against reciprocal concentrations. The order of samples in the crude trends outlined is essentially the same for Sr and Nd and corresponds to that given above for the isotope ratio correlation. Basalts from the ridge crest hole 525A thus have the highest Nd and Sr concentrations while the highly plagioclase phyric basalts from the flank holes 528 and 527 have the lowest. Differentiation and dilution effected by crystal liquid sorting would have changed reciprocal concentration values and contributed to scatter in Figure 1-4. Further scatter in the Sr plot in Figure 1-4 is attributable to alteration-induced increases in $^{87}\text{Sr}/^{86}\text{Sr}$ ratio discussed above.

A very crude positive correlation also exists between initial $^{143}\text{Nd}/^{144}\text{Nd}$ ratio and Sm/Nd ratio (Figure 1-5). Scatter in Sm/Nd ratio is again attributable to differentiation. Rb/Sr ratios are sufficiently scattered (combined effects of alteration and differentiation) to obscure any possible original positive correlation between $^{87}\text{Sr}/^{86}\text{Sr}$ and $^{87}\text{Rb}/^{86}\text{Sr}$ ratios (Figure 1-5).

1.5.3 Pb Isotope Variation

Whole rock Pb isotope ratios are listed in Table 1-1 and plotted in $^{207}\text{Pb}/^{204}\text{Pb}$ (β) - $^{206}\text{Pb}/^{204}\text{Pb}$ (α) and $^{208}\text{Pb}/^{204}\text{Pb}$ (γ) - $^{206}\text{Pb}/^{204}\text{Pb}$ (α) diagrams (Figures 1-6 and 1-7) along with fields of published data for MORB and several S. Atlantic ocean islands (Tatsumoto, 1978; Sun, 1980; Cohen et al, 1980; Dupre & Allegre, 1980). Since U, Th and Pb concentrations have not been measured, radiogenic Pb growth over the 70 Ma since basalt formation cannot be quantified. However, the magnitude of differential growth in the basalts relative to their mantle sources for possible differences in $^{238}\text{U}/^{204}\text{Pb}$ (μ) and $^{232}\text{Th}/^{204}\text{Pb}$ ($\mu \cdot \kappa$ where $\kappa = ^{232}\text{Th}/^{238}\text{U}$) is reasonably small (Figures 1-6 and 1-7). Its direction is sub-parallel to the data array and independent of $\Delta(\mu)$ in the α - β diagram (Figure 1-6). In the α - γ diagram, its direction is also likely subparallel to the data array, but dependent on $\Delta(\kappa)$ (Figure 1-7).

Notwithstanding analytical error and possible differential radiogenic Pb growth, the Walvis Ridge basalt Pb data describe essentially linear trends in both α - β and α - γ diagrams. Basalts from the ridge crest hole 525A have the lowest $^{206}\text{Pb}/^{204}\text{Pb}$, $^{207}\text{Pb}/^{204}\text{Pb}$ and $^{208}\text{Pb}/^{204}\text{Pb}$ ratios. Highly plagioclase phyric basalts from the lower flank hole 527 have the highest such ratios. Aphyric basalts from both flank sites have isotope ratios intermediate between the above extremes.

FIGURE 1-6

$^{207}\text{Pb}/^{204}\text{Pb}$ (β) - $^{206}\text{Pb}/^{204}\text{Pb}$ (α) diagram showing the Walvis Ridge basalt trend in relation to fields for MORB (Tatsumoto, 1978, Sun, 1980, Cohen et al, 1980, Dupre and Allegre, 1980) and recent S. Atlantic ocean island volcanics (Sun, 1980). Aphyric basalts from the ridge crest lie at the lower left end of this trend and highly plagioclase phyric basalts from the lower flank at its upper right end. The magnitude of differential radiogenic Pb growth in the basalts relative to their mantle sources [$\Delta(\alpha, \beta)$] for possible differences in $^{238}\text{U}/^{204}\text{Pb}$ ($\Delta(\mu)$) over the last 70 Ma is indicated at lower right. The enriched end member limit derived by extrapolation (see text) is shown at middle left. The 4.56 Ga geochron is constructed using conventional evolutionary parameters (Steiger & Jager, 1977) and a primordial Pb composition equivalent to that in Canyon Diablo troilite (Tatsumoto et al, 1973).

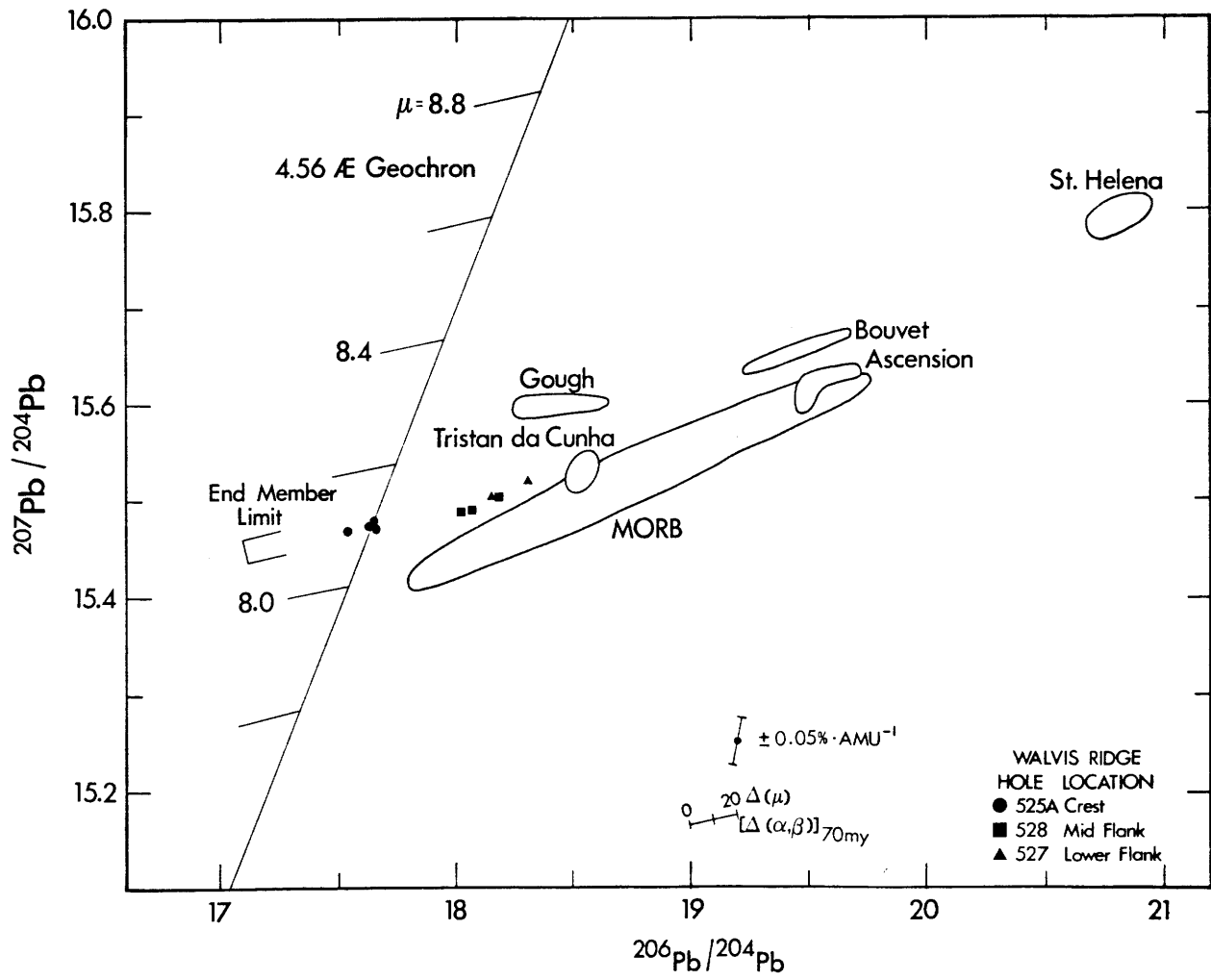
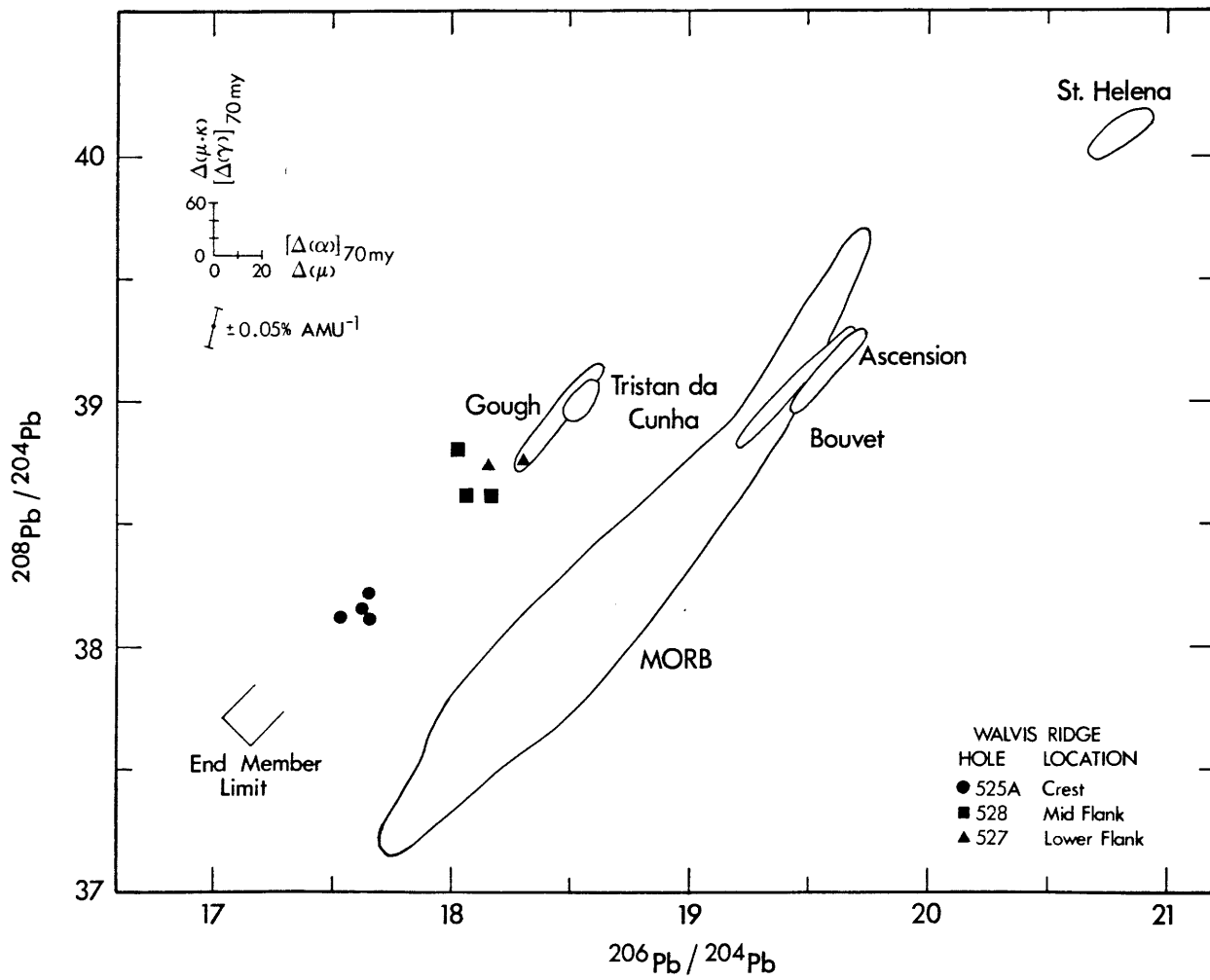


FIGURE 1-7

$^{208}\text{Pb}/^{204}\text{Pb}$ (γ) - $^{206}\text{Pb}/^{204}\text{Pb}$ (α) diagram showing the Walvis Ridge basalt trend in relation to fields for MORB and recent S. Atlantic ocean island volcanics (cf references in Fig. 1-6). Aphyric basalts from the ridge crest lie at the lower left end of this trend and highly plagioclase phyric basalts from the lower flank at its upper right end. The magnitude of differential radiogenic Pb growth in the basalts relative to their mantle sources [$\Delta(\alpha, \gamma)$] for possible differences in $^{238}\text{U}/^{204}\text{Pb}$ ($\Delta(\mu)$) and $^{232}\text{Th}/^{204}\text{Pb}$ ($\Delta(\mu \cdot \kappa)$ where $\kappa = ^{232}\text{Th}/^{238}\text{U}$) over the last 70 Ma is indicated at upper left. The enriched end member limit derived by extrapolation (see text) is shown at lower left.



1.6 Discussion

1.6.1 Relation to Oceanic Basalt Trace Element and Isotopic Systematics

Incompatible trace element contents and LREE enrichment in the Walvis Ridge transect basalts are in general greater than those observed in typical MORB (eg Erlank & Reid, 1974; Erlank & Kable, 1976; Schilling, 1971; Hart, 1969, 1971). Moreover, all the Walvis basalts have Zr/Nb ratios which are lower than those for normal, depleted or N-type MORB (Erlank & Reid, 1974; Kable, 1972) but similar to those for enriched or E-type MORB (represented by samples from the MAR at 45°N and the FAMOUS area (Erlank & Kable, 1976; Kable, 1972) as well as Atlantic island basalts, though within the range for Gough and Tristan da Cunha (Kable, 1972).

Alteration related changes in magmatic alkali element abundances and increases in $^{87}\text{Sr}/^{86}\text{Sr}$ isotope ratio suggested in previous sections are almost certainly due to exchange with seawater (Hart, 1969, 1971; Hart et al, 1974). Such exchange leaves the Zr and Nb abundances and Nd isotopic composition of submarine basalts essentially unchanged (eg Hart et al, 1974; O'Nions et al, 1978). Alteration of submarine basalts with substantial sediment cover is restricted to a short period (<5-10 Ma) after eruption (Hart & Staudigel, 1978; Richardson et al, 1980; Staudigel et al, 1981). Exchange between 70 Ma old seawater (~8 ppm Sr; $^{87}\text{Sr}/^{86}\text{Sr} \approx 0.7078$ (Hart & Staudigel, 1978)) and Walvis Ridge basalts (146-495 ppm Sr) would therefore produce mild increases in whole rock $^{87}\text{Sr}/^{86}\text{Sr}$ ratio. Alteration related changes in Rb/Sr ratio (soon after 70 Ma) were dominated by losses and gains in Rb. Calculated initial $^{87}\text{Sr}/^{86}\text{Sr}$ ratios are maximum values for magmatic initial ratios. The effects of seawater alteration on Pb isotope ratios are expected to be minimal (Hofmann &

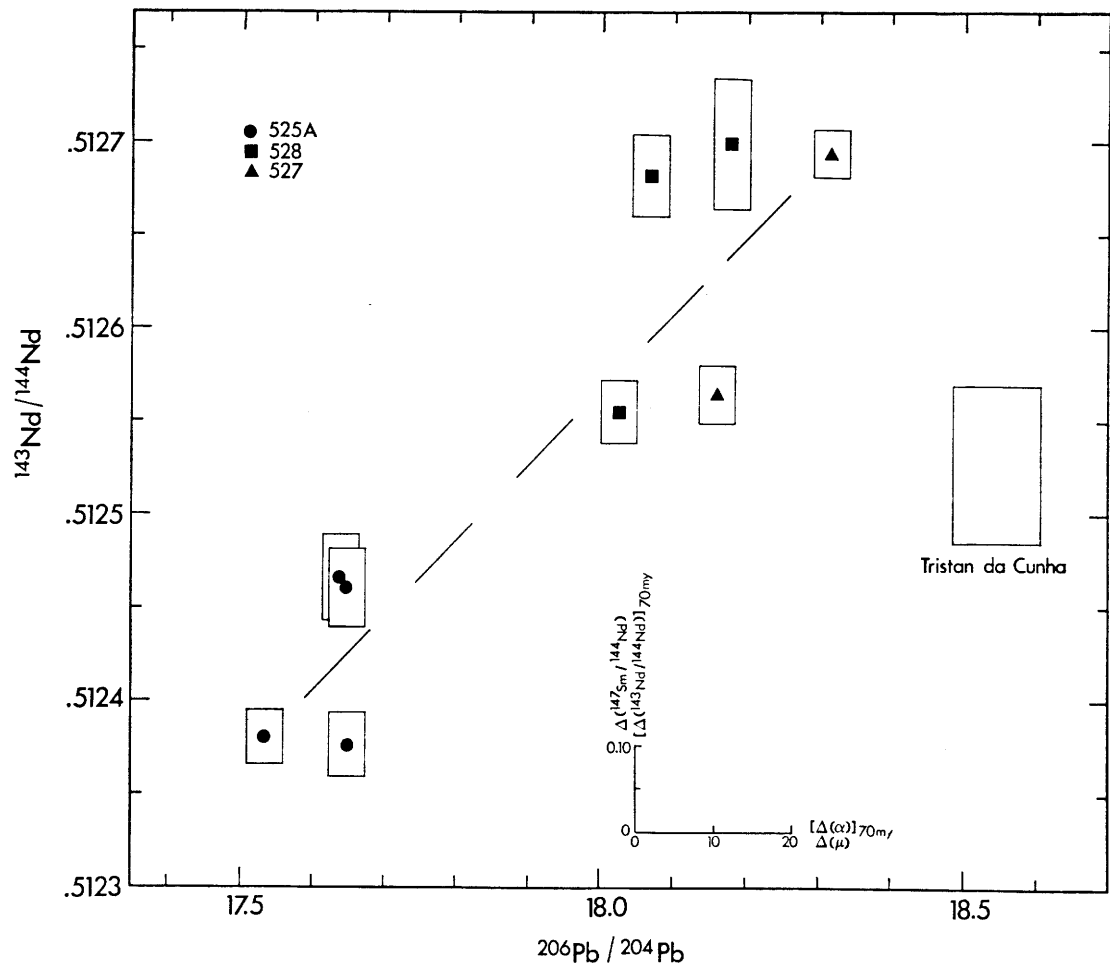
Hart, 1978) as also apparent from the coherency of observed trends (Figures 1-6 and 1-7).

The Walvis Ridge basalt Nd-Sr isotope correlation (Figure 1-3) parallels an extension of the mantle array (DePaolo & Wasserburg, 1979; Allegre et al, 1979) outlined by the data for MORB and some recent ocean island volcanics (Richard et al, 1976; DePaolo & Wasserburg, 1976b; O'Nions et al, 1977). Basalts from the crest of the Walvis Ridge lie at the low $^{143}\text{Nd}/^{144}\text{Nd}$, high $^{87}\text{Sr}/^{86}\text{Sr}$ end of this trend at slightly but distinctly lower $^{87}\text{Sr}/^{86}\text{Sr}$ ratios (for equivalent $^{143}\text{Nd}/^{144}\text{Nd}$ ratio) than alkaline basalts on the spatially associated island of Tristan da Cunha (O'Nions et al, 1977) and on the Kerguelen Island in the Indian Ocean (Dosso & Murthy, 1980). On the $^{207}\text{Pb}/^{204}\text{Pb}$ - $^{206}\text{Pb}/^{204}\text{Pb}$ diagram (Figure 1-6) the Walvis trend has a slope of approximately 0.059 which is shallower than that of the arrays for MORB and most islands (Cohen et al, 1980; Tatsumoto, 1978; Sun, 1980; Dupre & Allegre, 1980; White, 1979; Dosso et al, 1979). Only that for Gough Island at higher $^{207}\text{Pb}/^{204}\text{Pb}$ ratios displays a shallower slope, no greater than 0.041 (Sun, 1980). Basalts from the crest of the Walvis Ridge lie at $^{206}\text{Pb}/^{204}\text{Pb}$ ratios which are even lower than the lowest found for MORB. On the $^{208}\text{Pb}/^{204}\text{Pb}$ - $^{206}\text{Pb}/^{204}\text{Pb}$ diagram (Figure 1-7), basalts from the crest of the Walvis Ridge again lie at the low $^{208}\text{Pb}/^{204}\text{Pb}$, $^{206}\text{Pb}/^{204}\text{Pb}$ end of the trend. Those from the flank trend in the direction of Tristan da Cunha and Gough, displaced from and parallel to fields for MORB and most other islands (Cohen et al, 1980; Tatsumoto, 1978; Sun, 1980; Dupre & Allegre, 1980; White, 1979).

Nd, Sr and Pb isotope ratios of Walvis Ridge rocks are coherently correlated. This is best illustrated for $^{143}\text{Nd}/^{144}\text{Nd}$ and $^{206}\text{Pb}/^{204}\text{Pb}$ (Figure 1-8), notwithstanding differential radiogenic Pb and

FIGURE 1-8

Nd-Pb isotope correlation diagram showing the positive correlation for Walvis Ridge basalts and its relation to the field for Tristan da Cunha (O'Nions et al, 1977; Sun, 1980). Error boxes represent in-run precision for $^{143}\text{Nd}/^{144}\text{Nd}$ (Table 1 and O'Nions et al, 1977) and reproducibility (0.1%) for $^{206}\text{Pb}/^{204}\text{Pb}$ (Table 1 and Sun, 1980). The magnitude of differential radiogenic Nd and Pb growth in the basalts relative to their mantle sources [$\Delta(\alpha, ^{143}\text{Nd}/^{144}\text{Nd})$] for possible differences in $^{238}\text{U}/^{204}\text{Pb}$ ($\Delta(\mu)$) and $^{147}\text{Sm}/^{144}\text{Nd}$ over the last 70 Ma is indicated at lower right.



Nd growth in the basalts relative to their mantle sources over the last 70 Ma. The observed positive correlation (and negative correlation for $^{87}\text{Sr}/^{86}\text{Sr}$ and $^{206}\text{Pb}/^{204}\text{Pb}$) is opposite in sense to that reported for MORB (Allegre et al, 1980; Cohen et al, 1980; Dupre and Allegre, 1980). The distinction between the isotopic signature of Tristan da Cunha basalts and those of the Walvis Ridge suite is also more clearly illustrated (Figure 1-8).

1.6.2 Mantle Source Evolution

Three classes of models for the origin of the Walvis Ridge basalts derive from consideration of their distinct geochemical characteristics. Because of variation in incompatible inter-element and isotopic ratios, derivation of different magma types cannot be modelled simply by crystal-liquid sorting (differentiation/dilution) of compositionally equivalent magmas or by partial melting of a homogeneous source. Plausible models which might account for the isotopic and incompatible trace element variations include: 1. crustal contamination of melts from homogeneous mantle; 2. mixing of melts from heterogeneous mantle; 3. melting of mantle with small scale heterogeneity. These three models and their applicability to the Walvis Ridge basalts are discussed below.

1.6.2.1. Crustal contamination of melts from homogeneous mantle

Mantle-derived magmas of the Walvis Ridge could potentially undergo contamination by oceanic crust, continental crust or surficial marine sediments. If the original "primitive" magmas of the Walvis Ridge had MORB characteristics then contamination by pre-existing (Mesozoic) hydrothermally altered oceanic crust might cause small increases in $^{87}\text{Sr}/^{86}\text{Sr}$. However, such contamination would leave

$^{143}\text{Nd}/^{144}\text{Nd}$ and the Zr and Nb abundances essentially unchanged and is therefore not a viable mechanism to account for the geochemical characteristics of Walvis Ridge basalts.

Contamination by continental crust could potentially produce the low $^{143}\text{Nd}/^{144}\text{Nd}$ ratios, high $^{87}\text{Sr}/^{86}\text{Sr}$ ratios and high Ba contents observed in the Walvis Ridge basalts given the widespread occurrence of these characteristics in old continental crustal materials (eg Carter et al, 1978; DePaolo & Wasserburg, 1979). However, the Walvis Ridge basalt $^{208}\text{Pb}/^{204}\text{Pb}$ - $^{206}\text{Pb}/^{204}\text{Pb}$ data array is displaced from and parallel to the range of MORB type end members (Figure 1-7). This effectively precludes such a contamination scheme involving MORB, unless a case can be made for an as yet unidentified MORB source which has evolved with a high Th/U ratio. Moreover, magneto- and biostratigraphic age constraints and the character of recovered samples (Moore et al, 1983) argue against Walvis Ridge segments originating as blocks of continental crust as suggested by van der Linden (1980).

Contamination by surficial marine sediments could account for the high Ba and Nb abundances in Walvis ridge basalts but fails to explain the various incompatible element and isotope ratio correlations. Sediments with a significant terrigenous (continental) component which might be more suitable contaminants have not been recorded in the holes comprising the Walvis Ridge transect.

1.6.2.2 Mixing of melts from heterogeneous mantle

The classic interpretation of the Walvis Ridge as a mantle plume trace (Wilson, 1963) presupposes a two box mantle model in which the lower mantle source of the plume (Morgan, 1971, 1972) is compositionally distinct from the upper mantle. Passage of the rising plume through the

upper mantle ultimately results in binary mixing of end members melts. This is analogous to the LOM mantle model (large scale, old heterogeneity; mixing of melts) outlined by Zindler et al (1979) as the preferred explanation for the trace element and isotopic characteristics of the Reykjanes Peninsula basalts of Iceland. Adaption of this model to Walvis Ridge basalts would predict approximately linear arrays on Nd-Sr-Pb and Pb-Pb isotope correlation diagrams (Figures 1-3, 1-6, 1-7 and 1-8) because differences in Nd, Sr and Pb concentrations in the two end members would not be sufficiently extreme to induce obvious curvature (Langmuir et al, 1978). Approximate limits for the end member compositions in such a system can be derived from plots of initial Nd and Sr isotopic composition verses reciprocal concentration (Figure 1-4). A lower limit $^{143}\text{Nd}/^{144}\text{Nd}$ ratio of 0.5121 and upper limit $^{87}\text{Sr}/^{86}\text{Sr}$ ratio of 0.7058 can be obtained for the most enriched end member by extrapolation of the crude trends in Figure 1-4, which are variously affected by fractionation and alteration, to $1/\text{Nd} = 0$ and $1/\text{Sr} = 0$ (unattainable infinite enrichment). Significantly, this hypothetical composition lies on an extension of the Walvis Ridge basalt initial Nd-Sr isotope ratio correlation (Figure 1-3). Using an appropriate present day end member limit $^{143}\text{Nd}/^{144}\text{Nd}$ ratio of 0.5122, a corresponding $^{206}\text{Pb}/^{204}\text{Pb}$ ratio of 17.10 can be obtained by extrapolation of the Nd-Pb isotope correlation (Figure 1-8). Corresponding $^{207}\text{Pb}/^{204}\text{Pb}$ and $^{208}\text{Pb}/^{204}\text{Pb}$ values can in turn be obtained by extrapolation of the Pb-Pb trends (Figures 1-6 and 1-7). This represents the hypothetical limit of the most enriched (low $^{143}\text{Nd}/^{144}\text{Nd}$, $^{206}\text{Pb}/^{204}\text{Pb}$, $^{207}\text{Pb}/^{204}\text{Pb}$, $^{208}\text{Pb}/^{204}\text{Pb}$ and high $^{87}\text{Sr}/^{86}\text{Sr}$) end member composition. With increasing reciprocal Nd and Sr concentration (depletion) the trends in Figures 1-3 and 1-4 extrapolate in the general

direction of MORB. However, the $^{208}\text{Pb}/^{204}\text{Pb}$ - $^{206}\text{Pb}/^{204}\text{Pb}$ data array is parallel to and displaced from the range of MORB compositions (Figure 1-7) and such an end member can be discounted. Instead, an end member with a Pb isotopic composition equivalent to or more radiogenic than that of Tristan da Cunha would be required.

In such a binary mixing model correlations between isotope ratio and parent-daughter ratio (Figure 1-5) would be mixing lines. They would not have age significance except in the case of a simple two-source model where both sources differentiated from a common parent at a discrete time. In this case, the mixing lines would correspond to two point isochrons. As noted in Figure 1-5, correlations between isotope and parent-daughter ratios are poorly developed. This is especially so for the Rb-Sr system, where seawater alteration has undoubtedly been active.

The inferred $^{143}\text{Nd}/^{144}\text{Nd}$ ratio of the actual enriched end member lying somewhere between the limit (0.5122) and the minimum observed value of the Walvis Ridge crest basalts (0.51238), is distinctly lower than the average present-day chondritic value (0.51264) adopted for the bulk earth (Jacobsen & Wasserburg, 1980; Wasserburg et al, 1981). The B-type Pb isotopic composition of the enriched end member, again somewhere between that of the ridge crest basalts and the limit ($^{206}/^{204}\text{Pb} = 17.10$, $^{207}/^{204}\text{Pb} = 15.45$, $^{208}/^{204}\text{Pb} = 37.65$), lies to the left of the geochron (Figure 1-6) and thus bears no resemblance to a primitive bulk earth composition. The fact that the Walvis Ridge crest basalts lie close to the geochron is probably fortuitous. The above considerations imply that the source of at least one component in the petrogenetic scheme for the Walvis Ridge basalts underwent an ancient increase in Nd/Sm, Rb/Sr and Pb/U, relative to bulk earth values.

FIGURE 1-9

Variation between Zr/Nb and Ba/Nb ratios of basalts from holes 525A, 528 and 527 on the Walvis Ridge transect and comparison with other Atlantic sea floor and island basalts. All data obtained by XRF at the University of Cape Town. Data sources: MORB (N-type), Kable (1972), Erlank & Reid (1974); MORB (E-type), Famous area, le Roex et al (1981) and MAR at 45° N, Erlank & Kable (1976); Atlantic islands, Kable (1972). Specific fields for data from Gough and Tristan da Cunha are shown. Other Atlantic islands include Ascension, Azores Group, Bouvet, Fogo, Iceland, Jan Mayen, Madeira, Saint Helena and Tenerife. All samples contain <55% SiO₂. Any simple two component mixing should produce a straight line on this diagram between potential end members (effects of magmatic fractionation on these ratios are considered to be negligible).

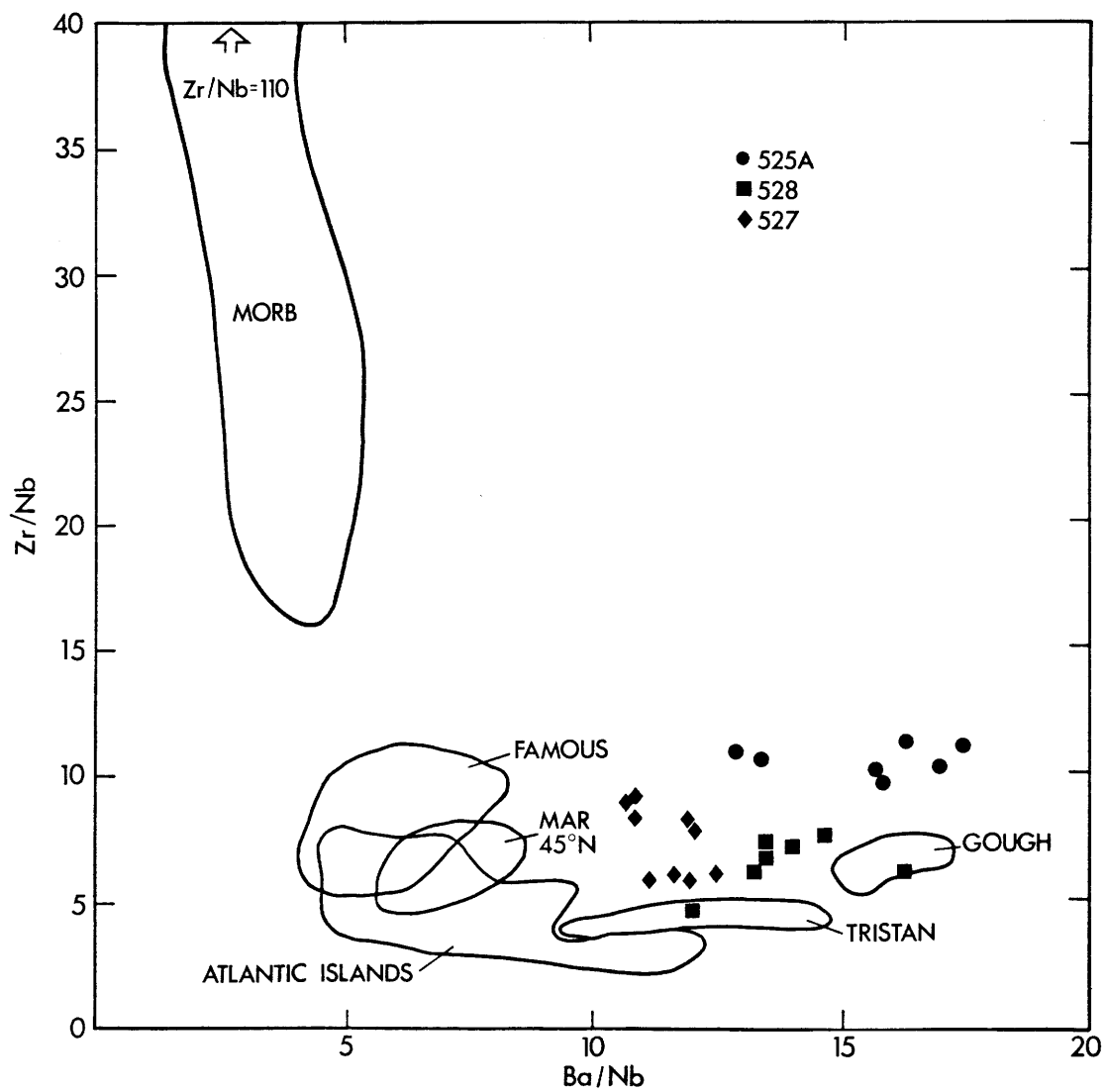
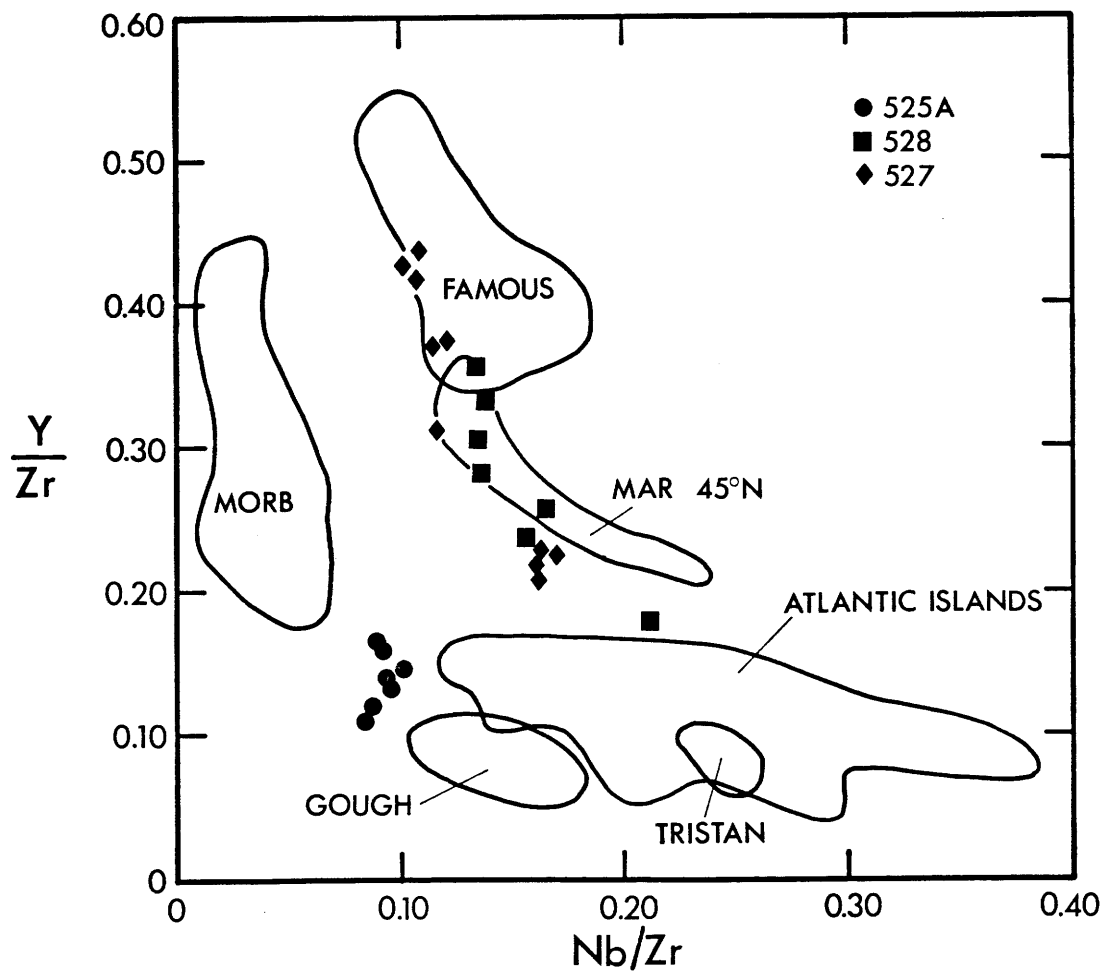


FIGURE 1-10

Variation between Y/Zr and Nb/Zr ratios of basalts from holes 525A, 528 and 527 on the Walvis Ridge transect and comparison with other Atlantic sea floor and island basalts. Data sources as in Figure 1-9.



A simple binary mixing model necessarily requires that all combinations of elements and ratios form mixing curves. As discussed above for Pb isotope ratios, Zr-Nb-Ba-Y inter-element relationships (Figures 1-9 and 1-10) effectively preclude any significant participation by N-type MORB as the depleted end member in a magma mixing model (Richardson et al, 1984). The high Ba/Nb ratios of the Walvis Ridge basalts (Figure 1-9) also appear to eliminate the possibility of E-type MORB being an end member in a two component model (Figure 1-9). Finally, the combined distribution of Zr/Nb and Zr/Y ratios (Figure 1-10) in the ridge flank basalts (Zr/Nb = 5-10; Zr/Y = 5-2) relative to those in the more evolved ridge crest basalts (Zr/Nb = 10-12; Zr/Y = 6-9) apparently rules out any mixing model which is restricted to two components, even when allowance is made for fractionation of inter-element ratios by magmatic differentiation.

1.6.2.3 Melting of mantle with small scale heterogeneity

An alternative model requiring a heterogeneous mantle involves the partial melting of a chemically modified mantle which has been variably enriched, such that the ridge crest basalts from hole 525A are representative of those portions of the mantle which show the greatest degree of enrichment. A simple example of such a model is the SOS mantle model (small scale, old heterogeneity; solid state, mixing of sources) of Zindler et al (1979). Volcanic products derived from a composite source in which the enriched and depleted portions had the same initial isotopic compositions describe the same Nd-Sr-Pb and Pb-Pb correlations and correlations of isotope ratio with reciprocal concentration and parent-daughter ratio as in the LOM model described in the previous section. In the SOS model, however, the Pb-Pb and isotope ratio vs.

parent-daughter ratio correlations are more likely to have real age significance. $^{207}\text{Pb}/^{204}\text{Pb}$ - $^{206}\text{Pb}/^{204}\text{Pb}$, $^{143}\text{Nd}/^{144}\text{Nd}$ - $^{147}\text{Sm}/^{144}\text{Nd}$ and $^{87}\text{Sr}/^{86}\text{Sr}$ - $^{87}\text{Rb}/^{86}\text{Sr}$ arrays represent secondary isochrons. In the ideal case where basalt parent-daughter ratios reflect those of their sources the age of the enrichment event can be obtained. The positive correlation of initial $^{143}\text{Nd}/^{144}\text{Nd}$ and $^{147}\text{Sm}/^{144}\text{Nd}$ ratios for Walvis Ridge basalts (Figure 1-5) is not well enough defined to yield a meaningful age directly. However, given that relative decreases in Sm/Nd ratio caused by differentiation are likely to be greater for the more evolved ridge crest basalts than for the highly phyric ridge flank basalts, a minimum age of 800 (+70) Ma can be obtained. The slope of the $^{207}\text{Pb}/^{204}\text{Pb}$ - $^{206}\text{Pb}/^{204}\text{Pb}$ array (uncorrected for differential radiogenic Pb growth since basalt formation; Figure 1-6) represents an age of approximately 600 Ma with a large uncertainty ($> \pm 600$ Ma in a York II regression (York, 1969) using errors of $\pm 0.05\% \cdot \text{AMU}^{-1}$). Clearly, if the event was not discrete or involved components with different initial isotopic compositions (> 2 stage model) its timing is necessarily obscure.

Although the presence of compositionally different upper mantle beneath the Walvis Ridge is supported by its anomalous Rayleigh wave dispersion characteristics (Chave, 1979) its precise nature cannot be defined at this stage. The positive Nd-Pb and negative Nd-Sr and Sr-Pb isotopic correlations of the Walvis basalts require coherent increases in Nd/Sm, Rb/Sr and Pb/U ratio in the enriched source component (crystallized fluid and/or melt) relative to those of the host source. The sense of the Nd-Pb correlations is opposite to that for MORB where increasing degree of time integrated source depletion (previous melt extraction) corresponds to decreasing Nd/Sm and Rb/Sr ratio but increasing Pb/U ratio (Allegre et al,

1980; Cohen et al, 1980; Dupre & Allegre, 1980). This may be accounted for by appealing, for example, to preferential enrichment of Rb and Nd over Sr and Sm in both fluids and melts, but enrichment of more volatile Pb over U in fluid, as opposed to U over Pb in melt. However, such empirical arguments do not constrain a choice of enrichment process and it is appropriate to discuss the following options for enrichment mechanisms and events:

(1) Invasion of a homogeneous mantle source by small volume enriched melts which crystallize as veins of enriched material and which do not subsequently equilibrate isotopically with the host mantle wall rock. Such melts could be derived in two ways: (a) by direct melting of mantle (eg Hanson, 1977; Wood, 1979; Zindler, 1979). In the simplest case the small volume melts are derived from material of the same composition as that which they invade (SOS model); and (b) by subduction induced melting as a consequence of recycling of subducted crust (eg O'Nions et al, 1979; Allegre et al, 1980; Hofmann & White, 1982; Chase, 1981). This could also effectively be a contamination model if the subducted material contributes directly to the small volume melts. In the simplest case this contribution does not occur, the subduction process merely acts as a triggering mechanism and the melting process is the same as that in the SOS model.

For the simple cases outlined in (a) and (b) above the previously noted minimum time of 800 Ma required to account for observed differences in Nd isotopic composition, can be viewed in the context of the geodynamic history of the regional lithosphere prior to opening of the South Atlantic. The Walvis Ridge meets the southern African continental margin in the vicinity of the SW-NE trending Damaran orogen of Pan-African age.

With regard to (a) it is pertinent to note that the earliest manifestations of Damaran volcanic activity (Naauwpoort volcanics and Matchless amphibolites) have yielded radiometric ages of approximately 800 Ma, well before the 500-600 Ma period of major orogenic activity (Hawkesworth et al, 1981). The Matchless amphibolites have higher Sm/Nd and $^{143}\text{Nd}/^{144}\text{Nd}$ ratios than the bulk earth value at the time of their emplacement, indicating the existence of an N-type MORB source when age differences are allowed for (Hawkesworth et al, 1981). In the context of (b) McWilliams and Kroner (1981) have recently proposed a complex, broadly defined model involving rifting, heating and stretching of the lithosphere beneath the Damara Belt followed by "intracrustal subduction". All of these processes could result in the generation and migration of melt in the upper mantle.

(2) Invasion of a homogeneous mantle source by metasomatic fluids which crystallize partly as veins and partly (as a consequence of re-equilibration) as replacement products of pre-existing minerals in the host mantle. The overall process is one of infiltration metasomatism. While this process is similar to that involving the introduction of small volume melts, it is likely that the chemical character of the metasomatic fluids will be different from that of melts, particularly for volatile and incompatible elements.

Mineralogical and chemical evidence for metasomatism of mantle-derived nodules is now widely documented (eg Lloyd and Bailey, 1975; Harte et al, 1975; Erlank & Rickard, 1977). Sr isotopic evidence for a suite of K-richrichterite bearing peridotites from a 90 Ma old southern African kimberlite (Bultfontein) suggests a maximum age of 150 Ma for the

metasomatic event (Erlank and Shimizu, 1977; Erlank et al, 1980) tentatively linked with the cessation of Karoo volcanicity. Such a metasomatic event is obviously too young for the postulated enrichment event in the upper mantle underlying the Walvis Ridge. However, Nd and Sr isotopic measurements on diopside and garnet separates from garnet peridotites (which lack K-richterite) from the Bultfontein kimberlite, indicate other much older enrichment (Menzies & Murthy, 1980; Chapter 2). Kimberlite nodules clearly carry evidence of the existence of metasomatised mantle which could potentially give rise to the Walvis Ridge basalts. However, progress has yet to be made in understanding the cause and timing of metasomatic event(s) and the identity and source of metasomatising fluids.

As noted in the previous section, any petrogenetic scheme for the Walvis Ridge basalts must provide more than two compositional components although only two isotopic components are required. In this respect the two models of small scale heterogeneity in the mantle which are discussed above suffer the same defect as the LOM model discussed in the previous section. However, there are two plausible ways to incorporate an extra component into the small scale heterogeneity models:

(a) The small volume melts or metasomatic fluids could be introduced into a mantle that is already heterogeneous as a result of some previous event.

(b) Both small volume melts and metasomatic fluids (of different composition) are introduced into homogeneous mantle, either simultaneously or sequentially.

The latter possibility is appealing since it seems highly probable that introduction of a metasomatic fluid could trigger small volume

partial melting as a consequence of depressing the mantle solidus. In either case it would appear that the SOS model is capable of satisfying the existing constraints which are imposed on the petrogenesis of the Walvis Ridge basalts by isotopic data and incompatible element inter-relationships.

1.7 Conclusions

Basement in a NNW-SSE trending block of the Walvis Ridge consists of submarine tholeiitic basalts (with minor intercalated sediments) erupted approximately 70 Ma ago (Moore et al, 1983). This age is equivalent to that of immediately adjacent oceanic crust in the Angola Basin and consistent with basalt formation at the paleo mid ocean ridge (Moore et al, 1983). The Nd, Sr and Pb isotopic compositions of ridge crest basalts indicate the existence of an old Nd/Sm, Rb/Sr and Pb/U enriched source component. The isotopic signature of the Walvis Ridge basalts is similar to that of alkaline basalts on the spatially associated island of Tristan da Cunha, but with distinctly lower Nd and Pb isotopic ratios. The incompatible element concentrations are similar to those in oceanic islands or E-type MORB, but detailed examination of Zr-Ba-Nb-Y interelement relationships (Richardson et al, 1984) shows that they are not consistent with any simple two component model of magma mixing, as might result from the rise of a lower mantle plume through the upper mantle. Incompatible element and Pb isotopic systematics also preclude extensive involvement of depleted (N-type) MORB material or its mantle sources in the petrogenesis of Walvis Ridge basalts. In the preferred petrogenetic model the Walvis Ridge basalts were derived by partial melting of upper mantle similar to an enriched (E-type) MORB source which

had become heterogeneous on a small scale due to the introduction of small volume melts and metasomatic fluids.

CHAPTER 2

EVOLUTION OF DEPLETED AND ENRICHED SUB-CONTINENTAL MANTLE
INFERRED FROM THE Nd AND Sr ISOTOPIC SYSTEMATICS OF
GARNET PERIDOTITES FROM KIMBERLITE

2.1 Introduction

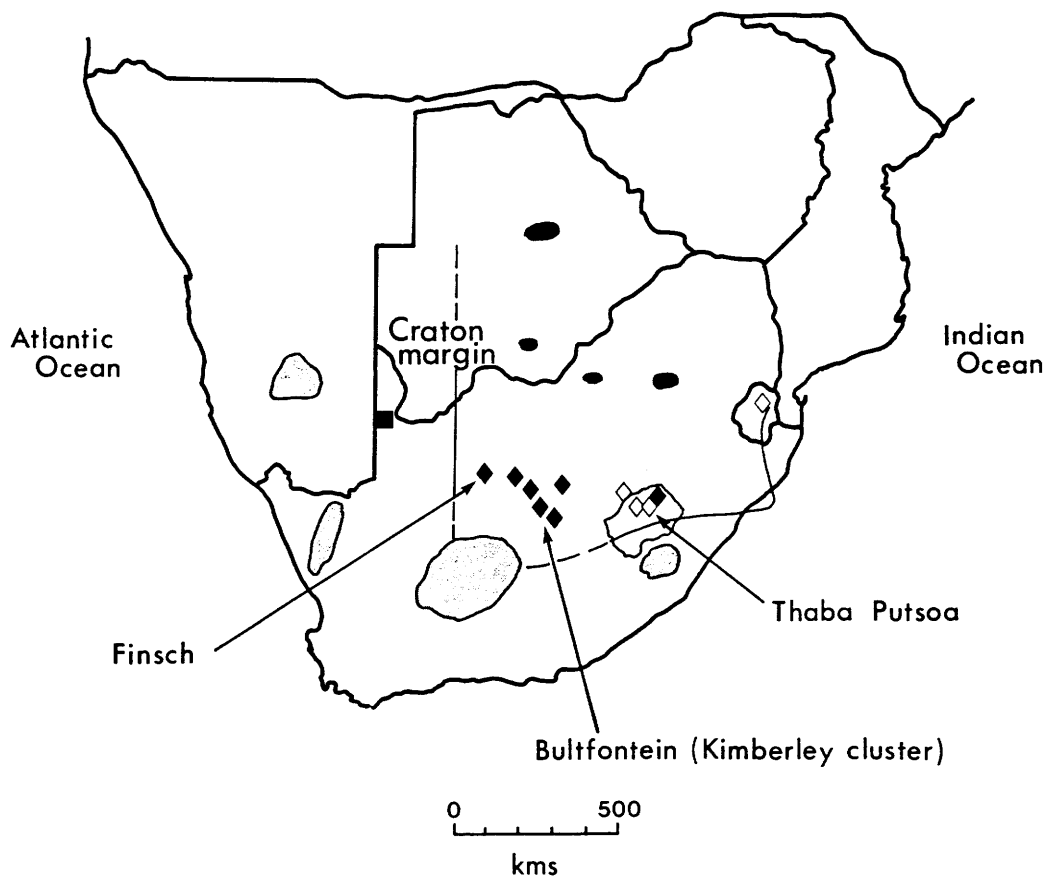
Current understanding of the evolution of the earth's mantle derives from numerous trace element and isotopic studies of ancient and modern mantle-derived magmas. Recognition that ocean floor basalts are derived from upper mantle sources with time integrated Rb/Sr, Pb/U and Nd/Sm ratio depletion relative to inferred bulk earth values (eg Tatsumoto et al 1965; Tatsumoto, 1966; Gast, 1968; Richard et al, 1976; DePaolo & Wasserburg, 1976a; O'Nions et al, 1977) led to concepts of episodic (Brooks et al, 1976a) or continuous (eg Armstrong, 1968; Russell, 1972) mantle differentiation. The material extracted from such mantle is presumed to give rise to continental crust, and various mass balance models have been constructed to try to constrain the proportion of the mantle thus depleted (O'Nions et al, 1979; Jacobsen & Wasserburg, 1979; DePaolo, 1980; Allegre et al, 1983). The generation of complementary enriched mantle that might be as durable as continental crust, is generally discounted in these models. However, some ocean island basalts such as those from the Walvis Ridge (Chapter 1) and Kerguelen (Dosso & Murthy, 1980) have isotopic signatures which require a contribution from such ancient enriched mantle. In this context, the most likely place for long-term storage of enriched mantle appears to be the sub-continental lithosphere. The existence of such enriched sub-continental mantle has also been inferred on the basis of the trace element and isotopic signatures of mantle-derived continental volcanics (Brooks et al, 1976b) including Mesozoic flood basalts (eg Brooks et al, 1978; Erlank et al, 1980; Hawkesworth et al, 1983) and some kimberlites (Smith, 1983; McCulloch et al, 1983). This inference has generally run counter to other claims of essentially undifferentiated bulk earth sources for flood

basalts (DePaolo & Wasserburg, 1976b; Wasserburg & DePaolo, 1979) and kimberlites (Basu & Tatsumoto, 1979, 1980). At the same time, both these alternatives have been clouded by the possibility that continental crustal contamination of magmas from depleted mantle might give rise to the same set of characteristics (cf Hawkesworth & Norry, 1983).

A direct approach to the chemical constitution of sub-continental mantle involves examination of peridotite xenoliths from alkalic basalts and kimberlites. Continental alkalic basalts with spinel peridotite xenolith suites are generally associated with rifts or areas of similarly elevated heat flow. In contrast, kimberlites with garnet peridotite xenolith suites are most commonly erupted through stable cratons with low surface heat flow. Kimberlites are therefore the most likely bearers of samples of long-lived sub-continental lithosphere. Several suites of peridotite xenoliths from southern African kimberlites have already been broadly characterized with respect to bulk and mineral major and trace element chemistry by numerous workers (cf Nixon, 1973a; Ahrens et al, 1975; Boyd & Meyer, 1979b). From these data, scenarios describing the physico-chemical evolution of host mantle materials have been constructed (cf Gurney & Harte, 1980; Harte, 1983). Definition of the time-integrated aspects of this evolution, using the isotopic systematics of these xenoliths, has generally been hampered by severe alteration problems and the consequent necessity for analysis of small pure samples of selected constituent minerals. A Nd and Sr isotopic study of garnet and diopside in various peridotites from three southern African kimberlites, Bultfontein (Kimberley cluster), Thaba Putsoa (northern Lesotho) and Finsch (northern Cape Province), was undertaken with a view to obtaining reliable data for well-characterized samples. Observed isotopic

FIGURE 2-1

Sketch map of distribution of various kimberlites in southern Africa (from Gurney & Harte, 1980), highlighting the location of Bultfontein ($28^{\circ} 46'S$, $24^{\circ} 48'E$; Kimberley cluster), Finsch ($28^{\circ} 16'S$, $23^{\circ} 06'E$; ~ 160 km WNW of Kimberley) and Thaba Putsoa ($28^{\circ} 55'S$, $28^{\circ} 40'E$; northern Lesotho). Black diamonds, diamond mines; white diamonds, diamondiferous kimberlites; black areas, clusters of diamondiferous kimberlites; black square, non-diamondiferous kimberlite; shaded areas, clusters of non-diamondiferous kimberlites. An estimate of the southern margin of the Archean Kaapvaal craton is also shown (other lines are boundaries of countries).



equilibrium and disequilibrium relationships are used to qualify the nature and evolution of depleted and enriched sub-continental mantle.

2.2 Peridotite Lithology & Chemistry

2.2.1 Petrography

Five broad categories of mantle-derived xenoliths are to be found in southern African kimberlites (Harte, 1978): 1. peridotites, including garnet-bearing and garnet-free lherzolites and harzburgites, 2. garnet pyroxenites, 3. eclogites, 4. megacrysts (diopside, garnet, orthopyroxene, olivine, ilmenite, phlogopite), and 5. MARID (mica, amphibole, rutile, ilmenite, diopside) suite rocks.

Garnet lherzolites from the northern Lesotho (Archean Kaapvaal craton margin) kimberlites at Thaba Putsoa (Figure 2-1) and nearby Mothae were originally divided into granular and sheared textural types (Boyd & Nixon, 1972, 1973; Boyd, 1973). These are now termed coarse and porphyroclastic (Harte, 1977). The coarse lherzolites are composed predominantly of olivine and orthopyroxene along with minor purple-red chrome pyrope, bright green chrome diopside and chromite. Phlogopite can also occur. The porphyroclastic lherzolites contain larger proportions of reddish-brown pyrope and dark green diopside than the coarse varieties and chromite and phlogopite are absent. The deformation observed in the porphyroclastic lherzolites is believed to have been produced in a period of minutes to days (Goetze, 1975; Mercier, 1979).

Coarse lherzolites and harzburgites, seemingly always with at least a trace of primary phlogopite, dominate the peridotite suite at Bultfontein (Figure 2-1) and other kimberlite pipes of the Kimberley (craton interior) cluster (Chen, 1971; Boyd & Nixon, 1978; Lawless, 1978). However, mineralogically equivalent deformed varieties also occur. Garnet free

members of the coarse suite containing the amphibole potassic richterite in addition to more abundant phlogopite have also been recognized (Erlank, 1973). Their mineralogy and associated replacement textures are considered to be the result of mantle metasomatic processes (Aoki, 1975; Erlank & Rickard, 1977; Jones et al, 1982; Haggerty et al, 1983a). The introduced metasomatic minerals bear similarities to those in the MARID suite (Dawson & Smith, 1977) of xenoliths.

2.2.2 Major & Trace Element Chemistry

Bulk major element compositions of the two major types of lherzolite at Thaba Putsoa show that the coarse lherzolites are depleted in Na, Ti, Fe, Ca and Al relative to the porphyroclastic lherzolites (Boyd & Nixon, 1973). Differences in bulk composition are largely reflected in respective clinopyroxene and garnet compositions. Paired clinopyroxene and orthopyroxene compositions have been used for geothermometry and geobarometry, indicating higher temperatures and greater depths of equilibration for the porphyroclastic lherzolites from northern Lesotho (Boyd, 1973; Boyd & Nixon, 1975; MacGregor, 1975). In contrast, deformed lherzolites from the Kimberley pipes resemble coarse varieties in their bulk and mineral chemistry and, hence, in lower temperatures and depths of equilibration (Dawson et al, 1975; Boyd & Nixon, 1978). Bulk major element compositions of such cold coarse and deformed peridotites suggest previous partial melt (basaltic component) extraction. In contrast, the hot deformed (and rarely undeformed) peridotites have more fertile compositions and compositional similarities with the ubiquitous Cr-poor megacryst suite, suggesting either lesser depletion or variable refertilization by diffusive equilibration with megacryst magmas (cf Gurney & Harte, 1980; Harte, 1983).

Trace element data (eg Erlank, 1973; Shimizu, 1975 a,b; Shimizu & Allegre, 1978; Nixon et al, 1981; Erlank et al, 1982) are generally inconsistent with simple major element relations, since cold basalt depleted peridotites have higher incompatible element concentrations and LREE enrichment than the hot more fertile peridotites. This is also reflected in the trace element chemistry of respective clinopyroxenes and garnets (Shimizu, 1975b; Erlank & Shimizu, 1977; Shimizu & Allegre, 1978) where, for instance, cold lherzolite clinopyroxenes (particularly those from the modally metasomatized suite) have some impressively high Sr contents (200-900 ppm, as compared to 70-100 ppm for hot lherzolite and megacryst clinopyroxenes).

2.2.3 Previous Sr, Nd and Pb Isotopic Studies

Extensive reconnaissance Sr isotopic studies of southern African kimberlite xenoliths were performed by Allsopp & Barrett (1975) and Barrett (1975). The former study documented mica ages of kimberlite emplacement, yielding initial $^{87}\text{Sr}/^{86}\text{Sr}$ ratios (~ 0.707) for peridotite phlogopites, compatible with approximate isotopic equilibrium between phlogopite and coexisting diopside at the time of kimberlite emplacement (~ 90 Ma). Barrett (1975) found that initial $^{87}\text{Sr}/^{86}\text{Sr}$ ratios of various kimberlite and xenolith components increased in the following order: megacryst diopsides (0.703 -0.704) < most basaltic kimberlites (0.704 -0.705) < eclogite omphacites (0.7047 -0.7062) < peridotite diopsides (0.7060 -0.7075). Kramers (1977) determined Sr and Pb isotope ratios in a set of porphyroclastic and coarse peridotite diopsides from Bultfontein. A large spread in $^{87}\text{Sr}/^{86}\text{Sr}$ ratios (0.7038 -0.7134) and Pb isotope ratios ($^{206}\text{Pb}/^{204}\text{Pb} = 17.8 -19.7$; $^{208}\text{Pb}/^{204}\text{Pb}: 37.3 -39.2$) was obtained. None of the above included hot deformed peridotite materials.

O'Nions et al (1978) measured whole rock $^{87}\text{Sr}/^{86}\text{Sr}$ and $^{143}\text{Nd}/^{144}\text{Nd}$ ratios on single porphyroclastic and coarse lherzolite nodules from Thaba Putsoa and found them to have low $^{87}\text{Sr}/^{86}\text{Sr}$ and high $^{143}\text{Nd}/^{144}\text{Nd}$ ratios requiring low time integrated Rb/Sr and Nd/Sm ratios not unlike those of sub-oceanic mantle. Subsequently, Allegre et al (1982) found apparent Sr isotopic disequilibrium between constituent minerals of a number of porphyroclastic nodules from the Thaba Putsoa pipe (~ 90 Ma old) as well as one from the Precambrian Premier pipe (~ 1.4 Ga old). While the Precambrian example effectively indicated isotopic equilibrium at the time of kimberlite emplacement, the Thaba Putsoa materials gave apparent ages (based on Rb-Sr data for garnet-diopside pairs) of up to 1.8 Ga, well in excess of the 90 Ma kimberlite emplacement age. Unfortunately, the nodule garnet Rb-Sr data, on which the above ages hinge, have been found to be quite unreliable, as discussed in section 2.6. Nevertheless, low initial $^{87}\text{Sr}/^{86}\text{Sr}$ ratios (from diopside) of < 0.703 (similar to the range of 0.7023 - 0.7029 for ocean ridge basalts; eg Hofmann & Hart, 1978) are reasonably well-established.

Intriguing sets of data on coarse modally metasomatized lherzolites from Bultfontein were generated by Erlank & Shimizu (1977) and Menzies & Murthy (1980). In the former study, whole rock Rb-Sr data were obtained for a suite of extensively metasomatized phlogopite K-richterite peridotites, yielding an apparent maximum 150 Ma age for the metasomatism. Minerals were considered to be in isotopic equilibrium on a nodule scale at the time of kimberlite emplacement (90 Ma). In the latter study, combined $^{87}\text{Sr}/^{86}\text{Sr}$ and $^{143}\text{Nd}/^{144}\text{Nd}$ ratios were obtained for a set of diopsides from phlogopite garnet lherzolites. A linear anti-correlation between $^{143}\text{Nd}/^{144}\text{Nd}$ (0.5125 - 0.5120) and $^{87}\text{Sr}/^{86}\text{Sr}$ (0.7046 - 0.7075) was

TABLE 2-0 List of mantle peridotite xenolith samples

| <u>Locality</u> | <u>Rock type</u> ¹ | <u>Mineralogy</u> ² | <u>Texture</u> ³ |
|-----------------|-------------------------------|----------------------------------------------------------|------------------------------------|
| Thaba Putsoa | | | |
| THA3 | garnet lherzolite | ol+opx+ga+cpx | coarse (incipient porphyroclastic) |
| Bultfontein | | | |
| AJE164 | garnet lherzolite | ol+opx+ga+cpx | porphyroclastic |
| BD2435 | garnet lherzolite | ol+opx+ga+cpx | porphyroclastic |
| AJE25 | garnet lherzolite | ol+opx+cpx+ga | coarse |
| AJE165 | garnet lherzolite | ol+opx+ga+cpx | coarse |
| JJG358 | garnet lherzolite | ol+opx+cpx+ga+phlog+chrom | coarse |
| AJE223 | garnet harzburgite | ol+opx+ga+phlog | coarse |
| BUL2 | garnet harzburgite | ol+opx+ga | coarse |
| AJE245 | harzburgite | ol+opx+phlog (substrate) K-richt+phlog+opaques (vein) | coarse |
| Finsch | | | |
| XM46 | garnet lherzolite | ol+opx+ga+cpx+diamond | coarse |

¹ Distinction between lherzolite and harzburgite is simply presence or absence of diopside.

² Listed in estimated overall order of decreasing modal abundance (often variable on a cm scale).

³ Consensus classification described by Harte (1977). Porphyroclastic and coarse lherzolites are respectively equivalent to the sheared and granular lherzolites of Nixon and Boyd (1973).

obtained, extending the mantle array previously observed in mantle-derived magmas (Richard et al, 1976; DePaolo & Wasserburg, 1976b; O'Nions et al, 1977) to less and more radiogenic values for Nd and Sr respectively. Menzies & Murthy (1980) contended that these diopsides (and, hence, whole nodules) represent enriched mantle that has existed for billions of years. Diopside and garnet from a similar coarse lherzolite from Bultfontein were found by Basu & Tatsumoto (1980) to be in approximate Nd isotopic equilibrium, with $^{143}\text{Nd}/^{144}\text{Nd}$ ratios in the range found by Menzies & Murthy (1980). Coexisting primary phlogopite, however, was clearly out of equilibrium with these phases. A distinction can thus be drawn between recent (<150 Ma) enrichment, represented by phlogopite and K-richterite metasomatism, and ancient enrichment apparent in the Nd and Sr isotopic signatures of diopside and garnet (Erlank et al, 1982; Hawkesworth et al, 1983). Furthermore, the liquids or fluids responsible for the young metasomatism appear to have had kimberlitic affinities and could also have given rise to the MARID suite of xenoliths (Kramers et al, 1983).

During the course of the above developments, a detailed isotopic study of coexisting minerals in peridotites from the range of textural and chemical types discussed above, was pursued by the author at MIT (cf Richardson et al, 1982). The kimberlite locality, rock type, major mineralogy and texture of the selected nodules are given in Table 2-0. The majority are from the Bultfontein dumps (Kimberley cluster; Archean Kaapvaal craton interior) and include two deformed and two coarse garnet lherzolites (AJE164, BD2435; AJE25, AJE165), one coarse phlogopite garnet lherzolite (JJG358), two coarse garnet harzburgites (AJE223, BUL2) and one K-richterite-veined harzburgite (AJE245). Several of these have variously featured in studies cited above (Kramers, 1977: BD2435; Shimizu &

Allegre, 1978: AJE25, JJG358; Erlank et al, 1982: BD2435, AJE25) and all (except BUL2 from N Shimizu) have been petrographically and chemically characterized by A J Erlank and coworkers (unpublished) at the University of Cape Town. The very mildly deformed garnet lherzolite (THA3) from Thaba Putsoa (northern Lesotho; craton margin) which features in Allegre et al (1982) has been confirmed to have the chemical characteristics of the hot deformed peridotite suite (P Tilke, pers comm, 1983). The exceptional coarse diamondiferous garnet lherzolite (XM46) from Finsch (northern Cape Province, craton interior) has been described in detail by Shee et al (1982). Further commentary on individual nodule characteristics appears in subsequent discussion of relevant isotopic data.

2.3 Analytical Techniques

Mineral separates were prepared using conventional mechanical and magnetic preconcentration techniques, followed by meticulous hand-picking. Grossly weathered nodule exteriors were discarded and, depending on sample availability, 100-200g of interior material were progressively crushed and sieved for maximum yield of a 200-400 μ m grain size fraction. After removal of fines, specific minerals were concentrated on a Frantz isodynamic separator. Because of variably pervasive alteration (serpentinization, kelyphitization and other lower temperature processes) and consequent dispersion of magnetic properties, these concentrates are necessarily crude. Pure separates were only obtainable by intensive hand-picking. This was performed using Dumont INOX #5 stainless steel tweezers under a Nikon SMZ2 binocular microscope with fiber-optic illumination.

The modally dominant minerals olivine and orthopyroxene were rejected because of very low levels of the elements of interest and consequent

formidable analytical and interpretational problems involved in discriminating between intrinsic and contaminant contributions. For garnet, only isotropic grain fragments entirely bounded by concoidal fracture surfaces and free of visible discoloration and surface pitting were accepted. For diopside, fracture morphology is partially cleavage controlled but similar acceptance criteria were applied. Potassic richterite cleaves profusely during crushing but retains sufficient transparency for a reasonable level of screening. Phlogopite is only marginally transparent and the edges of stacked sheets fracture poorly. Interlayered secondary calcite can sometimes be found. Screening of this mineral is therefore particularly problematic, with the extent of interlayer adsorption and exchange undetermined. Typical yields of acceptable garnet and diopside from original peridotite were 0.04% and 0.01% respectively.

Final garnet separates were subjected to successive ultrasonic cleaning in ultrapure 2.5N HCl, 5% HF, 2.5N HCl, water and acetone prior to limited grinding under acetone in a boron carbide mortar. Diopside was similarly cleaned but not pulverized. K-rich richterite was cleaned in 2.5N HCl, water and acetone while phlogopite was cleaned in water only.

For comparative purposes, whole rock powders of xenoliths and selected hypabyssal kimberlite samples were variously produced at MIT and the University of Cape Town. Preparatory cleaning was limited to water and acetone and powders were not leached.

Chemical and mass spectrometric techniques for determination of K, Rb and Sr concentrations and $^{87}\text{Sr}/^{86}\text{Sr}$ ratios are as described in Hart & Brooks (1977); for Sm and Nd concentrations and $^{143}\text{Nd}/^{144}\text{Nd}$ ratios as summarized in Zindler et al (1979) but with 1982 provision for precise

determination of Sm/Nd and $^{143}\text{Nd}/^{144}\text{Nd}$ ratios on totally spiked samples, as detailed in the Appendix. Total procedural blanks applicable to various data are listed in Tables 2-2 through 2-6. Blank corrections are generally insignificant other than for alkalis. Alkali contents of garnet and diopside samples are very low, with the Rb content of some separates within a factor of 3 of minimum procedural blank levels, which are dominated by ion exchange column contributions. For garnet, the effect of such blanks is increased by alkali elution peak dilation, peculiar to garnet column chemistry. Listed garnet K and Rb concentrations and diopside Rb concentrations should therefore be treated with caution in addition to that warranted by potentially imperfect mineral separate preparation.

In the latter stages of this investigation it became apparent that traces of a colorless secondary mineral (zeolite/carbonate), specifically associated with garnet, were escaping detection during screening of garnet separates. This secondary mineral is restricted to nodule garnet microfracture linings and is apparently a low temperature groundwater precipitate (no garnet substrate discoloration or pitting is discernible). Its mode of occurrence is particularly subversive in that preexisting (emplacement related) coincidental fracture surfaces with a perfectly transparent thin film of this material are difficult to detect. Furthermore, it appears to be present in garnet peridotites from all three localities investigated. A sufficient amount of this material for isotope analysis was separated from a Bultfontein garnet harzburgite (AJE 223). Its presence in garnet separates has demonstrably serious effects on garnet Sr concentrations and $^{87}\text{Sr}/^{86}\text{Sr}$ ratios but no effect on alkali and REE concentrations and $^{143}\text{Nd}/^{144}\text{Nd}$ ratios. Table footnote references

to large pure mineral separates indicate probable imperfect exclusion of this secondary component. References to small ultrapure separates or single ultrapure nodule grains indicate subsequent efforts to minimize this problem. These coincided with refinements in chemical and mass spectrometric procedures for analysis of small Sr samples, as summarized in section 3.4.

2.4 Host Kimberlites

The distribution of various kimberlites in southern Africa is shown in Figure 2-1 (from Gurney & Harte, 1980) with the particular locations of Bultfontein (Kimberley cluster), Finsch (northern Cape Province) and Thaba Putsoa (northern Lesotho) indicated. While a comprehensive study of kimberlite compositions was considered beyond the scope of this investigation, Sr and Nd isotopic data for selected kimberlite samples from the first two of the above three localities were variously acquired for reference purposes (Table 2-1). These samples represent the freshest available hypabyssal facies kimberlite with minimal xenolith fragment content, recovered through diamond mining operations. Sample numbers in Table 2-1 are those assigned by the Geology Department, De Beers Consolidated Mines, Kimberley, where parent specimens reside. The two Bultfontein samples, from the mine 580m level and 825m level drill core respectively, are reputedly monticellite kimberlites, and data (from various labs) are as presented by Erlank et al (1982). The three Finsch samples, two from the F4 intrusive phase and one from an internal dyke identified in the open pit mine, are phlogopite-serpentine, diopside-phlogopite and monticellite-phlogopite kimberlites respectively (J Robey, pers comm, 1982) and have been analyzed at MIT.

The Bultfontein and Finsch kimberlites are respectively

TABLE 2-1 Rb-Sr and Sm-Nd concentrations¹ and isotope ratios² for hypabyssal facies kimberlite specimens³ from the Bultfontein pipe, Kimberley cluster, and the Finsch pipe, northern Cape Province.

| | K | Rb | Cs | Sr | ⁸⁷ Rb/ ⁸⁶ Sr | ⁸⁷ Sr/ ⁸⁶ Sr _p | ⁸⁷ Sr/ ⁸⁶ Sr _i | Sm | Nd | ¹⁴⁷ Sm/ ¹⁴⁴ Nd | ¹⁴³ Nd/ ¹⁴⁴ Nd _p | ¹⁴³ Nd/ ¹⁴⁴ Nd _i |
|--------------------------|-------|-----|------|-------|------------------------------------|-------------------------------------------------|-------------------------------------------------|-------|-------|--------------------------------------|---------------------------------------------------|---------------------------------------------------|
| BULTFONTEIN ⁴ | | | | | | | | | | | | |
| 173/33/K8/12 | 1600 | 35 | | 1485 | 0.068 | 0.70452±2 | 0.70443 | | | | 0.51270±1 | |
| 173/33/K8/19 | 7200 | 57 | | 1675 | 0.098 | 0.70442±5 | 0.70429 | 20.3 | 145 | 0.0846 | 0.51270±1 | 0.51265 |
| FINSCH ⁵ | | | | | | | | | | | | |
| 173/24/K1/347 | 23300 | 154 | 3.11 | 837.4 | 0.5309 | 0.70968±2 | 0.70900 | 10.17 | 77.49 | 0.07930 | 0.512217±14 | 0.512170 |
| 173/24/K1/350 | 33560 | 174 | 2.89 | 666.0 | 0.7560 | 0.71004±2 | 0.70907 | 7.086 | 53.08 | 0.08069 | 0.512224±15 | 0.512176 |
| 173/24/K1/361 | 24070 | 184 | 2.86 | 1186 | 0.4498 | 0.70953±2 | 0.70895 | 11.29 | 85.58 | 0.07977 | 0.512210±13 | 0.512163 |

¹Concentrations in ppm (µg/g). All blanks negligible. Estimated precision of high level concentrations determined by isotope dilution at MIT: K(0.1%), Rb(0.5%), Cs(2%), Sr(0.05%), Sm(0.01%), Nd(0.01%).

²⁸⁷Sr/⁸⁶Sr ratios normalized to 0.70800 for E & A SrCO₃ [average measured value = 0.70783±3 (2σ, N=5, 1981-83) using ⁸⁶Sr/⁸⁸Sr = 0.1194]. ¹⁴³Nd/¹⁴⁴Nd ratios normalized to 0.51264 for BCR-1 [average measured value = 0.512622±14 (2σ, N=6, spiked, 1982-83) using ¹⁴⁶Nd/¹⁴⁴Nd = 0.7219]. In-run precision given by errors (2σ_{mean}) corresponding to least significant digits. Initial ratios calculated for a kimberlite emplacement age of 90 Ma using λ_{Rb} = 1.42 x 10⁻¹¹a⁻¹ and λ_{Sm} = 6.54 x 10⁻¹²a⁻¹.

³Sample numbers assigned by the Geology Department, De Beers Consolidated Mines Limited, Kimberley.

⁴Mine drill core specimens. Data, presented by Erlank et al. (1982), from University of Cape Town (K, Rb and Sr by XRF), University of the Witwatersrand (⁸⁷Sr/⁸⁶Sr), SUNY at Stony Brook (REE by IDMS) and Open University [¹⁴³Nd/¹⁴⁴Nd normalized to 0.51264 for BCR-1 (from 0.51262)].

⁵Mine excavation specimens. Also known as AJE180, AJE181 and AJE182 respectively.

representative of two classic types of kimberlite (basaltic and micaceous) recognizable on the basis of petrographic (cf Skinner & Clement, 1979), chemical and isotopic characteristics (Barrett & Berg, 1975; Smith, 1983). The distinct Nd and Sr isotopic signatures of Bultfontein and Finsch (Table 2-1) are thus representative of the two groups (I and II) identified by Smith (1983) in conjunction with previously published data (Barrett & Berg, 1975; Basu & Tatsumoto, 1979, 1980; Kramers, 1977; Kramers et al, 1981). The Thaba Putsoa kimberlite carries only traces of diamond (Nixon, 1973b) and so mined specimens are not available. However, all indications are that it is a basaltic (Group I) kimberlite.

While direct determination of accurate kimberlite emplacement ages is generally problematic, a variety of isotopic studies on kimberlite inclusions show broad agreement and existing discrepancies are of little consequence to this thesis. In detail, Davis et al (1976) obtained precise heavy mineral concentrate zircon U-Pb ages close to 90 Ma for Kimberley cluster kimberlites (Bultfontein: 91.2 Ma; De Beers: 92.0 Ma; Wesselton: 90.3 Ma; analytical error: $\pm 1.5\%$). An age of 87 Ma was similarly obtained for Mothae, a northern Lesotho kimberlite close to Thaba Putsoa. A comparable age of 94 Ma was later obtained for a single zircon apparently recovered from Finsch (Davis, 1977). At the same time, a Bultfontein peridotite nodule zircon (very low U concentration) yielded a duplicated age of 83 Ma. Subsequently, equivalent but less precise ages were obtained on the same or similar discrete zircons by fission track dating (Haggerty et al, 1983b).

On a different tack, Allsopp & Barrett (1975) obtained a multiple peridotite nodule phlogopite Rb-Sr age of 84 ± 3 Ma (recalculated for $\lambda_{Rb} = 1.42 \times 10^{-11} \text{ a}^{-1}$) for Kimberley cluster kimberlites. This result has

FIGURE 2-2

Rb-Sr isochron diagram showing an apparent isochron relationship between three hypabyssal facies kimberlite samples from the Finsch kimberlite pipe (Table 2-1). Isochron parameters (with nominal 2σ errors) are calculated using $\lambda_{\text{Rb}} = 1.42 \times 10^{-11} \text{ a}^{-1}$ and a York 1 regression (York, 1966). The resultant age (apparently 25% too high) is not considered as reliable as the errors might suggest. The system appears to be dominated by low and high Rb/Sr ratio end members (cf Figure 2-3), the latter of which (phlogopite) would be particularly susceptible to alkali element (Rb) exchange with circulating groundwater (see text).

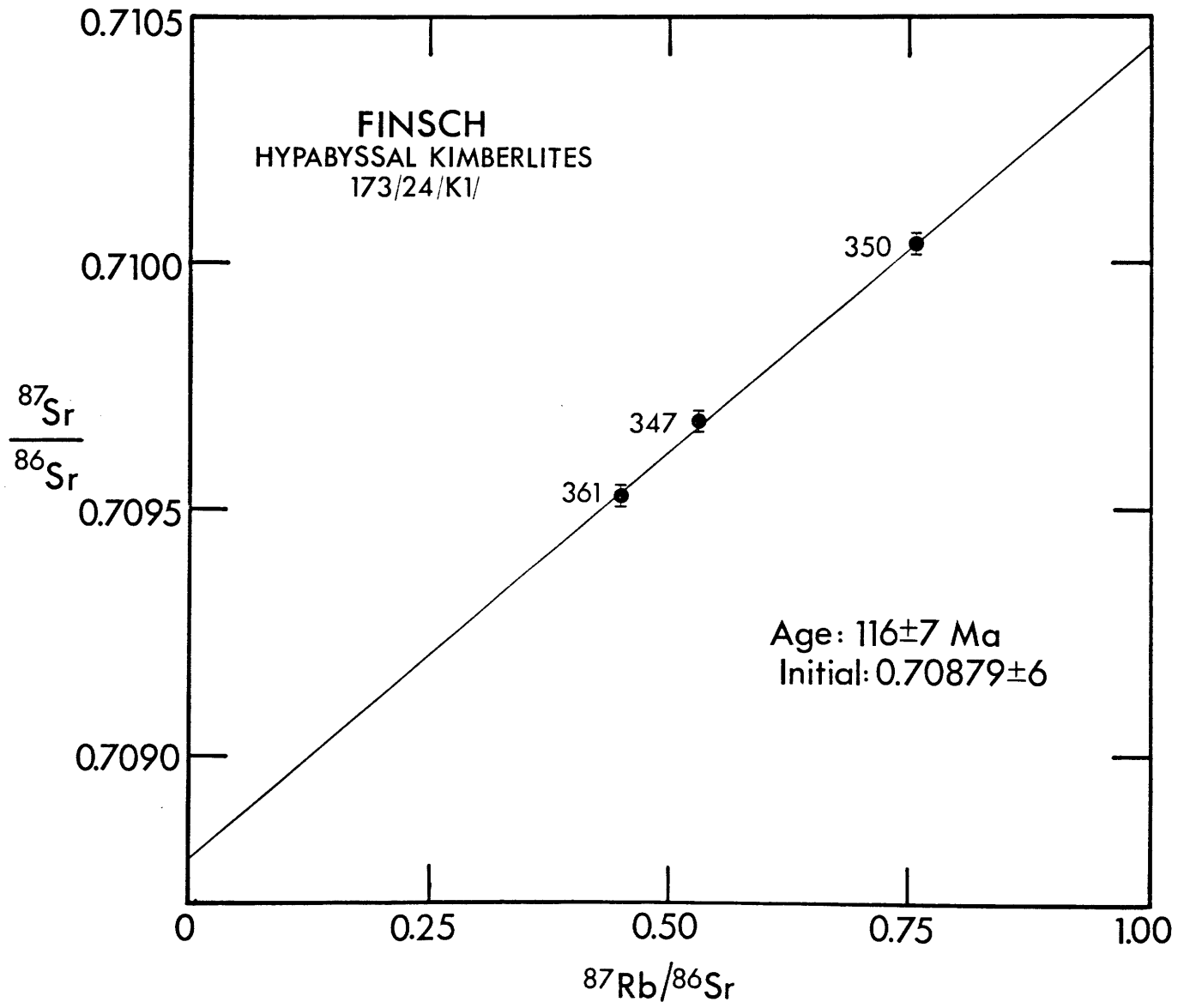
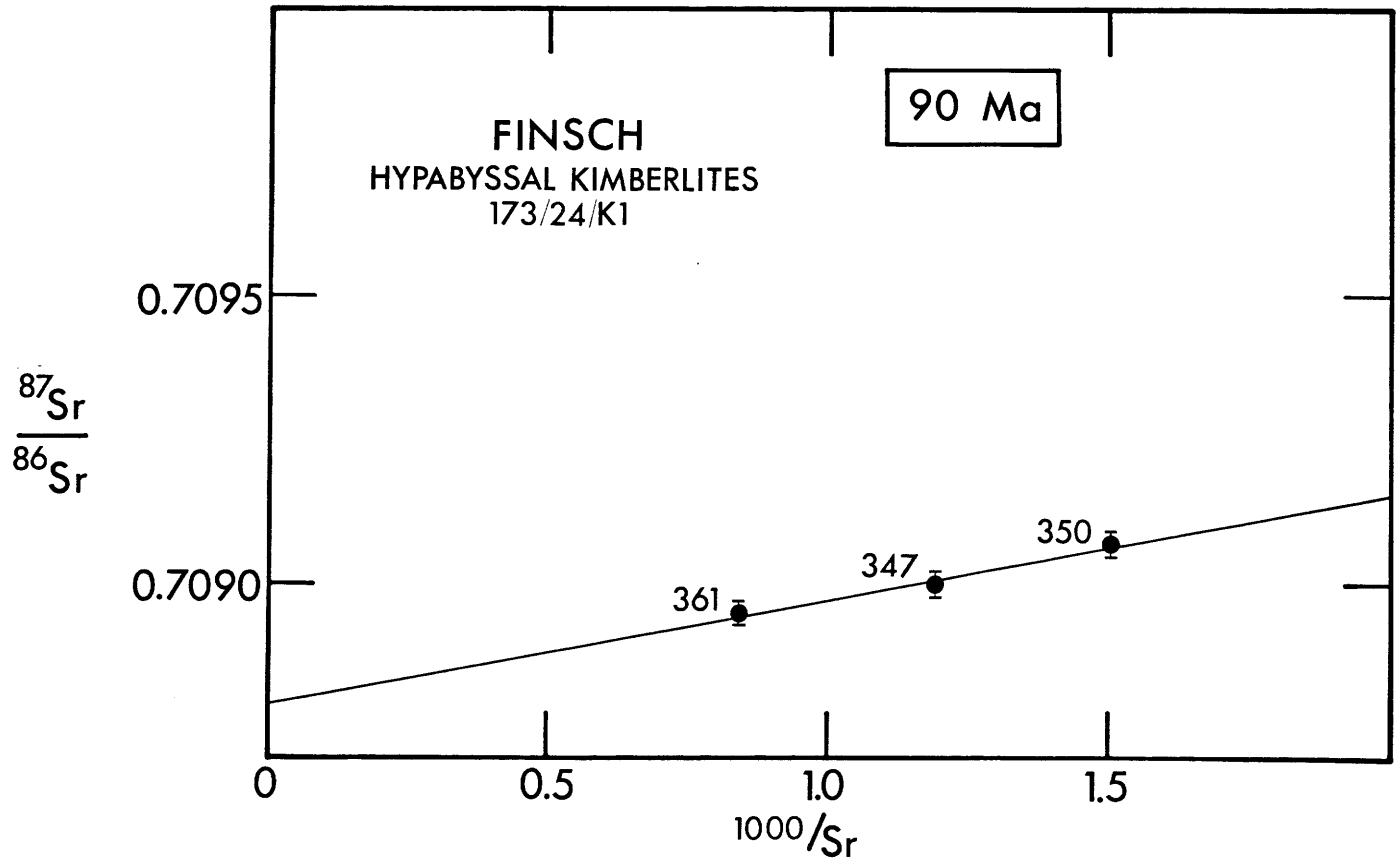


FIGURE 2-3

Variation between $^{87}\text{Sr}/^{86}\text{Sr}$ ratio and reciprocal Sr concentration for three Finsch kimberlite samples with an apparent isochron age of 116 Ma (Figure 2-2). While $^{87}\text{Sr}/^{86}\text{Sr}$ ratios are depicted at 90 Ma, the approximate kimberlite zircon U-Pb age (Davis, 1977), a positive linear relationship is equally apparent at 0 through 116 Ma. Variations in $^{87}\text{Sr}/^{86}\text{Sr}$ and Rb/Sr are thus primarily controlled by variation in Sr concentration rather than Rb concentration (cf Table 2-1) and the system appears to be dominated by two end-members: a high Sr concentration, low Rb/Sr and $^{87}\text{Sr}/^{86}\text{Sr}$ component (carbonate) and a low Sr concentration, high Rb/Sr and $^{87}\text{Sr}/^{86}\text{Sr}$ component (phlogopite).



been duplicated for Bultfontein peridotite phlogopites with apparently greater precision (84 ± 1 Ma) by Kramers et al (1983). Similar Rb-Sr ages have been obtained for K-richterite/diopside-phlogopite pairs in modally metasomatized peridotites from Bultfontein by Erlank et al (1982) and this study (JYG358: diopside-phlogopite = 82 Ma; AJE245: K-richterite-phlogopite = 83 Ma; AJE223: garnet-phlogopite = 81 Ma). Use of a ^{87}Rb decay constant of $1.39 \times 10^{-11} \text{a}^{-1}$ would increase all the above Rb-Sr ages by 2 Ma. It should be noted, however, that these are only approximations since phlogopite Sm-Nd systematics require either initial disequilibrium or partial open system behavior (section 2-7). In addition, more reliable, if less precise, Sm-Nd ages for garnet-diopside pairs in three Bultfontein garnet lherzolites (Figure 2-8) average 91 Ma (AJE25: 89 Ma; AJE164: 86 Ma; BD2435: 98 Ma).

For Finsch, Allsopp & Kramers (1977) reported two groundmass phlogopite Rb-Sr ages of 130 and 170 Ma whereas Smith (1983) refers to a lower phlogopite age of 118 Ma. Furthermore, Kramers & Smith (1983) report a whole rock U-Pb isochron age of 97 ± 42 Ma. A similar age derives from the Rb-Sr data for the three Finsch kimberlite whole rock samples in Table 2-1 as illustrated in a Rb-Sr isochron diagram (Figure 2-2). Least squares regression (York, 1966) yields an age of 116 ± 7 Ma (2σ). However, the resultant age is not considered as reliable as the errors might suggest. The system is dominated by low and high Rb/Sr ratio end members, as is apparent in the variation between $^{87}\text{Sr}/^{86}\text{Sr}$ ratio and reciprocal Sr concentration (Figure 2-3). Variation in Rb/Sr ratio is primarily controlled by variation in Sr concentration rather than Rb concentration (cf Table 2-1) and the two end members appear to be a high Sr concentration, low Rb/Sr and $^{87}\text{Sr}/^{86}\text{Sr}$ component (carbonate) and a low Sr

concentration, high Rb/Sr and $^{87}\text{Sr}/^{86}\text{Sr}$ component (phlogopite). By virtue of being a sheet silicate, phlogopite would be particularly susceptible to cation exchange with circulating groundwater. Appropriately pervasive alteration of phlogopite Rb-Sr systematics to give a 25% too high age can easily be envisaged, though this is obviously speculative. In short, the closed system character of such samples is clearly not established and phlogopite dominated ages should be treated with due caution.

For convenience, a uniform age of 90 Ma is used for all subsequent kimberlite emplacement age corrections. Averaged data from Table 1 are used for comparison with xenolith whole rock and mineral data in this chapter, as well as sub-calcic garnet data in Chapter 3. They are also referred to in a final speculative note on kimberlite isotopic signatures in section 3.8.

2.5 Xenolith Whole Rocks

While peridotite xenolith whole rocks appear to retain some original trace element characteristics (eg Nixon et al, 1981), their isotopic characteristics indicate the presence of extraneous Nd and Sr of kimberlite origin, as suggested by Erlank et al (1982). This is clearly illustrated by isotopic data for whole rocks and constituent minerals in diverse garnet lherzolites nodules from Bultfontein (Tables 2-3 & 2-4). On a Nd-Sr isotope correlation diagram (Figure 2-4), whole rock values generally show displacement from diopside-garnet tielines towards the host kimberlite value. If garnet and diopside are the original major carrier phases of Nd and Sr, kimberlitic Nd and Sr must have been introduced by secondary alteration processes during and/or after emplacement. This comes as no surprise, given the variably pervasive alteration apparent in macro- and microscopic inspection of all kimberlite-derived peridotite

FIGURE 2-4

Nd-Sr isotope correlation diagram showing present day data for diverse garnet lherzolite nodules (described in Table 2-0) and constituent garnet and diopside (original major carrier phases of Nd and Sr) from the Bultfontein kimberlite pipe (Tables 2-3 and 2-4). Intersection of dashed lines marks inferred present day bulk earth value. Whole rock values generally show displacement from garnet-diopside tielines towards the host kimberlite value (Table 2-1) indicating the presence of kimberlite-derived contaminants in nodules. Nodule whole rock data are therefore considered unreliable and do not feature in subsequent treatment.

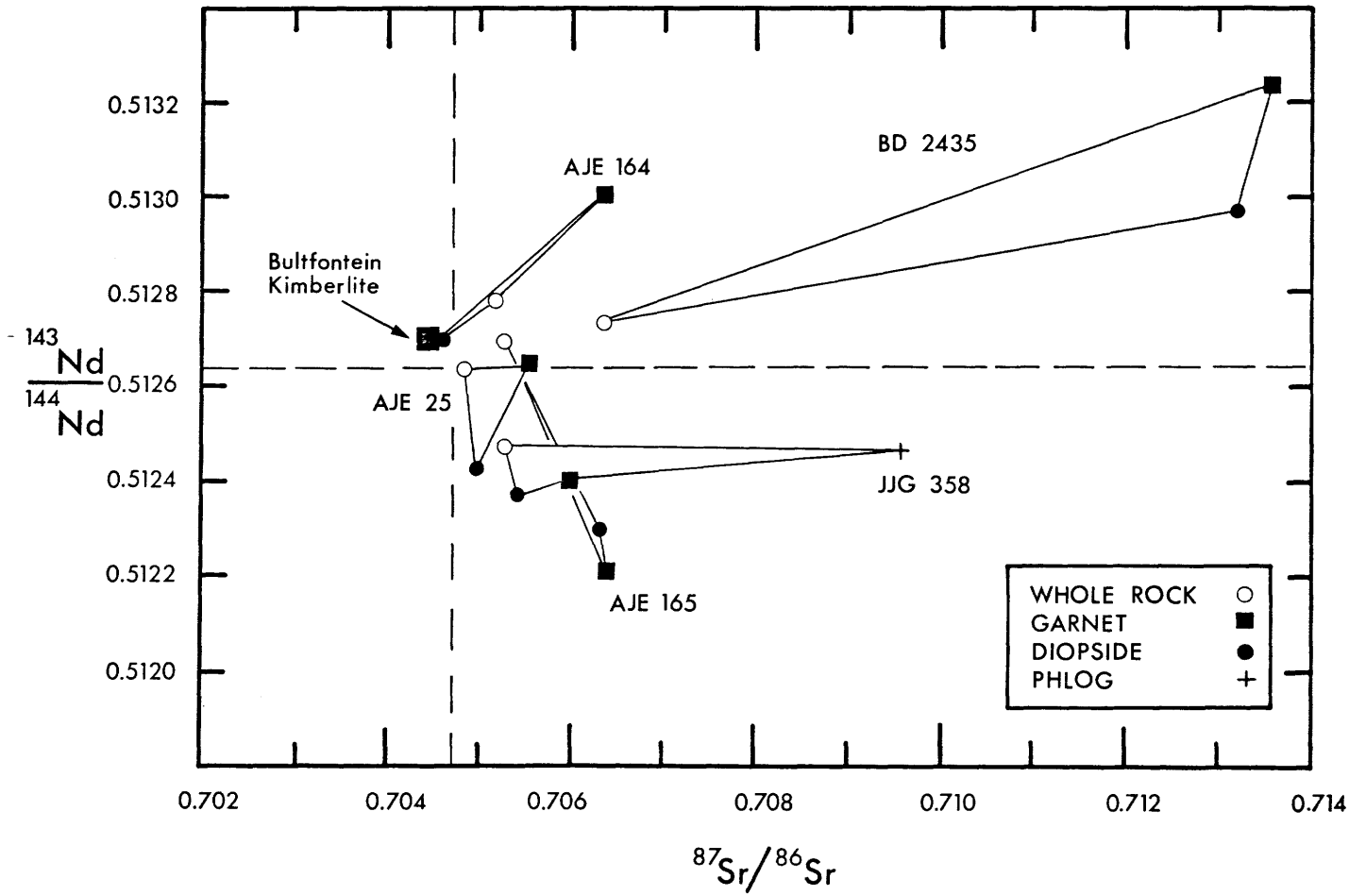


TABLE 2-2 Rb-Sr and Sm-Nd concentrations¹ and isotope ratios² for a garnet lherzolite nodule from the Thaba Putsoa kimberlite pipe, northern Lesotho.

| | weight mg | K | Rb | Sr | ⁸⁷ Rb/ ⁸⁶ Sr | ⁸⁷ Sr/ ⁸⁶ Sr _p | ⁸⁷ Sr/ ⁸⁶ Sr _i | Sm | Nd | ¹⁴⁷ Sm/ ¹⁴⁴ Nd | ¹⁴³ Nd/ ¹⁴⁴ Nd _p | ¹⁴³ Nd/ ¹⁴⁴ Nd _i |
|-----------------------|--------------|------|--------|-------|------------------------------------|-------------------------------------------------|-------------------------------------------------|-------|-------|--------------------------------------|---------------------------------------------------|---------------------------------------------------|
| THA3 | | | | | | | | | | | | |
| garnet ³ | | | 0.0427 | 2.20 | 0.056 | 0.70387±15 | 0.70381 | | | | | |
| garnet ⁴ | 65.50 | 0.31 | 0.0032 | 0.732 | 0.013 | 0.70309±7 | 0.70307 | 1.153 | 1.532 | 0.4547 | 0.513165±13 | 0.512897 |
| garnet ⁵ | 5.70 | | | 0.669 | | 0.70228±20 | | | | | | |
| diopside ³ | | | 0.016 | 83.3 | 0.00056 | 0.70251±6 | 0.70252 | | | | | |
| diopside ⁴ | 20.82 | 212 | 0.019 | 83.13 | 0.00066 | 0.70232±5 | 0.70232 | 1 174 | 4.722 | 0.1503 | 0.513012±13 | 0.512924 |

¹ Concentrations in ppm (µg/g) after correction for minimum applicable blanks: K(2ng), Rb(28pg), Sr (50pg), Sm(1.5pg), Nd(2.3pg). estimated analytical uncertainties in concentrations indicated by number of significant digits.

² ⁸⁷Sr/⁸⁶Sr ratios normalized to 0.70800 for E & A SrCO₃ [average measured value = 0.70783±3 (2σ, N=5, 1981-83) using ⁸⁶Sr/⁸⁸Sr = 0.1194]. ¹⁴³Nd/¹⁴⁴Nd ratios normalized to 0.51264 for BCR-1 [average measured value = 0.512622±14 (2σ, N=6, spiked, 1982-83) using ¹⁴⁶Nd/¹⁴⁴Nd = 0.7219]. In-run precision given by errors (2σ_{mean}) corresponding to least significant digits. Blank effects on isotope ratios insignificant. Initial ratios calculated for a kimberlite emplacement age of 90 Ma using λ_{Rb} = 1.42 x 10⁻¹¹a⁻¹ and λ_{Sm} = 6.54 x 10⁻¹²a⁻¹.

³ Data from Allegre et al (1982) with ⁸⁷Sr/⁸⁶Sr normalized to 0.71022 for NBS SRM987 (from 0.71014) , equivalent to 0.70800 for E & A SrCO₃ (S R Hart, pers comm).

⁴ 1982 analysis. Large pure mineral separate (cf Section 2.3).

⁵ 1983 analysis with refined Sr(15 pg) blank. Small ultrapure mineral separate (cf Section 2.3).

xenoliths. Whole rock isotopic data are therefore considered unreliable and do not feature in subsequent detailed treatment of mineral equilibrium and disequilibrium relationships.

2.6 Thaba Putsoa Peridotites

The interpretive results of a Rb-Sr isotopic study of garnet lherzolite xenoliths from Thaba Putsoa by Allegre et al (1982) are illustrated in Figure 2-5. Apparent isochron ages and initial ratios for diopside-garnet pairs from hot deformed peridotites describe a depleted (low Rb/Sr) mantle evolution curve analogous to that required for mid-ocean ridge basalts (MORB). These ages effectively hinge on the Rb-Sr systematics of garnet as shown for actual mineral data from Allegre et al (1982) in Figure 2-6. The nodule (THA3) showing the greatest apparent Rb-Sr age (1.8 Ga) was singled out for reinvestigation. This nodule is in better than average physical condition given an essentially coarse texture (incipient deformation is observable in thin section). Nevertheless its mineral chemistry (P Tilke, pers comm, 1983) indicates that it belongs to the hot deformed peridotite suite (cf section 2.2.2).

Combined Sm-Nd and Rb-Sr isotopic systematics of constituent garnet and diopside were determined to test the reliability of the above old age. The Sm-Nd data (Table 2-2) were found to immediately preclude such an age. These data are illustrated in Figure 2-8 where a two point isochron age of 77 ± 13 Ma is indicated. This is within errors of the assumed kimberlite emplacement age of 90 Ma (cf section 2.4).

Refining the Rb-Sr data (Table 2-2) proved to be more of a challenge, because of residual alteration-related contamination effects apparent in garnet Sr concentrations and $^{87}\text{Sr}/^{86}\text{Sr}$ ratios. Comparison of data for a large (65 mg) and nominally pure mineral separate of garnet with that from

FIGURE 2-5

$^{87}\text{Sr}/^{86}\text{Sr}$ evolution diagram showing the depleted (low Rb/Sr) mantle evolution curve apparently described by Rb-Sr isochron ages and initial $^{87}\text{Sr}/^{86}\text{Sr}$ ratios (Figure 2-6) for garnet-diopside pairs in garnet lherzolites from the Cretaceous Thaba Putsoa kimberlite pipe and one from the Precambrian Premier pipe (from Allegre et al, 1982). A Sm-Nd and refined Rb-Sr study of the Thaba Putsoa nodule (THA3) showing the greatest apparent age, reveals that this age is spurious and that constituent phases were actually in isotopic equilibrium at the time of kimberlite emplacement (~ 90 Ma). This revisionary result likely applies to the other nodules with Rb-Sr ages significantly greater than that of the kimberlite. However, diopside $^{87}\text{Sr}/^{86}\text{Sr}$ ratios remain a useful indicator of nodule $^{87}\text{Sr}/^{86}\text{Sr}$ ratios immediately prior to kimberlite emplacement.

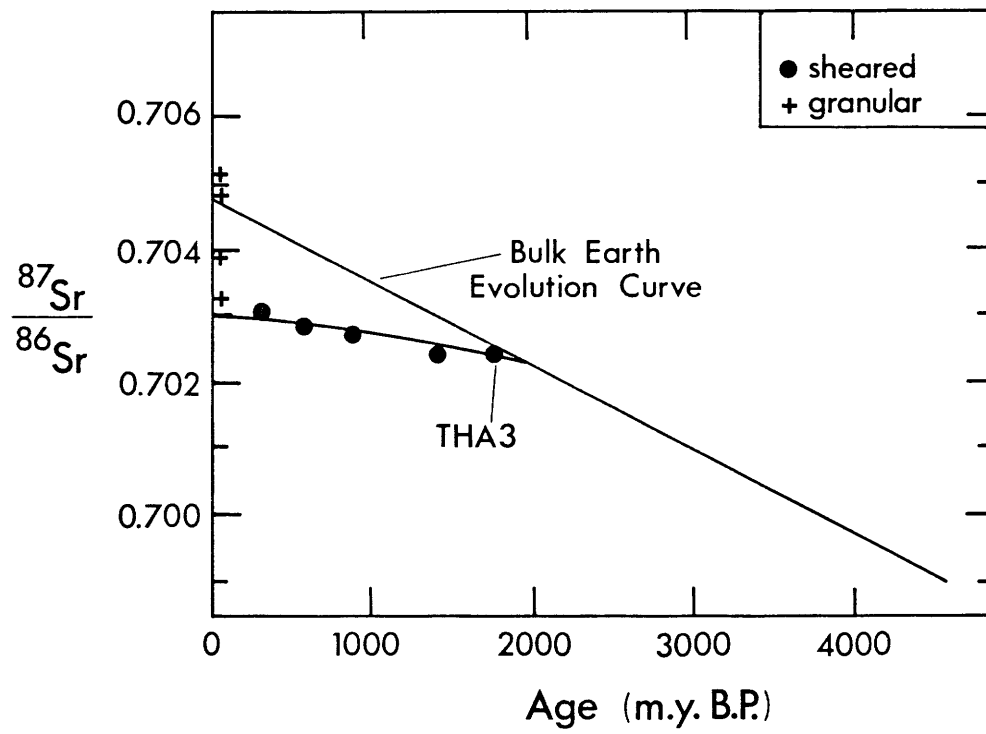


FIGURE 2-6

Rb-Sr isochron diagram for garnet-diopside pairs in garnet lherzolites from the Thaba Putsoa and Bultfontein kimberlite pipes. Data are from Allegre et al (1982) and present study with nodules THA3 (Thaba Putsoa) and AJE 25 (Bultfontein) common to both data sets (cf Tables 2-2 and 2-4). Measurement errors are smaller than the size of plotted points except where otherwise indicated. In present study, garnets show dramatically lower Rb/Sr ratios as well as lower $^{87}\text{Sr}/^{86}\text{Sr}$ ratios, indicating severe alteration-related problems for nodule garnet Rb-Sr systematics. Data for garnet from two Bultfontein garnet harzburgites are also presented. Garnet $^{87}\text{Sr}/^{86}\text{Sr}$ ratios in present study are still suspect, except where extra special effort has been expended in specimen preparation and analysis (see text). Diopside $^{87}\text{Sr}/^{86}\text{Sr}$ ratios are more reliable and span the range 0.7023 to 0.7132. Note that this encompasses the entire range of values for modern (<200 Ma) mantle-derived oceanic and continental volcanics.

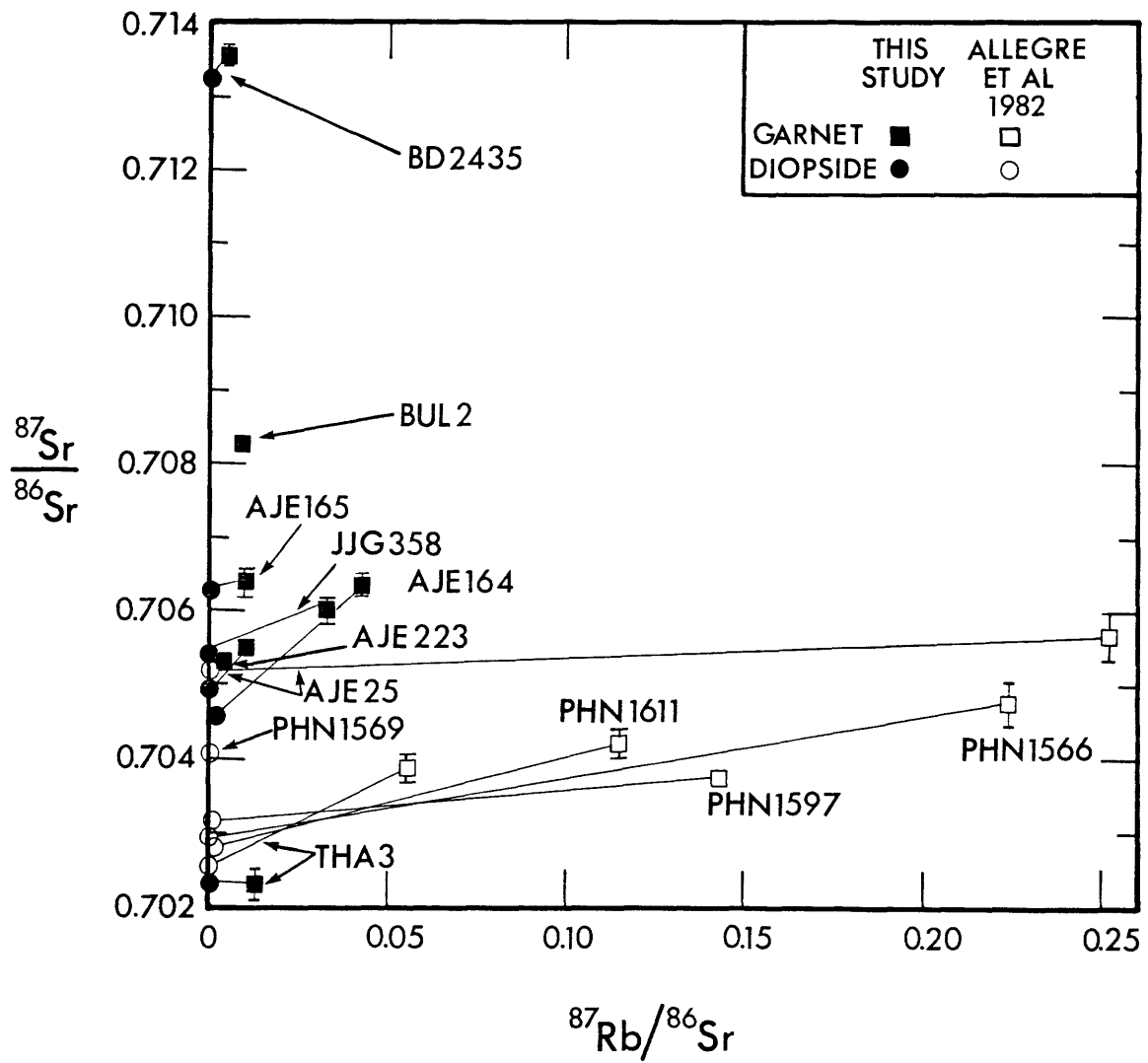
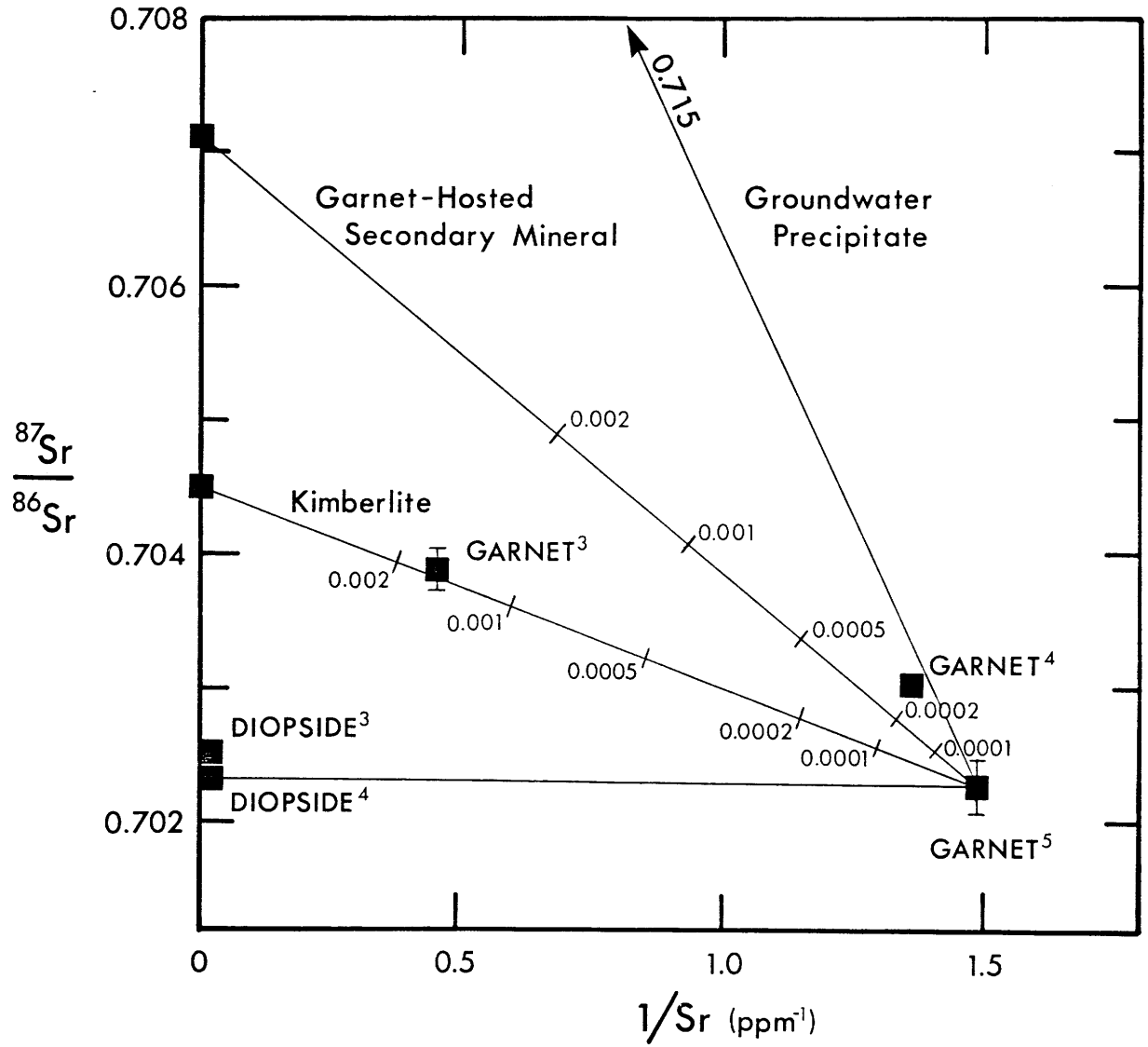


FIGURE 2-7

Correlation between measured $^{87}\text{Sr}/^{86}\text{Sr}$ ratio and reciprocal Sr concentration for various separates of garnet and diopside in garnet lherzolite THA3 from the Thaba Putsoa kimberlite pipe. Label superscripts refer to identifying footnotes in Table 2-2. Measurement errors are smaller than the size of plotted points except where otherwise indicated. Corrections for radiogenic growth of ^{87}Sr from intrinsic ^{87}Rb since Kimberlite emplacement (~ 90 m.y.) are effectively insignificant (less than measurement errors). In the absence of measured values for secondary sources of Sr in the Thaba Putsoa pipe, values for equivalent species at Bultfontein are used for reference: kimberlite (Table 2-1); garnet-hosted secondary mineral in garnet harzburgite AJE223 (Table 2-5); mine groundwater (Barrett & Berg, 1975). Reference mixing lines radiating from purest garnet (0.669 ppm Sr) are graduated in fractional proportions of kimberlite (1000 ppm Sr) and garnet-hosted secondary mineral (400 ppm Sr). The Sr concentration of hypothetical groundwater precipitate is unknown, but assumed to be within an order of magnitude of that of the garnet-hosted secondary mineral, since latter is probably groundwater related. Nodule garnet $^{87}\text{Sr}/^{86}\text{Sr}$ ratios significantly higher than those of coexisting diopside can reasonably be ascribed to such secondary mineral contamination in analysed separates (see text).



Allegre et al (1982) indicates an order of magnitude drop in Rb concentration. A factor of 3 drop in Sr concentration from 2.2 ppm to 0.73 ppm and a drop in $^{87}\text{Sr}/^{86}\text{Sr}$ ratio from 0.70387 to 0.70309 is also apparent. The reduced concentrations were initially attributed to more efficient exclusion of kelyphite (high Rb) substrate surfaced grains from garnet separates. Intrinsic garnet Rb/Sr ratios are evidently much lower than indicated by data from Allegre et al (1982) in Figure 2-6. As for diopside, 90 Ma age corrections for radiogenic growth of ^{87}Sr in garnet since kimberlite emplacement are actually negligible. A significant contribution to discrepancies in Sr concentration and $^{87}\text{Sr}/^{86}\text{Sr}$ ratio was subsequently attributed to the effects of a clear colorless secondary mineral (low temperature zeolite/carbonate) specifically occurring as concoidal fracture linings in garnet in this and other peridotite xenoliths investigated. Because this secondary phase was generally difficult to detect and its significance overlooked, it was originally not rigorously sought out and avoided (see section 2.3). However, analysis of a crude separate of this material from garnet in a diopside-free harzburgite (AJE223) from Bultfontein (Table 2-5) revealed a Sr concentration of 400 ppm and $^{87}\text{Sr}/^{86}\text{Sr}$ ratio of 0.707 (but insignificant alkali and REE concentrations). At this point, a second small (6 mg) ultrapure mineral separate of garnet from THA3 was prepared with more stringent exclusion of grain fragments which may have been in contact with this secondary phase. This separate (with a total Sr content of less than 4 ng) yielded a marginally lower Sr concentration of 0.67 ppm and a lower $^{87}\text{Sr}/^{86}\text{Sr}$ ratio of 0.70228 ± 20 . These iniquitous relationships between measured garnet $^{87}\text{Sr}/^{86}\text{Sr}$ ratio and Sr concentration are illustrated in Figure 2-7. The difference between the two garnet separates analyzed in

this study can be accounted for by the presence of 0.01-0.02% of the secondary component in the first separate.

The $^{87}\text{Sr}/^{86}\text{Sr}$ ratio of the second garnet separate is within errors of the measured diopside $^{87}\text{Sr}/^{86}\text{Sr}$ ratio of 0.70232 ± 5 . Sr isotopic equilibrium between garnet and diopside at the time of kimberlite emplacement has thus been demonstrated, but not without a caveat. The Rb-Sr system is clearly unreliable for peridotite nodule garnets because of the above-mentioned alteration-related contamination problems. However, it should be emphasized that discrete heavy mineral concentrate garnets and garnet inclusions in diamonds (Chapter 3) are not similarly indisposed, since interiors of such garnet grains are exceptionally fresh and uncracked. In addition, the Sm-Nd system provides reasonably reliable data and a real indication of equilibrium and disequilibrium relationships for all types of garnet and diopside.

While the first order reliability of diopside $^{87}\text{Sr}/^{86}\text{Sr}$ ratios is not in doubt, in detail there do appear to be problems. For instance, the value for THA3 diopside measured in this study (0.70232 ± 5) is significantly lower than that reported in Allegre et al (1982) after appropriate normalization of the latter for interlaboratory bias (0.70251 ± 6). In turn, a value of 0.70272 ± 4 for diopside from the legendary deformed garnet lherzolite PHN1611 measured by Allegre et al (1982), is substantially lower than the value of 0.70352 ± 14 previously obtained by Shimizu (1975a). This further illustrates problems attributable to sample quality. Considerable caution should thus be exercised in using even the spread of deformed peridotite diopside $^{87}\text{Sr}/^{86}\text{Sr}$ ratios in Allegre et al (1982) to further the cause of chemical geodynamics (Allegre, 1982).

On the basis of Sm-Nd and refined Rb-Sr systematics, the hot deformed garnet lherzolites from northern Lesotho clearly retain no age information beyond that of kimberlite emplacement. They were thus in internal isotopic equilibrium on at least a mineral scale at the time of sampling by kimberlite. The initial $^{143}\text{Nd}/^{144}\text{Nd}$ (0.5129) and $^{87}\text{Sr}/^{86}\text{Sr}$ (0.7023) ratios for THA3 at 90 Ma (Figure 2-12) indicate a depleted mantle source analogous to that of MORB. Chondrite-normalized whole rock rare earth patterns for hot deformed garnet lherzolites, reconstructed from mineral data (Shimizu, 1975b; Basaltic Volcanism Study Project, 1981) are flat or LREE depleted and thus also analogous to those of MORB type sources. In short, trace element and isotopic systematics of these relatively more fertile peridotites do not require an origin involving diffusive introduction of a basaltic component from megacryst magmas (Gurney & Harte, 1980; Harte, 1983), but cannot be used to argue against it if such signatures are dominated by the added component. However, the apparent restriction of this peridotite suite to kimberlites near the margins of and off the Archean craton (cf Harte, 1983) suggests that they may well represent samples of MORB type sources abutting the shallowing cratonic root.

2.7 Bultfontein Peridotites

The major mineralogy of cold coarse and deformed peridotites from Bultfontein (Kimberley cluster) featured in this study, is given in Table 2-0. Based on the presence or absence of diopside, five are lherzolites and three are harzburgites. All are garnet-bearing except for one veined harzburgite. In addition, all carry at least a trace of primary (texturally equilibrated) phlogopite. While such phlogopite is reasonably abundant in some coarse garnet peridotites such as JJG358 (~ 5%), in

others such as AJE25 and AJE165 which are superficially phlogopite-free, isolated grains are generally only revealed by processing appropriately large volumes of rock (50-100 cm³ or more). At the other extreme, the garnet-free harzburgite, AJE245, carries a clearcut vein dominated by K-richterite, phlogopite and opaque phases. Thus, strictly speaking, all these rocks are modally metazomatized, though for the majority of the common coarse peridotites this is not immediately apparent. In addition, both lherzolites and harzburgites are variably depleted in major elements such as Ca, Al and Fe, consistent with prior removal of a basaltic component.

2.7.1 Deformed Garnet Lherzolites

Porphyroclastic garnet lherzolite nodules AJE164 and BD2435 display the textures of the hot deformed peridotites from various craton margin kimberlite pipes, but the mineral chemistry of their cold coarse counterparts from Kimberley cluster and other craton interior pipes (cf section 2.2.2 and Harte, 1983). Diopside in BD2435 was previously analyzed for K, Rb, Sr and ⁸⁷Sr/⁸⁶Sr by Kramers (1977). In that study, BD2435 yielded the highest ⁸⁷Sr/⁸⁶Sr ratio for a suite of diopsides from coarse and deformed peridotites, and was thus singled out for further investigation.

Rb-Sr and Sm-Nd data for garnet and diopside in AJE164 and BD2435 appear in Table 2-3. On a Sm-Nd isochron diagram (Figure 2-8) these two nodules yield two point isochron ages of 86±8 Ma and 98±11 Ma respectively, which are within errors (derived from maximum and minimum slopes allowed by in-run precision ($2\sigma_{\text{mean}}$)) of the approximate kimberlite emplacement age of 90 Ma (cf section 2.4). These rocks were clearly in internal Nd isotopic equilibrium at the time of sampling by kimberlite, as

TABLE 2-3 Rb-Sr and Sm-Nd concentrations¹ and isotope ratios² for porphyroclastic garnet lherzolite nodules from the Bultfontein kimberlite pipe, Kimberley cluster.

| | weight mg | K | Rb | Sr | ⁸⁷ Rb/ ⁸⁶ Sr | ⁸⁷ Sr/ ⁸⁶ Sr _p | ⁸⁷ Sr/ ⁸⁶ Sr _i | Sm | Nd | ¹⁴⁷ Sm/ ¹⁴⁴ Nd | ¹⁴³ Nd/ ¹⁴⁴ Nd _p | ¹⁴³ Nd/ ¹⁴⁴ Nd |
|-----------------------|--------------|------|--------|-------|------------------------------------|-------------------------------------------------|-------------------------------------------------|--------|-------|--------------------------------------|---------------------------------------------------|--------------------------------------|
| AJE164 | | | | | | | | | | | | |
| wr | 300 | 812 | 3.89 | 43.91 | 0.256 | 0.70517±4 | 0.70484 | 0.5542 | 2.455 | 0.1365 | 0.512783±14 | 0.512703 |
| garnet ³ | 84.97 | 10.7 | 0.0090 | 0.611 | 0.043 | 0.70636±14 | 0.70631 | 2.697 | 2.296 | 0.7101 | 0.513008±13 | 0.512590 |
| diopside | 18.93 | 144 | 0.161 | 285.1 | 0.00165 | 0.70456±3 | 0.70456 | 4.285 | 16.17 | 0.1602 | 0.512699±14 | 0.512605 |
| BD2435 | | | | | | | | | | | | |
| wr ⁴ | | | | | | 0.70636±4 | | | | | 0.51274±3 | |
| garnet ⁵ | 73.41 | | | 0.670 | | | | 3.669 | 3.951 | 0.5615 | 0.513237±15 | 0.512906 |
| garnet ⁶ | 6.87 | | 0.001 | 0.568 | 0.005 | 0.71356±12 | 0.71355 | | | | | |
| diopside ⁷ | | 153 | 0.22 | 317 | 0.0020 | 0.7134±2 | | | | | | |
| diopside | 14.29 | 144 | 0.0073 | 314.6 | 0.00007 | 0.71322±4 | 0.71322 | 3.031 | 12.27 | 0.1493 | 0.512971±15 | 0.512883 |

¹Concentrations in ppm (µg/g) after correction for minimum applicable blanks: K(2ng), Rb(28pg), Sr(50pg), Sm(1.5pg), Nd(2.3pg). Estimated analytical uncertainties in concentrations indicated by number of significant digits.

²⁸⁷Sr/⁸⁶Sr ratios normalized to 0.70800 for E & A SrCO₃ [average measured value = 0.70783±3 (2σ, N=5, 1981-83) using ⁸⁶Sr/⁸⁸Sr = 0.1194]. ¹⁴³Nd/¹⁴⁴Nd ratios normalized to 0.51264 for BCR-1 [average measured value = 0.512622±24 (2σ, N=15, unspiked & spiked, 1981-83) using ¹⁴⁶Nd/¹⁴⁴Nd = 0.7219]. In-run precision given by errors (2σ_{mean}) corresponding to least significant digits. Blank effects on isotope ratios insignificant. Initial ratios calculated for a kimberlite emplacement age of 90 Ma using λ_{Rb} = 1.42×10⁻¹¹a⁻¹ and λ_{Sm} = 6.54×10⁻¹²a⁻¹.

³1981 analysis. Large pure mineral separate (cf Section 2.3).

⁴Data, presented by Erlank et al (1982), from Open University with ¹⁴³Nd/¹⁴⁴Nd normalized to 0.51264 for BCR-1 (from 0.51262).

⁵1982 analysis. Large pure mineral separate (cf Section 2.3). Failed ⁸⁷Sr/⁸⁶Sr analysis.

⁶1983 analysis with refined Rb(20pg) and Sr(15pg) blanks. Single ultrapure nodule grain (cf Section 2.3).

⁷Data from Kramers (1977).

illustrated in Figure 2-9.

Such equilibrium no doubt existed for Sr but this has so far only been imperfectly demonstrated. Kimberlite emplacement age corrections are negligible and remaining discrepancies (Figure 2-6) reflect aberrant garnet $^{87}\text{Sr}/^{86}\text{Sr}$ ratios, attributable to a nodule-garnet-specific secondary phase with high Sr concentration and high $^{87}\text{Sr}/^{86}\text{Sr}$ ratio (cf sections 2.3 & 2.6). This is particularly the case for AJE164, with $^{87}\text{Sr}/^{86}\text{Sr}$ ratios of 0.70636 ± 14 for garnet and 0.70456 ± 3 for diopside. For BD2435, the discrepancy between garnet $^{87}\text{Sr}/^{86}\text{Sr}$ ratio (0.71356 ± 12 using $<4\text{ng}$ Sr from a single ultrapure 6 mg grain) and diopside $^{87}\text{Sr}/^{86}\text{Sr}$ ratio (0.71322 ± 4) is much smaller (3 x garnet in-run precision) and may be analytical. The diopside $^{87}\text{Sr}/^{86}\text{Sr}$ ratio is also within errors of the previous value (0.7134 ± 2) obtained by Kramers (1977). By analogy with arguments in section 2.6, calculation of garnet-diopside Rb-Sr ages (eg AJE164: 3.0 Ga; BD2435: 4.7 Ga) is meaningless. Clearly, diopsides with 2 to 3 orders of magnitude higher Sr concentrations than garnet, yield the more reliable $^{87}\text{Sr}/^{86}\text{Sr}$ ratios.

Combined Sr and Nd isotopic data are illustrated in a Nd-Sr isotope correlation diagram (Figure 2-12). Allowing for an aberrant garnet $^{87}\text{Sr}/^{86}\text{Sr}$ ratio, nodule AJE164 lies within the oceanic mantle array in the presumably fortuitous vicinity of host kimberlite and bulk earth values. In contrast, nodule BD2435 is representative of a rather novel domain with high $^{143}\text{Nd}/^{144}\text{Nd}$ similar to that of depleted (low Sm/Nd) MORB sources but anomalously high $^{87}\text{Sr}/^{86}\text{Sr}$ indicative of an enriched (high Rb/Sr) component. Neither diopside nor garnet contain sufficient Rb to account for such radiogenic Sr and there is no obviously modally abundant mineral repository of radiogenic Sr (eg phlogopite) with which they may

FIGURE 2-8

Sm-Nd isochron diagram showing present day data for garnet and diopside in garnet lherzolites, and garnet in garnet harzburgites, from the Bultfontein kimberlite pipe. Also shown are values for primary phlogopite in a garnet lherzolite (JJG358), a garnet harzburgite (AJE223) and a veined harzburgite (AJE245), together with a value for potassic richterite from the large vein in the latter. Data for nodule B33 (open symbols) are from Basu & Tatsumoto (1980). Also included is the garnet lherzolite from Thaba Putsoa (THA3) featured in Figures 2-5 through 2-7. Measurement errors are smaller than the size of plotted points except where otherwise indicated. The average present day chondritic value (CHUR) used as a bulk earth reference is from Jacobsen & Wasserburg (1980). Two point ages were calculated for diopside-garnet tielines with significant positive slopes, using $\lambda_{Sm} = 6.54 \times 10^{-12} \text{a}^{-1}$. Assigned errors derive from maximum and minimum slopes allowed by $2\sigma_{\text{mean}}$ measurement errors (Tables 2-2 through 2-4). The average of three Bultfontein nodule ages is 91 Ma. Tielines with close to zero or negative slope indicate inter-mineral disequilibrium prior to kimberlite emplacement, suggesting metasomatic component addition (see Figure 2-9 and text). Note that inferred whole rock $^{143}\text{Nd}/^{144}\text{Nd}$ ratios encompass virtually the entire range of values for modern (<200 Ma) mantle-derived oceanic and continental volcanics.

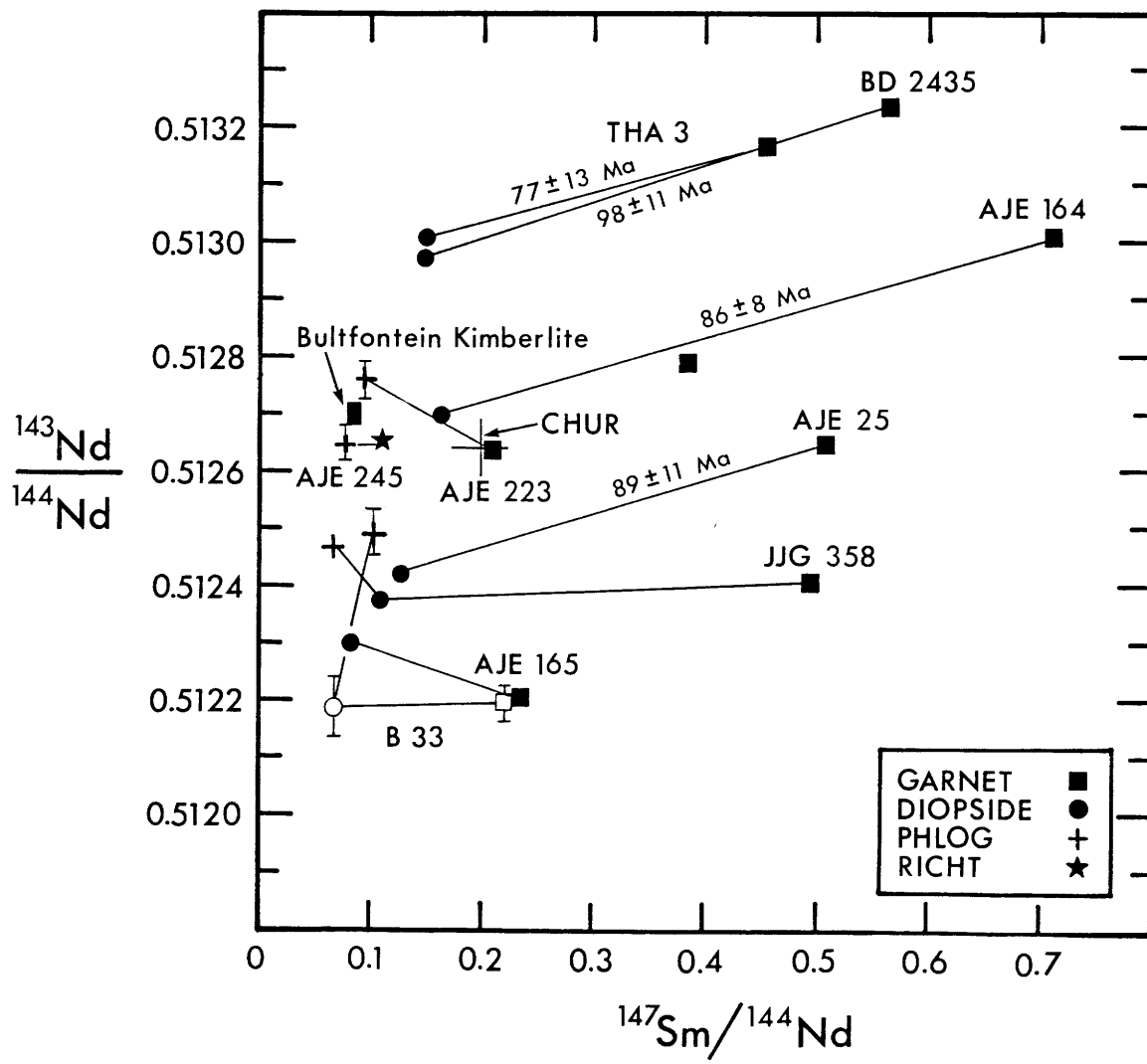


FIGURE 2-9

Sm-Nd isochron diagram with $^{143}\text{Nd}/^{144}\text{Nd}$ ratios corrected to 90 Ma, the age of Bultfontein kimberlite emplacement. Equilibrium and disequilibrium relationships between coexisting nodule minerals featured in Figure 2-8 are better illustrated. Nodules AJE25, AJE164, BD2435 and THA3 (Thaba Putsoa) were in Nd isotopic equilibrium in the mantle immediately prior to sampling by kimberlite. However, negative slopes of diopside-garnet tielines for nodules JJG358, AJE165 (and B33) indicate inter-mineral disequilibrium, which cannot be ascribed to in-situ aging. A similar relation also applies to all phlogopite-garnet tielines, although data for phlogopite is less convincing because of the possibility of inter-layer incorporation of a secondary kimberlite-derived component. Metasomatic addition of diopside and phlogopite is suggested (see text).

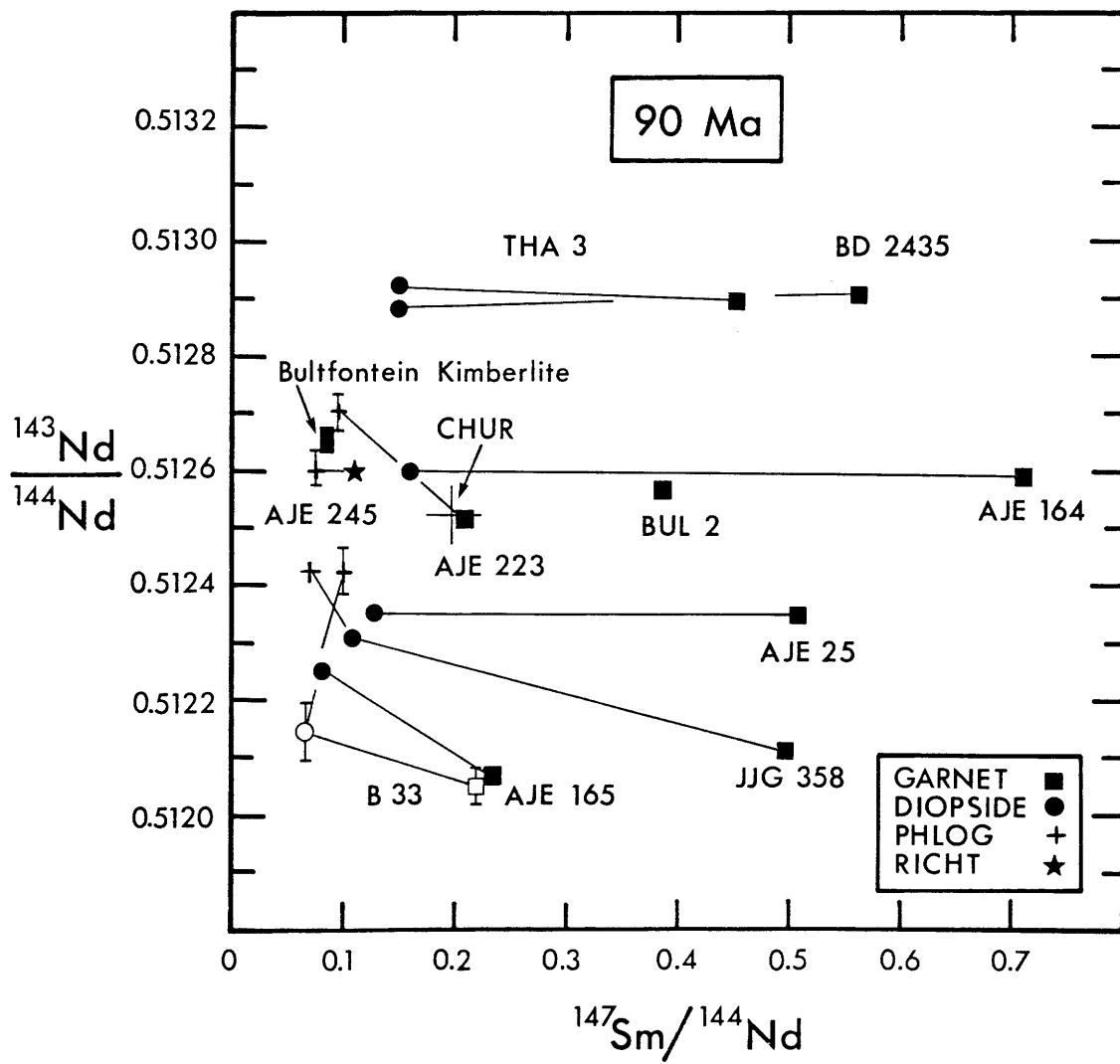


TABLE 2-4 Rb-Sr and Sm-Nd concentrations¹ and isotope ratios² for coarse garnet lherzolite nodules from the Bultfontein kimberlite pipe, Kimberley cluster.

| | weight mg | K | Rb | Sr | ⁸⁷ Rb/ ⁸⁶ Sr | ⁸⁷ Sr/ ⁸⁶ Sr _p | ⁸⁷ Sr/ ⁸⁶ Sr _i | Sm | Nd | ¹⁴⁷ Sm/ ¹⁴⁴ Nd | ¹⁴³ Nd/ ¹⁴⁴ Nd _p | ¹⁴³ Nd/ ¹⁴⁴ Nd _i |
|-----------------------|--------------|------|--------|-------|------------------------------------|-------------------------------------------------|-------------------------------------------------|--------|-------|--------------------------------------|---------------------------------------------------|---------------------------------------------------|
| AJE25 | | | | | | | | | | | | |
| wr ³ | | | 1.2 | 37 | 0.0938 | 0.70485±4 | 0.70473 | 0.394 | 2.37 | 0.1005 | 0.512638±25 | 0.512579 |
| garnet ⁴ | | | 0.105 | 1.21 | 0.252 | 0.7057±2 | 0.7054 | | | | | |
| garnet ⁵ | 45.90 | 0.28 | 0.0021 | 0.738 | 0.0082 | 0.70554±9 | 0.70553 | 2.095 | 2.488 | 0.5090 | 0.512648±15 | 0.512348 |
| diopside ⁴ | | | 0.032 | 209 | 0.00044 | 0.70520±10 | 0.70521 | | | | | |
| diopside | 16.52 | 308 | 0.034 | 205.2 | 0.00048 | 0.70498±3 | 0.70498 | 2.001 | 9.433 | 0.1282 | 0.512426±13 | 0.512351 |
| AJE165 | | | | | | | | | | | | |
| wr | 300 | 192 | 0.818 | 18.53 | 0.0441 | 0.70529±3 | 0.70523 | 0.3578 | 2.157 | 0.1003 | 0.512692±13 | 0.512633 |
| garnet ⁶ | 91.30 | | | 0.619 | | 0.7069±10 | | 1.429 | 3.694 | 0.2338 | 0.512209±15 | 0.512071 |
| garnet ⁷ | 14.30 | 0.53 | 0.002 | 0.567 | 0.010 | 0.70640±11 | 0.70639 | | | | | |
| diopside | 14.95 | 138 | 0.021 | 362.6 | 0.00017 | 0.70631±2 | 0.70631 | 2.182 | 16.00 | 0.0825 | 0.512303±14 | 0.512254 |
| JJG358 | | | | | | | | | | | | |
| wr | 200 | 1158 | 4.42 | 105.0 | 0.1218 | 0.70529±2 | 0.70513 | 1.344 | 9.129 | 0.0890 | 0.512476±14 | 0.512424 |
| garnet ⁵ | 41.30 | 9.9 | 0.026 | 2.32 | 0.033 | 0.70599±16 | 0.70595 | 2.731 | 3.331 | 0.4956 | 0.512407±13 | 0.512115 |
| diopside | 14.90 | 17.6 | 0.069 | 697.1 | 0.00029 | 0.70543±3 | 0.70543 | 7.639 | 42.57 | 0.1085 | 0.512377±13 | 0.512313 |
| phlogopite | 76.32 | | 208 | 172.1 | 3.501 | 0.70952±3 | 0.70504 | 0.1781 | 1.530 | 0.0704 | 0.512465±14 | 0.512424 |

¹ Concentrations in ppm (µg/g) after correction for minimum applicable blanks: K(2ng), Rb(28pg), Sr(50pg), Sm(1.5pg), Nd(2.3pg). Estimated analytical uncertainties in concentrations indicated by number of significant digits.

² ⁸⁷Sr/⁸⁶Sr ratios normalized to 0.70800 for E & A SrCO₃ [average measured value = 0.70783±3 (2σ, N=5, 1981-83) using ⁸⁶Sr/⁸⁸Sr = 0.1194]. ¹⁴³Nd/¹⁴⁴Nd ratios normalized to 0.51264 for BCR-1 [average measured value = 0.512622±24 (2σ, N=15, unspiked & spiked, 1981-83) using ¹⁴⁶Nd/¹⁴⁴Nd = 0.7219]. In-run precision given by errors (2σ_{mean}) corresponding to least significant digits. Blank effects on isotope ratios insignificant. Initial ratios calculated for a kimberlite emplacement age of 90 Ma using λ_{Rb} = 1.42x10⁻¹¹ a⁻¹ and λ_{Sm} = 6.54x10⁻¹² a⁻¹.

³ Data, presented by Erlank et al. (1982), from University of Cape Town (Rb and Sr by XRF), University of Oxford (⁸⁷Sr/⁸⁶Sr), SUNY at Stony Brook (REE by IDMS) and Open University [¹⁴³Nd/¹⁴⁴Nd normalized to 0.51264 for BCR-1 (from 0.51262)].

⁴ Data from Allegre et al (1982) with ⁸⁷Sr/⁸⁶Sr normalized to 0.71022 for NBS SRM 981 (from 0.71014), equivalent to 0.70800 for E & A SrCO₃ (S R Hart, pers comm).

⁵ 1982 analysis. Large pure mineral separate (cf Section 2.3).

⁶ 1981 analysis. Large pure mineral separate (cf Section 2.3). Dissolved without pulverization.

⁷ 1983 analysis with refined Rb(20pg) and Sr(15pg) blanks. Single ultrapure nodule grain (cf Section 2.3).

have equilibrated. The history of such a rock remains enigmatic. However, its isotopic character underscores the expanse of Nd-Sr isotopic space accessible in the sub-continental lithosphere.

2.7.2 Coarse Garnet Lherzolites

Coarse garnet lherzolite nodules AJE25, AJE165, and JJG358 respectively contain increasingly extensive mineralogical, textural and chemical evidence for mantle metasomatic enrichment. At one end of the spectrum, AJE25 shows little evidence of modal metasomatism, while at the other, JJG358 displays abundant phlogopite and subtle replacement textures with phlogopite and diopside displacing garnet and leaving accessory chromite.

Rb-Sr and Sm-Nd data for garnet and diopside, as well as phlogopite from JJG358, appear in Table 2-4. On a Sm-Nd isochron diagram (Figure 2-8), AJE25 yields a garnet-diopside isochron age of 89 ± 11 Ma, which is nominally very close to the kimberlite emplacement age of 90 Ma. This rock was evidently in internal Nd isotopic equilibrium at the time of sampling by kimberlite (Figure 2-9). In contrast, garnet and diopside in JJG358 appear to be in Nd isotopic equilibrium at the present time (which is fortuitous since they have been closed systems for 90 Ma) while in AJE165 they exhibit inverse isotopic disequilibrium (Figure 2-8). Thus, when corrected back to 90 Ma (Figure 2-9), $^{147}\text{Sm}/^{144}\text{Nd}$ and $^{143}\text{Nd}/^{144}\text{Nd}$ ratios of garnet and diopside in AJE165 and garnet, diopside and phlogopite in JJG358 are inversely correlated, precluding conventional Sm-Nd isochron age relationships. This requires exotic metasomatic component addition without reequilibration. The modal expression of this component is diopside in AJE165 and diopside + phlogopite in JJG358. Both diopside and phlogopite have low Sm/Nd ratios similar to that of host

FIGURE 2-10

Variation of Sr concentration with distance across two grains of diopside in coarse garnet lherzolite JJG358. In-situ ion microprobe traverses are crudely edge-to-edge. High diopside Sr concentration measurements were found to be reproducible to within 1% (sequential duplicate analyses on same 5-10 μ m diameter point), so that precision is better than the size of plotted points. Overall accuracy is considered to be better than 5%, as qualitatively confirmed by simple comparison of the unweighted average SIMS value (727 ppm) with the IDMS value for a 15 mg grain composite (697 ppm, Table 2-4; horizontal dashed line). Observed range of 495 to 875 ppm shows no obvious relationship with distance from grain boundaries or proximity to garnet. Metasomatic introduction of diopside is suggested (see also Figure 2-11 and text).

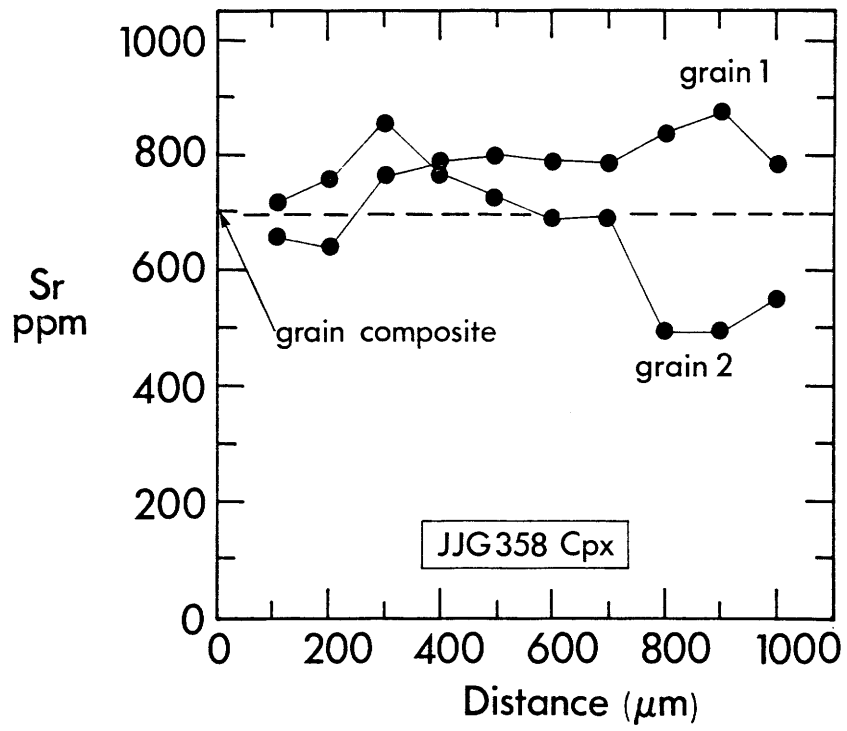
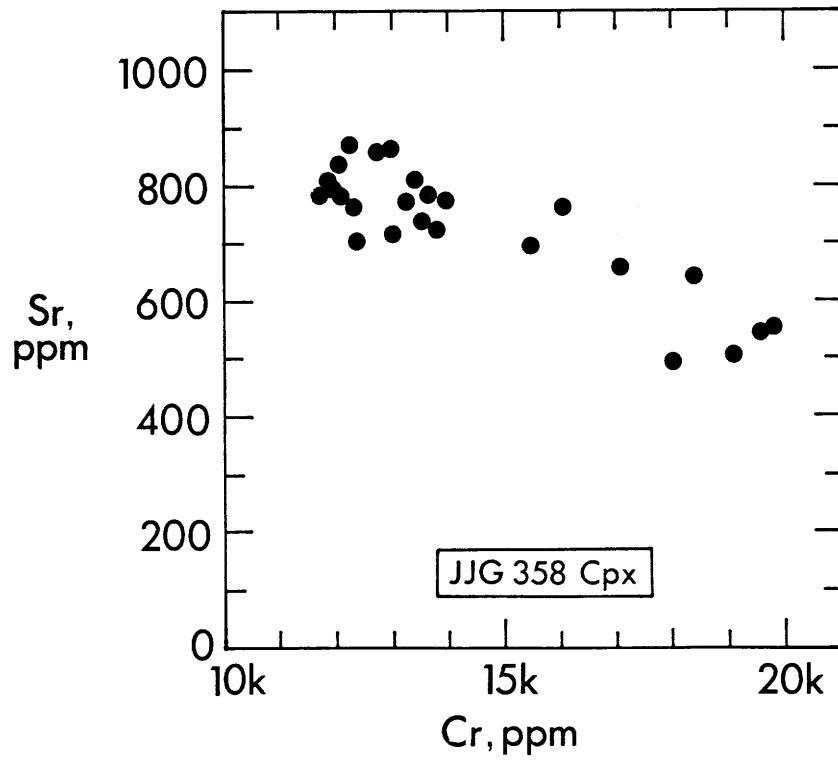


FIGURE 2-11

Covariation of point Sr and Cr concentrations within two diopside grains in coarse garnet lherzolite JJG358. Precision of these ion microprobe measurements is better than 1% for both elements and reasonably represented by the size of plotted points. The inverse correlation, taken together with subtle petrographic replacement textures and inter-mineral isotopic disequilibrium, suggest metasomatic replacement of garnet (2.7% Cr, ≤ 2 ppm Sr) by diopside (1-2% Cr, 500-900 ppm Sr), with excess Cr accommodated in modal chromite.



kimberlite and $^{143}\text{Nd}/^{144}\text{Nd}$ ratios intermediate between nodule garnet and host kimberlite (Figure 2-9). Unfortunately, the closed system character of phlogopite cannot be independently established, and the difference between phlogopite and diopside $^{143}\text{Nd}/^{144}\text{Nd}$ ratios may equally well be attributed to the presence of either some precursor diopside in an otherwise garnet harzburgite substrate or some secondary kimberlitic Nd (and Sr) in phlogopite.

Sr isotopic data are broadly consistent with the above relationships but suffer from various limitations which preclude complementarily detailed interpretation. Firstly, while diopsides with Sr concentrations of 200 ppm (AJE25) to 700 ppm (JJG358) give reasonably reliable $^{87}\text{Sr}/^{86}\text{Sr}$ ratios, garnets, with 2 to 3 orders of magnitude lower Sr concentrations, tend to give mildly aberrant (high) $^{87}\text{Sr}/^{86}\text{Sr}$ ratios attributable to residual alteration effects (cf sections 2.3 & 2.6). Specifically, even after reducing the AJE25 garnet Sr concentration by a factor of 2 and Rb/Sr ratio by a factor of 30 compared to those reported by Allegre et al (1982), the measured $^{87}\text{Sr}/^{86}\text{Sr}$ ratio of 0.70554 ± 9 for a large nominally pure garnet separate was still significantly higher than that of 0.70498 ± 3 for coexisting diopside (Figure 2-6). The resulting absurd 4.9 Ga Rb-Sr isochron age belies demonstrable Nd isotopic equilibrium at 90 Ma. The relative merits of measured AJE165 and JJG358 garnet $^{87}\text{Sr}/^{86}\text{Sr}$ ratios cannot be similarly assessed because of inverse Nd isotopic disequilibrium at 90 Ma. Secondly, phlogopite Rb/Sr ratios are sufficiently high that initial $^{87}\text{Sr}/^{86}\text{Sr}$ ratio calculation is very sensitive to kimberlite emplacement age, in addition to considerations of open/closed system character. In point of fact, JJG358 gives an apparent phlogopite-diopside Rb-Sr isochron age of 82 Ma, so that correction to 90

Ma necessarily produces an inverse correlation between $^{87}\text{Rb}/^{86}\text{Sr}$ and $^{87}\text{Sr}/^{86}\text{Sr}$ which carries the same alternative implications as for Nd.

Chemical disequilibrium relationships in JJG358 were further investigated by testing for compositional homogeneity of constituent diopside. Selected trace element concentration profiles were determined using ion microprobe techniques summarized in Shimizu & Allegre (1978) and Shimizu (1981). The variation of Sr concentration across two grains of diopside is shown in Figure 2-10. The dramatic range of 495 to 875 ppm compares with an average of 697 ppm (Table 2-4) with no obvious relation to grain boundaries or proximity to garnet. Nevertheless, diopside Sr concentration is inversely correlated with Cr concentration (Figure 2-11) with a similar relative magnitude of variation for both elements (50% of the median). Partial metasomatic replacement of garnet (2.7% Cr; < 2 ppm Sr) by diopside (2-1% Cr; 500-900 ppm Sr) and phlogopite has apparently occurred, with excess Cr accommodated in chromite.

Combined Sr and Nd isotopic data are illustrated in a Nd-Sr isotope correlation diagram (Figure 2-12). All three coarse garnet lherzolites lie within an extension of the oceanic mantle array as previously found for a suite of diopsides from diverse coarse peridotites (Menzies & Murthy, 1980) including one retrospectively identified as K-richterite bearing (Erlank et al, 1982).

Coarse garnet lherzolites provide some of the most convincing chemical evidence for ancient and modern enrichment in the sub-continental lithosphere. Ancient enrichment is particularly apparent in garnet $^{143}\text{Nd}/^{144}\text{Nd}$ ratios which are significantly lower than bulk earth and which require low time-integrated Sm/Nd ratios for periods in excess of 1 Ga, the opposite of those conventionally expected for the residua of basaltic

FIGURE 2-12

Nd-Sr isotope correlation diagram constructed at 90 Ma, the age of Bultfontein kimberlite emplacement. Data for constituent minerals in diverse garnet lherzolites and harzburgites from Bultfontein (Kimberley cluster) and one garnet lherzolite from Thaba Putsoa (northern Lesotho) are shown. Analytical precision is reasonably represented by the size of plotted points. Garnet and diopside $^{143}\text{Nd}/^{144}\text{Nd}$ ratios and diopside $^{87}\text{Sr}/^{86}\text{Sr}$ ratios are reliable. However, some measured garnet $^{87}\text{Sr}/^{86}\text{Sr}$ ratios are too high (eg. AJE164, AJE25) because of alteration-related Sr contamination (see text). Phlogopite $^{87}\text{Sr}/^{86}\text{Sr}$ ratios are very sensitive to age correction and only that with the smallest such correction is plotted. Phlogopites may also contain secondary kimberlitic Nd and Sr. The metasomatic K-richterite is from a veined harzburgite. Garnet and diopside in garnet lherzolites THA3, BD2435, AJE164 and AJE25 were in isotopic equilibrium prior to sampling by kimberlite, whereas inter-mineral disequilibrium existed in JYG358 and AJE165, indicating relatively recent metasomatic component addition. The oceanic mantle array (cf DePaolo & Wasserburg, 1979; Allegre et al, 1979) and a bulk earth evolution curve, based on average chondritic Nd isotopic evolution (Jacobsen & Wasserburg, 1980), are shown for reference. Also shown are published data for diopsides (open circles) in a suite of peridotites from Bultfontein (Menzies & Murthy, 1980). Nodule mineral data generally conform to an extension of the mantle array, but are not confined to it, as is clearly the case for otherwise unexceptional garnet lherzolite BD2435. Garnet lherzolite THA3 from Thaba Putsoa (craton margin) has characteristics of a depleted (low time-integrated Rb/Sr and Nd/Sm) MORB-type source which diverged from the bulk earth evolution curve at least 2 Ga ago. Conversely, peridotites from Bultfontein (craton interior) at lower right represent complexly enriched (high time-integrated Rb/Sr and Nd/Sm) subcontinental mantle which diverged from the bulk earth curve at least 1 Ga ago.

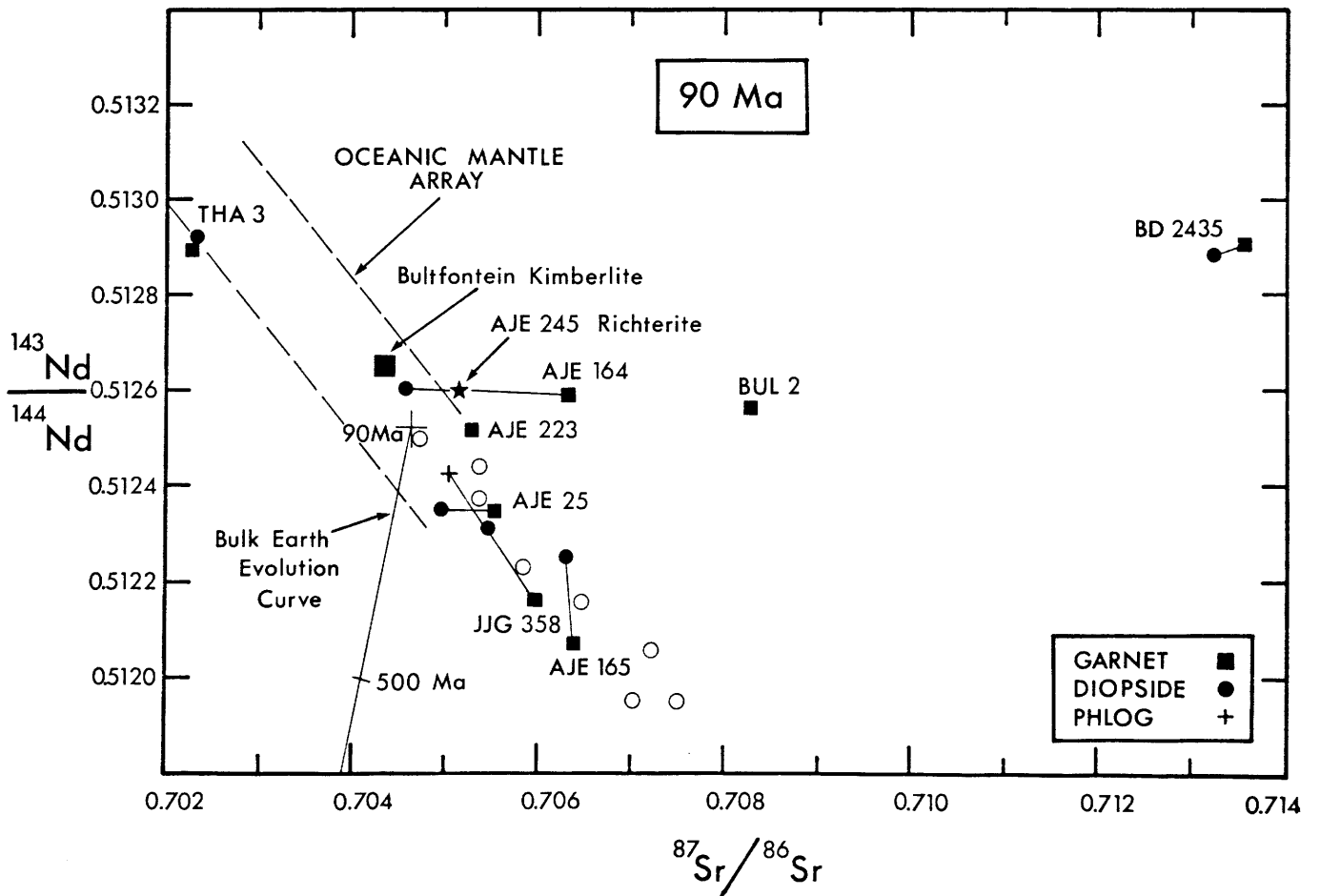


TABLE 2-5 Rb-Sr and Sm-Nd concentrations¹ and isotope ratios² for harzburgites from the Bultfontein kimberlite pipe, Kimberley cluster.

| | weight mg | K | Rb | Sr | ⁸⁷ Rb/ ⁸⁶ Sr | ⁸⁷ Sr/ ⁸⁶ Sr _p | ⁸⁷ Sr/ ⁸⁶ Sr _f | Sm | Nd | ¹⁴⁷ Sm/ ¹⁴⁴ Nd | ¹⁴³ Nd/ ¹⁴⁴ Nd _p | ¹⁴³ Nd/ ¹⁴⁴ Nd _f |
|-------------------------|--------------|-------|--------|-------|------------------------------------|-------------------------------------------------|-------------------------------------------------|---------|--------|--------------------------------------|---------------------------------------------------|---------------------------------------------------|
| AJE223 | | | | | | | | | | | | |
| wr | 100 | 129 | 1.10 | 18.26 | 0.1745 | 0.70524±3 | 0.70502 | 0.3632 | 1.890 | 0.1161 | 0.512706±14 | 0.512638 |
| garnet | 52.48 | 0.095 | 0.0013 | 1.086 | 0.0035 | 0.70530±5 | 0.70530 | 2.026 | 5.950 | 0.2058 | 0.512634±15 | 0.512513 |
| ga sec ³ | 3.02 | 26 | 0.14 | 314 | 0.0013 | 0.70711±5 | 0.70711 | 0.618 | 1.52 | 0.246 | | |
| phlogopite | 44.52 | 88150 | 315 | 32.46 | 28.15 | 0.73776±4 | (0.70176) | 0.09300 | 0.5923 | 0.09492 | 0.512761±32 | 0.512705 |
| BUL2 | | | | | | | | | | | | |
| garnet ⁴ | 33.39 | 0.40 | 0.0031 | 1.14 | 0.0079 | 0.70828±7 | 0.70827 | 1.496 | 2.354 | 0.3842 | 0.512792±13 | 0.512566 |
| AJE245 | | | | | | | | | | | | |
| wr ⁵ | 100 | 708 | 3.09 | 30.64 | 0.2916 | 0.70592±3 | 0.70555 | 0.4658 | 3.245 | 0.08677 | 0.512690±24 | 0.512639 |
| richterite ⁶ | 99.61 | 39300 | 56.5 | 445.4 | 0.3671 | 0.70562±2 | 0.70515 | 0.7574 | 4.158 | 0.1101 | 0.512659±14 | 0.512594 |
| phlogopite ⁷ | 24.17 | 79430 | 557 | 49.71 | 32.54 | 0.74346±2 | (0.70185) | 0.08838 | 0.6789 | 0.07870 | 0.512651±32 | 0.512605 |

¹Concentrations in ppm (µg/g) after correction for minimum applicable blanks: K(2ng), Rb(28pg), Sr(100pg), Sm(1.5pg), Nd(2.3pg). Estimated analytical uncertainties indicated by number of significant digits. Ba concentrations: AJE223 phlogopite, 1640 ppm; AJE245 phlogopite, 867 ppm.

²⁸⁷Sr/⁸⁶Sr ratios normalized to 0.70800 for E & A SrCO₃ [average measured value = 0.70783±3 (2σ, N=5, 1981-83) using ⁸⁶Sr/⁸⁸Sr = 0.1194]. ¹⁴³Nd/¹⁴⁴Nd ratios normalized to 0.51264 for BCR-1 [average measured value = 0.512622±14 (2σ, N=6, spiked, 1982-83) using ¹⁴⁶Nd/¹⁴⁴Nd = 0.7219]. In-run precision given by errors (2σ_{mean}) corresponding to least significant digits. Blank effects on isotope ratios insignificant. Initial ratios calculated for a kimberlite emplacement age of 90 Ma using λ_{Rb}=1.42×10⁻¹¹a⁻¹ and λ_{Sm}=6.54×10⁻¹²a⁻¹.

³Clear colorless secondary mineral (zeolite/carbonate) occurring as microfracture linings in garnet. Host garnet fragments accounted for approximately one quarter of the crude separate with corresponding dilution of the Sr concentration. Sm and Nd contents are entirely accounted for by garnet.

⁴Separate prepared by refining 50mg concentrate obtained from N Shimizu.

⁵Harzburgite substrate.

⁶Potassic richterite from vein.

⁷Phlogopite from harzburgite substrate (phlogopite in vein too altered for analysis).

melt extraction. Additional more recent trace element enrichment is manifest in variably equilibrated modal metasomatic minerals including diopside (high Sr and LREE concentrations) and phlogopite (high alkali and Ba concentrations).

2.7.3 Coarse Harzburgites

Coarse garnet harzburgites were studied in an effort to detect unenriched material. If they were residual after ancient basaltic melt extraction and unenriched, then constituent garnet should have high Sm/Nd ratios and consequent kimberlite emplacement age $^{143}\text{Nd}/^{144}\text{Nd}$ ratios significantly higher than the bulk earth value. However, at least the latter of the two harzburgites investigated, BUL2 and AJE223 was found to contain minor dispersed primary phlogopite. Finally, AJE245, a garnet free harzburgite with similarly dispersed phlogopite and a clearcut vein containing K-richterite, phlogopite and opaques, was used to characterize the relative isotopic signatures of substrate and vein metasomatic phases, as more extensively investigated by Kramers et al (1983).

Sm-Nd and Rb-Sr data for garnet from BUL2 and AJE223, dispersed phlogopite from AJE223 and AJE245, and vein K-richterite from AJE245 appear in Table 2-5. Contrary to early expectations, garnet initial $^{143}\text{Nd}/^{144}\text{Nd}$ ratios are neither significantly higher nor significantly lower than a bulk earth value (Figure 2-9). They apparently resemble neither entirely unenriched residua nor inferred garnet harzburgite precursors of coarse garnet lherzolites discussed in the previous subsection (2.7.2). As in coarse garnet lherzolite JGG358, phlogopite and garnet in AJE223 display inverse Nd isotopic disequilibrium (Figures 2-8 & 2-9). In contrast, AJE245 substrate phlogopite and vein K-richterite have essentially identical $^{143}\text{Nd}/^{144}\text{Nd}$ ratios along with similar Sm/Nd ratios.

As for phlogopite in AJE223, their Sm-Nd systematics resemble those of host kimberlite, suggesting kimberlitic affinities for the metasomatizing agents.

The reliability of garnet $^{87}\text{Sr}/^{86}\text{Sr}$ ratios is indeterminate, but the potential effects of a secondary phase with high Sr concentrations and high $^{87}\text{Sr}/^{86}\text{Sr}$ ratio (but negligible alkali and REE concentrations), separated from AJE223 garnet microfracture surfaces, should be noted (cf sections 2.3 & 2.6). AJE223 yields a phlogopite-garnet Rb-Sr isochron age of 81 Ma while AJE245 gives a similar phlogopite-K-richterite age of 83 Ma. Calculated phlogopite initial $^{87}\text{Sr}/^{86}\text{Sr}$ ratios for a slightly older emplacement age of 90 Ma are almost certainly too low (0.7018) suggesting partial open system behavior. In contrast, the initial $^{87}\text{Sr}/^{86}\text{Sr}$ ratio for K-richterite (0.70515) with a Sr concentration of 445 ppm and 2 orders of magnitude lower Rb/Sr ratio, is considered to be reasonably reliable. This is significantly higher than the corresponding host kimberlite $^{87}\text{Sr}/^{86}\text{Sr}$ ratio of approximately 0.7043 (Table 2-1) but still consistent with a general kimberlitic affinity for the metasomatizing agent (cf Kramers et al, 1983).

As for garnet and diopside in garnet lherzolites, these modal metasomatic minerals clearly do not retain any internal age information beyond that of kimberlite emplacement. However, their pre-emplacement origin is confirmed by examples of phlogopite K-richterite peridotites with deformation textures affecting both minerals (Erlank et al, 1982). In addition, phlogopite K-richterite peridotite whole rock Rb-Sr relationships allow an apparent maximum age of 150 Ma for the metasomatism (Erlank & Shimizu, 1977; Erlank et al, 1982). Recent enrichment is thus chemically manifest in modal metasomatic minerals including diopside,

phlogopite, K-richterite and various minor opaque phases such as lindsleyite, mathiasite and armalcolite (Haggerty et al, 1983a; Jones et al, 1982). Moreover, K-richterite and associated opaque phases generally only appear in garnet-free (Al poor) assemblages (Erlank & Rickard, 1977) and their stability relations suggest shallower depths of origin (75-100 km on a shield geotherm) than for most garnet-bearing peridotites (Haggerty et al, 1983a).

2.8 Finsch Peridotites

Because of intense alteration in the upper parts of the Finsch kimberlite pipe, sufficiently large and unaltered peridotite xenoliths were not available for study until the recent discovery of suitable specimens in a minor kimberlite phase exposed in the mine open pit (Shee et al, 1982). Two coarse garnet lherzolites were found to contain numerous small diamonds and subjected to detailed petrographic and mineral chemical analysis by Shee et al (1982). Geothermobarometry confirmed derivation within the diamond stability field at slightly greater depths (> 160 km on a shield geotherm) than most coarse garnet lherzolites from kimberlite. In addition, Ca and Cr contents of garnet (coexisting with diopside) from these two nodules lie on the lherzolite trend and these garnets are thus not sub-calcic (cf Shee et al, 1982 and Chapter 3 for significance of sub-calcic garnet and diamond association). Thus, these occurrences do not appear to represent a primary source of the majority of diamonds from Finsch. In any event, a reconnaissance study of the isotopic compositions of garnet and diopside in one of these xenoliths, XM46, was undertaken with a view to documenting any potentially extreme isotopic signatures. It should be emphasized that the overall physical condition of the xenolith is not conducive to recovery of high quality mineral separates.

TABLE 2-6 Rb-Sr and Sm-Nd concentrations¹ and isotope ratios² for a diamond-bearing garnet lherzolite nodule³ from the Finsch kimberlite pipe, northern Cape Province.

| | weight mg | K | Rb | Sr | ⁸⁷ Rb/ ⁸⁶ Sr | ⁸⁷ Sr/ ⁸⁶ Sr _p | ⁸⁷ Sr/ ⁸⁶ Sr _i | Sm | Nd | ¹⁴⁷ Sm/ ¹⁴⁴ Nd | ¹⁴³ Nd/ ¹⁴⁴ Nd _p | ¹⁴³ Nd/ ¹⁴⁴ Nd _i |
|----------|--------------|------|--------|-------|------------------------------------|-------------------------------------------------|-------------------------------------------------|--------|-------|--------------------------------------|---------------------------------------------------|---------------------------------------------------|
| XM46 | | | | | | | | | | | | |
| garnet | 68.46 | 0.19 | 0.0027 | 0.326 | 0.024 | 0.70528±16 | 0.70525 | 0.4031 | 1.230 | 0.1982 | 0.512617±14 | 0.512500 |
| diopside | 8.13 | 759 | 0.081 | 96.71 | 0.0024 | 0.70490±3 | 0.70490 | 0.2507 | 2.488 | 0.0609 | 0.512398±34 | 0.512362 |

¹Concentrations in ppm (µg/g) after correction for minimum applicable blanks: K(2ng), Rb(28pg), Sr(100pg), Sm(1.5pg), Nd(2.3pg). Estimated analytical uncertainties in concentrations indicated by number of significant digits.

²⁸⁷Sr/⁸⁶Sr ratios normalized to 0.70800 for E & A SrCO₃ [average measured value = 0.70783±3 (2σ, N=5, 1981-83) using ⁸⁶Sr/⁸⁸Sr = 0.1194]. ¹⁴³Nd/¹⁴⁴Nd ratios normalized to 0.51264 for BCR-1 [average measured value = 0.512622±14 (2σ, N=6, spiked, 1982-83) using ¹⁴⁶Nd/¹⁴⁴Nd = 0.7219]. In-run precision given by errors (2σ_{mean}) corresponding to last significant digits. Blank effects on isotope ratios insignificant. Initial ratios calculated for a kimberlite emplacement age of 90 Ma using λ_{Rb}=1.42x10⁻¹¹a⁻¹ and λ_{Sm}=6.54x10⁻¹²a⁻¹. Differential effects of a slightly older age for Finsch (Smith, 1983) are negligible.

³One of two nodules, XM46 and XM48, the petrography, petrology and diamond content of which are described in detail by Shee et al (1982). Nodule is highly altered and constituent diopside is in poor physical condition.

Diopside is particularly poorly preserved and detailed interpretation of original inter-mineral isotopic equilibrium/disequilibrium relationships is perhaps not merited.

Sm-Nd and Rb-Sr data for garnet and diopside in XM46 appear in Table 2-6. Garnet has initial $^{143}\text{Nd}/^{144}\text{Nd}$ (0.51250) and $^{87}\text{Sr}/^{86}\text{Sr}$ (0.70525) ratios similar, for example, to those for garnet in harzburgite AJE223 from Bultfontein (cf Figure 2-12). Diopside has apparent values for these ratios of 0.51236 and 0.70490 respectively, similar, for example, to those for diopside in lherzolite AJE25 from Bultfontein (cf Figure 2-12). Simple-minded treatment of these differences as closure age-related, gives inconsistent Sm-Nd and Rb-Sr isochron ages of 240 Ma and 1100 Ma respectively. Metasomatic introduction of diopside, as suggested for constituent diamonds (Shee et al, 1982), is plausible but available isotopic data do not permit exclusive arguments. Nevertheless, XM46 garnet and diopside do not have obviously extreme (enriched) Nd and Sr isotopic signatures such as those for sub-calcic garnets associated with the majority of diamonds from Finsch and Kimberley (cf Chapter 3).

2.9 Conclusions

Constituent minerals of hot deformed garnet lherzolites from northern Lesotho were in Nd and Sr isotopic equilibrium at the time of sampling by kimberlite (90 Ma). Previous evidence of ancient internal Rb-Sr ages from such peridotites (Allegre et al, 1982) is predicated on analysis of garnet with incomplete exclusion of secondary alteration-related contamination. The common cold coarse and deformed garnet lherzolites from the Kimberley area variously display inter-mineral isotopic equilibrium or inverse isotopic disequilibrium requiring pre-emplacement metasomatic component addition. The modal expression of this component is diopside \pm phlogopite

in garnet-bearing peridotites and diopside \pm phlogopite \pm K-richterite \pm opaques in garnet-free peridotites.

None of the peridotite xenoliths appears to retain internal age information beyond the time of kimberlite emplacement. However, emplacement age Nd and Sr isotopic signatures indicate time-integrated chemical histories. Hot deformed garnet peridotites (with more fertile major element compositions) from the craton margins have trace element and isotopic signatures resembling depleted (high Sm/Nd, low Rb/Sr) MORB type sources such as those conventionally associated with the convecting asthenosphere. In contrast, cold coarse and deformed peridotites (with residual major element compositions) from the craton interior bear isotopic signatures indicative of enriched (low Sm/Nd, high Rb/Sr) sources stabilized in the sub-continental lithosphere for at least 1 Ga. Additional incompatible trace element enrichment of the peridotites is manifest in modal metasomatic phases with kimberlitic affinities, introduced prior to sampling by host kimberlite. Together, these provide an extreme range of incompatible trace element and isotopic signatures for potential incorporation in continental basalts such as those of the Karoo province (cf Hawkesworth et al, 1983), as well as some peripheral oceanic basalts such as those of the Walvis Ridge (cf Chapter 1).

CHAPTER 3

ORIGIN OF DIAMONDS IN OLD ENRICHED MANTLE:
Sm-Nd and Rb-Sr AGE CONSTRAINTS FROM SUB-CALCIC GARNETS
IN DIAMONDS AND HOST KIMBERLITE CONCENTRATE

3.1 Introduction

While diamonds have been recovered directly from kimberlite pipes for over a century, their particular relation to host kimberlite has remained controversial (eg Ringwood, 1977; Harte et al, 1980; Boyd & Finnerty, 1980). The debate centers on whether diamonds are phenocrysts or xenocrysts in the proto-kimberlite magma. More broadly, diamond crystallization may be temporally and spatially associated with kimberlite genesis or, alternatively, segments of mantle within the diamond stability field may be littered with diamonds so that sampling by kimberlite is strictly accidental. Diamond is in fact only a trace constituent of kimberlite, with abundances varying from zero to an order of magnitude maximum of 1 ppm. Moreover, in southern Africa, kimberlites erupted within the boundaries of the Archean craton are diamondiferous while those in adjacent younger mobile belts are barren (Gurney & Harte, 1980).

A small fraction of diamonds (<1%) contains syngenetic monomineralic and rarely multimineralic inclusions belonging to peridotitic or eclogitic parageneses. Apart from a greater proportion of macles (twins), these diamonds are morphologically indistinguishable from the majority of inclusion free diamonds (Harris et al, 1979). The peridotitic inclusion assemblage, which includes olivine, orthopyroxene, chromite and distinctive lilac chrome-pyrope garnet, is on average far more abundant than the eclogitic assemblage of orange pyrope-almandine garnet and omphacitic clinopyroxene (see reviews in: Meyer & Tsai, 1976; Sobolev, 1977; Harris & Gurney, 1979). This

categorization and relative abundance are apparently also reflected in host diamond carbon isotopic composition (Sobolev et al, 1979) and, by association, in spectral type and carbon isotopic composition of inclusion free diamonds (Milledge et al, 1983). Since peridotitic inclusion bearing diamonds are apparently of spectral type 1A which has a restricted range in carbon isotopic composition and accounts for 99% of all diamonds (Milledge et al, 1983), constraints on diamond origin derived from such inclusions, may be considered applicable to the vast majority of inclusion free diamonds.

Diamond inclusion assemblages parallel the mineralogy of the two most important categories of mantle xenolith in kimberlites, garnet peridotite and eclogite. However, there are significant differences in chemical composition between the dominant peridotitic diamond inclusions and constituent minerals of garnet peridotites. For example, garnets in diamond have significantly higher Mg and Cr and lower Ca contents than their peridotite xenolith counterparts, which are generally saturated with Ca (Figure 3-1). The former are here referred to as sub-calcic garnets. Garnets of similar but less extreme composition have also been found in kimberlite concentrate (Gurney & Switzer, 1973). The distribution of these discrete sub-calcic garnets in southern African kimberlites generally mirrors that of diamonds, implying an intimate genetic association between such garnets and diamonds (Boyd & Gurney, 1982). However, sub-calcic garnet bearing xenoliths are conspicuous by their absence. If sub-calcic garnets and the majority of diamonds reside in residual harzburgites, an efficient means of disaggregation during transport to the surface is required. Disruption by decomposition of disseminated magnesite (Boyd & Gurney, 1982; Wyllie et al, 1983) or

FIGURE 3-1

Distribution of CaO and Cr₂O₃ in selected sub-calcic garnets from Bultfontein (Kimberley cluster) and Finsch kimberlite heavy mineral concentrates. Garnet major element compositions determined by EMP analysis of fragments from single grains used for Nd and Sr isotopic analysis. Also shown for comparison are fields enclosing greater than 95% of sub-calcic garnet inclusions in Finsch diamonds (Gurney et al, 1979), garnets in Finsch peridotites (Shee et al, 1982) and garnets in Bultfontein lherzolites and harzburgites (Lawless, 1978). The positive correlations described by the peridotite garnets, generally observable for kimberlite peridotite xenolith suites, have become known as the lherzolite trend (Sobolev et al, 1973), since they reflect equilibration in the presence of diopside. Sub-calcic concentrate garnet compositions scatter away from this trend toward diamond inclusion garnet compositions, suggesting diopside-free host assemblages. Similar distributions of concentrate garnet compositions have been found in a variety of southern African kimberlites erupted within the boundaries of the Archean Kaapvaal craton (Boyd & Gurney, 1982).

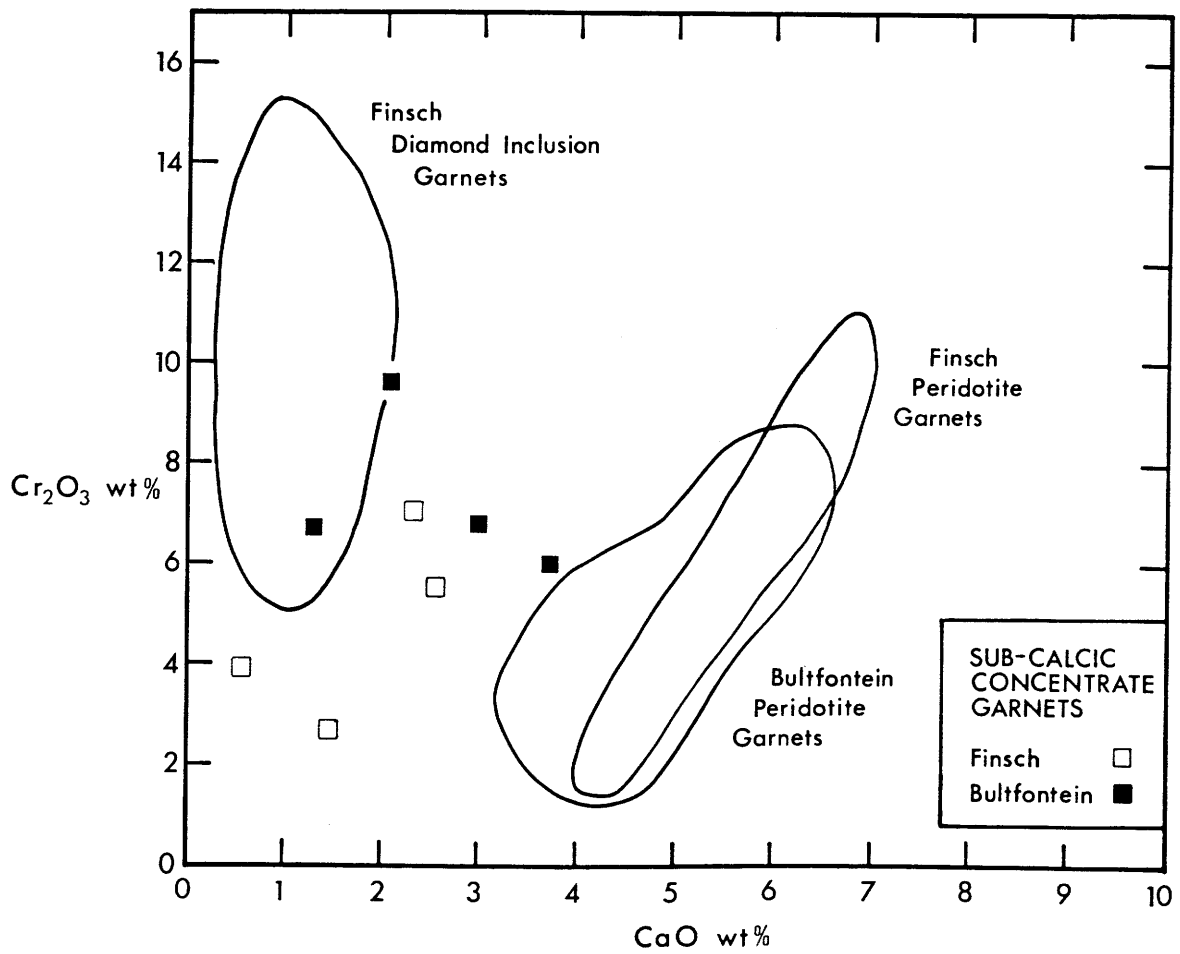


TABLE 3-1 Major element compositions¹ of sub-calcic garnets² from Bultfontein and Finsch kimberlite heavy mineral concentrates.

| | BULTFONTEIN | | | | FINSCH | | | |
|----------------------------------------|------------------------|---------|----------|----------|---------|---------|----------|--------------|
| | COMPOSITE ³ | JJG/SR4 | JJG/SR10 | JJG/SR20 | FINCON5 | FINCON7 | FINCON11 | FINCON/07/18 |
| SiO ₂ | 41.73 | 41.57 | 41.38 | 41.40 | 42.5 | 42.6 | 42.1 | 42.22 |
| TiO ₂ | N.D. | N.D. | 0.05 | N.D. | N.D. | N.D. | 0.05 | 0.04 |
| Al ₂ O ₃ | 19.07 | 18.93 | 19.56 | 17.01 | 22.8 | 21.8 | 20.5 | 19.40 |
| Cr ₂ O ₃ | 6.86 | 6.78 | 6.00 | 9.66 | 2.71 | 3.91 | 5.51 | 7.06 |
| FeO | 5.87 | 6.25 | 6.59 | 5.90 | 5.14 | 5.02 | 6.02 | 5.54 |
| MnO | 0.27 | 0.41 | 0.41 | 0.38 | 0.22 | 0.24 | 0.33 | 0.40 |
| MgO | 22.57 | 23.69 | 21.61 | 22.94 | 24.6 | 25.1 | 23.0 | 23.16 |
| CaO | 2.98 | 1.32 | 3.72 | 2.08 | 1.45 | 0.57 | 2.56 | 2.31 |
| TOTAL | 99.35 | 98.95 | 99.32 | 99.40 | 99.42 | 99.24 | 100.07 | 100.13 |
| ATOMIC PROPORTIONS BASED ON 12 OXYGENS | | | | | | | | |
| Si | 2.993 | 2.988 | 2.980 | 2.991 | 2.978 | 2.993 | 2.982 | 2.995 |
| Ti | 0.000 | 0.000 | 0.003 | 0.000 | 0.000 | 0.000 | 0.003 | 0.002 |
| Al | 1.612 | 1.604 | 1.660 | 1.448 | 1.883 | 1.805 | 1.712 | 1.622 |
| Cr | 0.389 | 0.385 | 0.342 | 0.552 | 0.150 | 0.217 | 0.309 | 0.396 |
| Fe ²⁺ | 0.352 | 0.376 | 0.397 | 0.357 | 0.301 | 0.295 | 0.357 | 0.329 |
| Mn | 0.016 | 0.025 | 0.025 | 0.023 | 0.013 | 0.014 | 0.020 | 0.024 |
| Mg | 2.414 | 2.538 | 2.320 | 2.470 | 2.570 | 2.629 | 2.429 | 2.449 |
| Ca | 0.229 | 0.102 | 0.287 | 0.161 | 0.109 | 0.043 | 0.194 | 0.176 |
| SUM | 8.005 | 8.017 | 8.015 | 8.006 | 8.005 | 7.996 | 8.005 | 7.993 |

¹ Determined by J J Gurney at University of Cape Town using EMP techniques summarized in Gurney et al (1979). N.D.=not detected

² Fragments split from single grains subsequently used for Rb-Sr and Sm-Nd isotope analysis (Table 3-2)

³ Average of individual analyses of six separate grains composited for isotope analysis.

simple dissociation due to the presence of interstitial melt (Harte et al, 1980), are viable alternative mechanisms.

Previous radiogenic isotope studies on trace constituents of diamond-related materials have been viewed with some skepticism given identification and potentially severe contamination problems. For example, a U-Pb study of presumed sulphide inclusions in diamonds yielded model Pb ages in excess of 2 Ga but was clouded by uncertainty regarding inclusion identity and paragenesis (Kramers, 1979). Similarly, results of a He isotopic study of industrial-grade diamonds required somewhat arbitrary speculation on He entrapment by diamonds soon after accretion of the earth (Ozima & Zashu, 1983; Ozima et al, 1983).

The present study involves an investigation of the Sm-Nd and Rb-Sr isotopic systematics of carefully screened sub-calcic garnets in concentrate and diamonds from two of the best documented localities in southern Africa, Kimberley and Finsch (cf Figure 2-1). These kimberlites are respectively representative of two classic types of kimberlite (basaltic and micaceous), recognizable on the basis of petrographic, chemical and isotopic characteristics (Barrett & Berg, 1975; Smith, 1983). The consistent results preclude a genetic connection between diamonds and host kimberlites and provide strong age and chemical constraints on an ultimate origin of diamonds in old enriched mantle.

3.2 Sub-calcic Garnets in Diamonds

Garnet inclusions in diamond are easily recognized in-situ by their distinctive colors. Peridotitic inclusions, of which 10-20% are garnets, comprise more than 98% of inclusions in Finsch diamonds (Harris & Gurney, 1979) and more than 90% of those in Kimberley diamonds (Harris et al, 1982). A comprehensive study of major element

compositions by Gurney et al (1970) revealed that more than 95% of peridotitic garnets in Finsch diamonds have extremely high Mg and Cr and low Ca contents. Associated olivine and orthopyroxene inclusion compositions are also extremely magnesian with average values of $Mg/(Mg+Fe)$ of 0.941 and 0.949 respectively (Gurney et al, 1979). Peridotitic diopside inclusions are conspicuous by their absence, emphasizing the residual major element character of the peridotitic inclusion paragenesis. The vast majority of peridotitic garnet inclusions, which are referred to as sub-calcic on the basis of Ca and Cr contents (Figure 3-1), also qualify as G10 garnets in the classification of Dawson & Stephens (1975), which considers all major elements. A similarly comprehensive study of Kimberley diamond inclusion compositions has not been performed to date but the same general relations are presumed to apply there as they do on a worldwide basis (cf Meyer & Tsai, 1976; Sobolev, 1977; Harris & Gurney, 1979).

Lilac garnet inclusion bearing diamonds were selected from the -6 + 5 diamond sieve fraction (average diameter ~ 2 mm; average weight ~ 10 mg (0.05 carats); Harris et al, 1979) of the general production from Finsch and the Kimberley Pool. The latter represents output from the common diamond recovery plant for Bultfontein, De Beers, Dutoitspan and Wesselton, the four kimberlite pipes currently mined at Kimberley, which are close enough at surface to have possibly had the same in-depth source. The relatively small diamond size used is convenient in terms of both economy and scale, since there is no obvious correlation between diamond and inclusion sizes (Gurney et al, 1979). Selected specimens represented approximately 1 in 1000 of all diamonds in this size category. The unperturbed encapsulation of inclusions can often not be verified

in-situ because the majority of diamonds have external irregularities, frosted surfaces and internal reflections which impair visibility. To avoid potential induration of contaminants and preserve host diamond material, diamonds were not burned. Instead, garnets were liberated by breaking diamonds in a Burrhus design steel cracker, and recovered intact, or occasionally in a few pieces, under a binocular microscope. Whole inclusions, often displaying diamond controlled morphologies, averaged 100-200 μ m in diameter and 10-15 μ g in weight (Tables 3-3 and 3-4). Inclusions from otherwise internally flawless diamonds were found to be in pristine condition. Partial alteration of some inclusions in other diamonds could generally be traced to emplacement-related fractures in diamonds, which were open to penetration by deuteric solutions.

In view of the small inclusion size, coupled with Nd and Sr concentrations of only a few ppm, as determined in a pilot study (Table 3-3), several hundred garnets from each locality were composited for isotope analysis (Table 3-4). Approximately 15% of Finsch and 30% of Kimberley inclusion garnets were rejected on the basis of the slightest trace of alteration, discoloration, coating or surface pitting visible during microscopic examination of all grain surfaces, before and after successive ultrasonic cleaning in ultrapure 2.5N HCl, 5% HF, 2.5N HCl, water and acetone. For the benefit of a duplicate determination, Finsch garnets were further divided into two fractions prior to final cleaning: the first, designated Finsch P, consisted of the largest flawless inclusions; the second, designated Finsch C, contained remaining irregular whole and fragmented inclusions, including those enclosing minute chromite grains (Table 3-4).

TABLE 3-2 Rb-Sr and Sm-Nd concentrations¹ and isotope ratios² for sub-calcic garnets³ from Bultfontein and Finsch kimberlite heavy mineral concentrates.

| weight mg | K | Rb | Sr | ⁸⁷ Rb/ ⁸⁶ Sr | ⁸⁷ Sr/ ⁸⁶ Sr _p | ⁸⁷ Sr/ ⁸⁶ Sr _i | Sm | Nd | ¹⁴⁷ Sm/ ¹⁴⁴ Nd | ¹⁴³ Nd/ ¹⁴⁴ Nd _p | ¹⁴³ Nd/ ¹⁴⁴ Nd _i | |
|------------------------|-------|-----|--------|------------------------------------|-------------------------------------------------|-------------------------------------------------|---------|--------|--------------------------------------|---------------------------------------------------|---------------------------------------------------|----------|
| BULTFONTEIN | | | | | | | | | | | | |
| COMPOSITE ⁴ | 13.25 | 5.2 | 0.022 | 2.97 | 0.021 | 0.71397±4 | 0.71394 | 2.797 | 9.042 | 0.1870 | 0.512253±15 | 0.512143 |
| JJG/SR4 | 2.67 | 2.8 | 0.0059 | 1.23 | 0.014 | 0.71020±46 | 0.71018 | 1.982 | 8.202 | 0.1462 | 0.512202±20 | 0.512116 |
| JJG/SR10 | 3.73 | 3.5 | 0.0070 | 0.671 | 0.030 | 0.71230±23 | 0.71226 | 1.558 | 3.111 | 0.3027 | 0.512574±25 | 0.512396 |
| JJG/SR20 | 2.77 | 4.4 | 0.0004 | 0.993 | 0.001 | 0.75510±33 | 0.75510 | 1.294 | 3.871 | 0.2020 | 0.511409±35 | 0.511290 |
| FINSCH | | | | | | | | | | | | |
| FINCON5 | 3.27 | 1.5 | 0.0006 | 0.642 | 0.003 | 0.70734±20 | 0.70734 | 0.8288 | 3.094 | 0.1619 | 0.512015±37 | 0.511920 |
| FINCON7 | 3.40 | 2.9 | 0.0023 | 2.66 | 0.0025 | 0.70889±24 | 0.70889 | 0.7954 | 7.327 | 0.06561 | 0.511800±17 | 0.511761 |
| FINCON11 | 2.26 | 3.9 | 0.0040 | 5.44 | 0.0021 | 0.73213±7 | 0.73213 | 1.714 | 12.149 | 0.08526 | 0.511250±17 | 0.511200 |
| FINCON/07/18 | 2.90 | 4.4 | 0.0015 | 12.17 | 0.00036 | 0.71424±3 | 0.71424 | 3.342 | 15.282 | 0.1322 | 0.511781±16 | 0.511703 |

¹ Concentrations in ppm (µg/g) after correction for minimum applicable blanks; Bultfontein: K(2ng), Rb(26pg), Sr(100pg), Sm(1.5pg), Nd(2.3pg); Finsch: K(1ng), Rb(20pg), Sr(15pg), Sm(1.5pg), Nd(2.3pg). Estimated analytical uncertainties in concentrations (ignoring small-sample weighing errors) indicated by number of significant digits.

² ⁸⁷Sr/⁸⁶Sr ratios normalized to 0.70800 for E & A SrCO₃ [average measured value = 0.70783±3 (2σ, N=5, 1981-83) using ⁸⁶Sr/⁸⁸Sr = 0.1194] and corrected for an identified reagent blank ⁸⁷Sr/⁸⁶Sr of 0.70783±15. Latter corrections all less than in-run precision (2σ_{mean} errors corresponding to least significant digits) except for JJG/SR20 (factor of 5; measured ⁸⁷Sr/⁸⁶Sr=0.75344). ¹⁴³Nd/¹⁴⁴Nd ratios normalized to 0.51264 for BCR-1 [average measured value = 0.512622±14 (2σ, N=6, spiked, 1982-83) using ¹⁴⁶Nd/¹⁴⁴Nd=0.7219]. Blank effects on Nd isotope ratios insignificant. Initial ratios calculated for a kimberlite emplacement age of 90 Ma using λ_{Rb}=1.42x10⁻¹¹a⁻¹ and λ_{Sm} = 6.54x10⁻¹²a⁻¹.

³ Major element compositions in Table 3-1.

⁴ Composite of six 1-3 mg sub-calcic garnet grains (cf Table 3-1).

3.3 Sub-calcic Garnets from Kimberlite Concentrate

Garnet crystals up to a few mm in diameter are generally abundant in the heavy mineral concentrate recovered from kimberlites. Among the variety of colors and associated chemical compositions, red to lilac chrome-pyrope crystals are dominant. The majority of these fall in the range of compositions for peridotite garnets, which display a positive correlation between Ca and Cr (Figure 3-1). This has become known as the lherzolite trend (Sobolev, 1973) since it reflects equilibration in the presence of diopside. However, a significant fraction of lilac garnets scatter between the lherzolite trend and the majority of diamond inclusion compositions (Gurney & Switzer, 1973; Boyd & Gurney, 1982), suggesting diopside free host assemblages. They similarly resemble garnets in diamonds in having high Mg, low Fe and very low Ti contents. As with the garnets in diamonds, these garnets are referred to as sub-calcic on the basis of Ca and Cr contents. At Finsch, such sub-calcic garnets comprise approximately 100 ppm of the kimberlite as a whole (Gurney & Switzer, 1973) as compared to a diamond abundance of 0.2 ppm (Shee et al, 1982) . At Kimberley, they account for some 15% of the lilac garnet population preselected from concentrate (Boyd & Gurney, 1982).

For this study, a number of sub-calcic garnets from Bultfontein (Kimberley cluster) and Finsch concentrates, were identified by J J Gurney on the basis of electron microprobe analysis of fragments split from pre-selected lilac garnet grains. Full major element compositions of the subset selected for isotope analysis are given in Table 3-1. Ca and Cr contents of individual grains (and a pilot six grain composite) are indicated in Figure 3-1. While grains have interiors that are extremely fresh and uncracked, they invariably carry remnants of kelyphite crusts

TABLE 3-3 Pilot study Rb-Sr and Sm-Nd concentrations¹ and isotope ratios² for sub-calcic garnet inclusions in diamonds³ from Kimberley Pool⁴ and Finsch kimberlite pipes.

| | weight mg | K | Rb | Sr | ⁸⁷ Rb/ ⁸⁶ Sr | ⁸⁷ Sr/ ⁸⁶ Sr _p | Sm | Nd | ¹⁴⁷ Sm/ ¹⁴⁴ Nd | ¹⁴³ Nd/ ¹⁴⁴ Nd _p |
|------------------------|--------------|----|------|-----|------------------------------------|-------------------------------------------------|------|------|--------------------------------------|---------------------------------------------------|
| KIMBERLEY POOL | | | | | | | | | | |
| composite ⁵ | 0.356 | 40 | 0.1 | 1.8 | 0.2 | 0.7054±7 | 0.87 | 3.37 | 0.16 | 0.51146±10 |
| single inclusion | 0.1046 | | | | | | 0.88 | 2.86 | 0.19 | |
| FINSCH | | | | | | | | | | |
| composite ⁵ | 0.301 | 20 | 0.03 | 8.8 | 0.01 | 0.7032±4 | 1.7 | 7.47 | 0.14 | 0.51132±12 |

¹ Concentrations in ppm (µg/g) after correction for minimum applicable blanks: K(2ng), Rb(28pg), Sr(100pg), Sm(17pg), Nd(2.3pg). Estimated analytical uncertainties in concentrations (ignoring small-sample weighing errors) indicated by number of significant digits.

² ⁸⁷Sr/⁸⁶Sr ratios normalized to 0.70800 for E & A SrCO₃ [average measured value = 0.70783±3 (2σ, N=5, 1981-83) using ⁸⁶Sr/⁸⁸Sr = 0.1194] and corrected for an identified reagent blank ⁸⁷Sr/⁸⁶Sr of 0.70783±15. Latter corrections less than nominal in-run precision (2σ_{mean} errors corresponding to least significant digits). ¹⁴³Nd/¹⁴⁴Nd ratios normalized to 0.51264 for BCR-1 [average measured value = 0.512622±14 (2σ, N=6, spiked, 1982-83) using ¹⁴⁶Nd/¹⁴⁴Nd = 0.7219]. Uncertainties for isotope ratios may be larger than indicated given lower-than-normal signal intensities (3x10⁻¹²A for ⁸⁸Sr; 1x10⁻¹²A for ¹⁴⁴Nd) and low sample-to-spike and sample-to-blank ratios.

³ Inclusions liberated by breaking diamonds in a Burrhus design steel cracker, followed by successive ultrasonic cleaning in ultrapure 2.5N HCl, 5% HF, 2.5N HCl, water and acetone.

⁴ Kimberley Pool includes Bultfontein, De Beers, Dutoitspan and Wesselton pipes.

⁵ Composite of ~ 30 inclusions with an average individual inclusion weight of ~ 10 µg.

or underlying pitted surfaces. All such exterior surfaces were removed using thin sliver splitting techniques, under a binocular microscope. Remaining whole 2-4 mg grains were then subjected to successive ultrasonic cleaning in 2.5N HCl, 5% HF, 2.5N HCl, water and acetone, followed by piece-by-piece grain size reduction in a Burrhus design steel cracker, and final inspection and cleaning.

3.4 Analytical Techniques

In order to minimize contamination, garnet samples were not pulverized (except for one pilot concentrate composite; Table 3-2) and final handling and transfer were performed using only teflon beakers and aqueous suspension. After weighing and total spiking with precisely calibrated mixed Sm-Nd and Rb-Sr tracer solutions, samples were dissolved with HF and HClO₄ in unsealed teflon beakers in 5-15 days. All were residue and precipitate free, except for one diamond inclusion composite with an expected tiny modal chromite residue (< 10µg; Table 3-4).

Chemical and mass spectrometric techniques for determination of K, Rb and Sr concentrations and ⁸⁷Sr/⁸⁶Sr ratios are as described in Hart & Brooks (1977); for Sm and Nd concentrations and ¹⁴³Nd/¹⁴⁴Nd ratios as summarized in Zindler et al (1979) but with provision for precise determination of Sm/Nd and ¹⁴³Nd/¹⁴⁴Nd ratios on totally spiked samples, as detailed in the Appendix. Apart from pilot study extremes (Table 3-3 and first entry in Table 3-2), available quantities of garnet Sr and Nd were 2-35 ng and 10-45 ng respectively. In-run precision ($2\sigma_{\text{mean}}$) of 0.007% for ⁸⁷Sr/⁸⁶Sr and 0.005% for ¹⁴³Nd/¹⁴⁴Nd was attainable for as little as 10 ng of each element from the same garnet sample, in runs with standard ⁸⁸Sr and ¹⁴⁴Nd ion beam intensities of $1 \times 10^{-11}\text{A}$ and $3 \times 10^{-12}\text{A}$ respectively, lasting up to 2 hours. Overall ion yields for chemical

TABLE 3-4 Rb-Sr and Sm-Nd concentrations¹ and isotope ratios² for sub-calcic garnet inclusions in diamonds³ from Kimberley Pool⁴ and Finsch kimberlite pipes.

| | weight mg | K | Rb | Sr | ⁸⁷ Rb/ ⁸⁶ Sr | ⁸⁷ Sr/ ⁸⁶ Sr _p | ⁸⁷ Sr/ ⁸⁶ Sr _i | Sm | Nd | ¹⁴⁷ Sm/ ¹⁴⁴ Nd | ¹⁴³ Nd/ ¹⁴⁴ Nd _p | ¹⁴³ Nd/ ¹⁴⁴ Nd _i |
|--------------------------|--------------|-----|--------|-------|------------------------------------|-------------------------------------------------|-------------------------------------------------|--------|-------|--------------------------------------|---------------------------------------------------|---------------------------------------------------|
| KIMBERLEY | | | | | | | | | | | | |
| composite ⁵ | 5.93 | 3.1 | 0.0025 | 1.985 | 0.0036 | 0.70621±5 | 0.70621 | 0.6115 | 2.920 | 0.1265 | 0.511058±36 | 0.510984 |
| FINSCH | | | | | | | | | | | | |
| composite P ⁶ | 3.81 | 17 | 0.013 | 6.379 | 0.0059 | 0.70380±4 | 0.70379 | 1.287 | 6.569 | 0.1184 | 0.510919±15 | 0.510849 |
| composite C ⁷ | 3.79 | 12 | 0.015 | 8.610 | 0.0050 | 0.70356±8 | 0.70355 | 1.186 | 6.301 | 0.1137 | 0.510892±22 | 0.510825 |

¹Concentrations in ppm (µg/g) after correction for minimum applicable blanks: K(1.1ng), Rb(20pg), Sr(15pg), Sm(1.5pg), Nd(2.3pg). Estimated analytical uncertainties in concentrations (ignoring small-sample weighing errors) indicated by number of significant digits.

²⁸⁷Sr/⁸⁶Sr ratios normalized to 0.70800 for E & A SrCO₃ [average measured value = 0.70783±3 (2σ, N=5, 1981-83) using ⁸⁶Sr/⁸⁸Sr = 0.1194]. ¹⁴³Nd/¹⁴⁴Nd ratios normalized to 0.51264 for BCR-1 [average measured value = 0.512622±14 (2σ, N=6, spiked, 1982-83) using ¹⁴⁶Nd/¹⁴⁴Nd = 0.7219]. In-run precision given by errors (2σ_{mean}) corresponding to least significant digits. Blank effects on isotope ratios insignificant. Initial ratios calculated for a kimberlite emplacement age of 90 m.y. using λ_{Rb}=1.42x10⁻¹¹yr⁻¹ and λ_{Sm}=6.54x10⁻¹²yr⁻¹.

³Inclusions liberated by breaking diamonds in a Burrhus design steel cracker, followed by meticulous sorting and successive ultrasonic cleaning in ultrapure 2.5N HCl, 5% HF, 2.5N HCl, water and acetone.

⁴Kimberley cluster includes Bultfontein, De Beers, Dutoitspan and Wesselton pipes, as well as exhausted Kimberley (Big Hole) pipe. Mined kimberlite from the first four pipes is channelled through common diamond recovery plant yielding Kimberley Pool diamonds.

⁵Composite of ~ 600 flawless and more irregular whole and fragmented sub-calcic garnet inclusions. Garnet inclusions enclosing minute chromite grains excluded. Altered, coated and otherwise suspect garnet inclusions excluded. Average individual inclusion weight approximately 10µg. Largest individual inclusion weight approximately 60µg.

⁶Composite of ~ 200 flawless sub-calcic garnet inclusions. Average individual inclusion weight 19µg. Largest individual inclusion weight approximately 80µg.

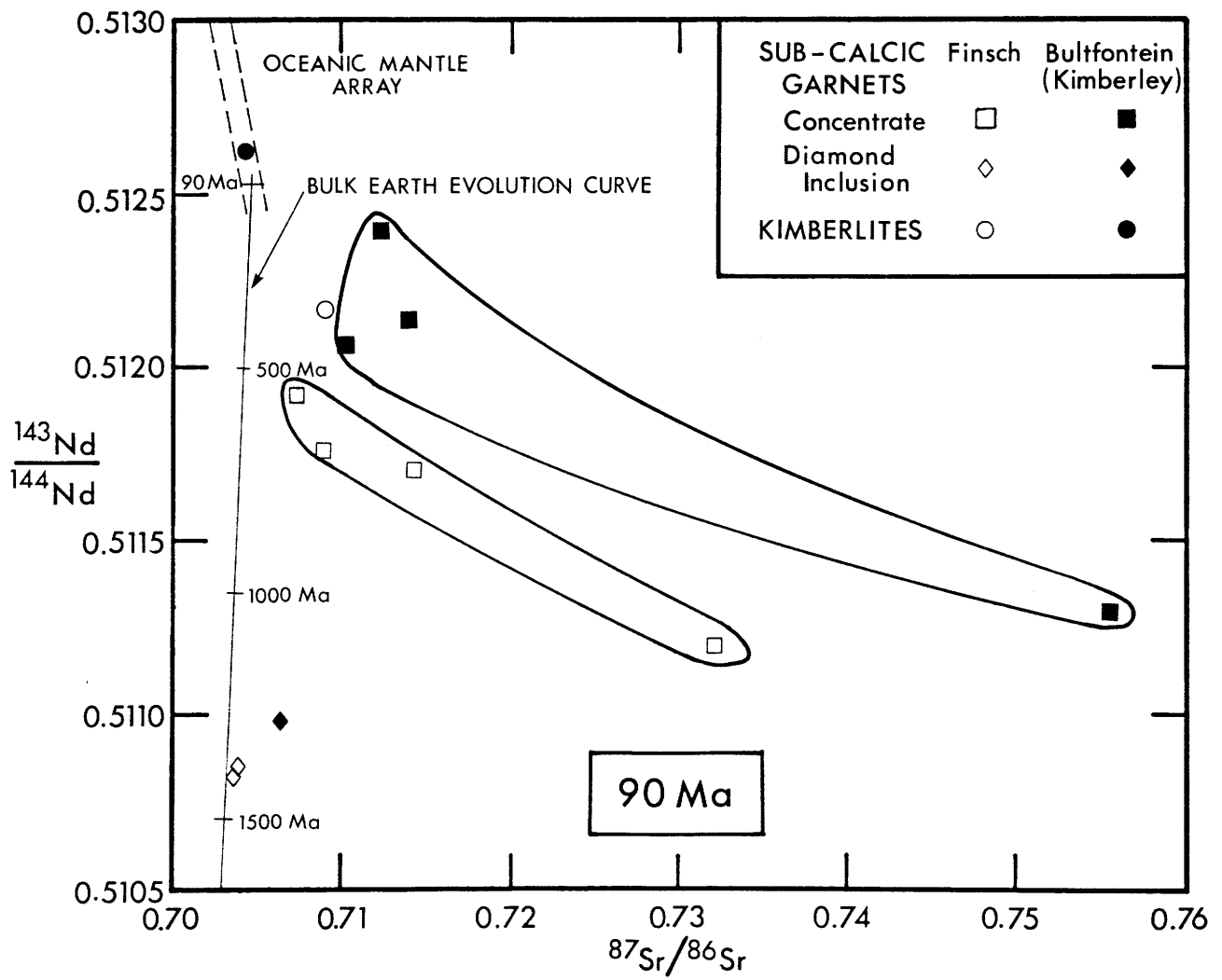
⁷Composite of ~ 300 more irregular whole and fragmented inclusions of which ~10% enclosed minute chromite grains (residual after garnet dissolution with total weight <10µg). Altered, coated and otherwise suspect garnet inclusions excluded. Average individual inclusion weight 13µg.

separation, thermal ionization and instrumental transmission were thus up to 0.6% for Sr and 1.3% for Nd. For garnet Sr contents in the 2-4 ng range, ^{88}Sr ion beam intensities were reduced to $3 \times 10^{-12}\text{A}$ with corresponding decrease in precision. No obvious differential instrumental bias attributable to use of this scaled reduction in intensity, has been detected within the precision of standard runs. Standard values used in normalization of isotope ratios for mass discrimination and systematic instrumental bias are given in Tables 3-2, 3-3, 3-4.

During the course of this project, total procedural blanks for some elements were progressively reduced (see Tables 3-2, 3-3 and 3-4 for minimum blanks applicable to various data). Aside from the diamond inclusion garnet pilot study, where sample-to-blank ratios were an order of magnitude lower than for subsequent analyses (Table 3-3), blank corrections to elemental concentrations are barely significant other than for alkalis. Alkali contents of garnets are so low as to be only 1-3 times minimum procedural blank levels, which are dominated by ion exchange column contributions. The effect of such blanks is increased by alkali elution peak dilation, peculiar to garnet column chemistry. Listed garnet K and Rb concentrations should therefore be treated with due caution, in that blank corrections are effectively underestimated and actual sample values are probably in many cases even lower than indicated. In addition, these data do not allow for calculation of meaningful K/Rb ratios. Blank corrections to isotope ratios are less than in-run precision (see Table 3-2 for one exception) or insignificant for Sr, and all insignificant for Nd.

FIGURE 3-2

Nd-Sr isotope correlation diagram, constructed at 90 Ma (time of kimberlite emplacement), showing data for sub-calcic garnets from Kimberley and Finsch. Concentrate garnets are single grains from Bultfontein (Kimberley cluster) and Finsch kimberlite heavy mineral concentrates (Table 3-2), while inclusion garnets are composites of many individual specimens from Kimberley Pool and Finsch diamonds (Table 3-4). Analytical precision is better than the size of plotted points. The oceanic mantle array (cf DePaolo & Wasserburg, 1979; Allegre et al, 1979), a bulk earth evolution curve, based on average chondritic Nd isotopic evolution (Jacobsen & Wasserburg, 1980), and host kimberlite values (Table 2-1) are shown for reference. Diamond inclusion garnet values clearly bear no relation to those of host kimberlites, or any other modern mantle-derived volcanics. Model age arguments (Figures 3-6 & 3-7) indicate ancient diamond formation in enriched mantle at 3.2-3.3 Ga. Concentrate garnets show crude inverse arrays, extending from the extreme high $^{87}\text{Sr}/^{86}\text{Sr}$ and low $^{143}\text{Nd}/^{144}\text{Nd}$ ratios back towards kimberlite and oceanic mantle values. Values for phlogopite kimberlites from southern Africa (Smith, 1983), as well as kimberlites and lamproites from western Australia (McCulloch et al, 1983), plot in the vicinity of the top left end of these arrays, as for the Finsch kimberlite. Such alkali rich kimberlites appear to have inherited a greater share of the enriched component, represented by hypothetical sub-calcic garnet host material, than "basaltic" kimberlites such as Bultfontein. Significantly, the degree of enrichment in this material shows some geographic variability, as is evident in the sympathetic displacement of Finsch and Bultfontein concentrate garnet arrays and corresponding diamond inclusion garnet values.



3.5 Sm-Nd and Rb-Sr Isotopic Systematics

Sub-calcic garnet $^{143}\text{Nd}/^{144}\text{Nd}$ and $^{87}\text{Sr}/^{86}\text{Sr}$ ratios (Tables 3-2 and 3-4) are illustrated on a Nd-Sr isotope correlation diagram (Figure 3-2) constructed at 90 Ma, the approximate time of host kimberlite emplacement (see section 2.4). Corresponding age corrections are small for $^{143}\text{Nd}/^{144}\text{Nd}$, since Sm/Nd ratios are low (0.1 - 0.5), and generally insignificant for $^{87}\text{Sr}/^{86}\text{Sr}$, since Rb/Sr ratios are negligible (< 0.01).

The immediate first order observation is that diamond inclusion garnets, concentrate garnets and host kimberlites (from Table 2-1) have distinct isotopic signatures. Sub-calcic diamond inclusion garnets have by far the lowest $^{143}\text{Nd}/^{144}\text{Nd}$ ratios measured in any modern mantle-derived materials. Such inclusion garnets clearly carry an ancient Nd isotopic component and host diamonds must necessarily be xenocrysts in kimberlites. Sub-calcic concentrate garnets have a large spread in $^{143}\text{Nd}/^{144}\text{Nd}$ ratios negatively correlated with extremely high $^{87}\text{Sr}/^{86}\text{Sr}$ ratios. Such concentrate garnets are also necessarily xenocrysts in kimberlites but clearly isotopically differentiated from their diamond inclusion counterparts. Yet both types of sub-calcic garnet show sympathetic differences in isotopic signature from place to place. Specifically, the Finsch concentrate garnet array and diamond inclusion composites lie at relatively lower $^{143}\text{Nd}/^{144}\text{Nd}$ and $^{87}\text{Sr}/^{86}\text{Sr}$ ratios than their Kimberley counterparts.

The next obvious observation is that sub-calcic garnet $^{87}\text{Sr}/^{86}\text{Sr}$ ratios are entirely unsupported by intrinsic Rb contents, even over the age of the earth. Therefore, the garnets must have inherited such $^{87}\text{Sr}/^{86}\text{Sr}$ ratios by diffusive equilibration with mantle hosts which

had higher time-integrated Rb/Sr ratios. Concentrate garnets with extremely high $^{87}\text{Sr}/^{86}\text{Sr}$ ratios require either much higher host Rb/Sr ratios or much longer integration times than their diamond inclusion counterparts. The latter alternative is immediately favored in that encapsulation by diamond provides for a unique difference in physical storage environment. Nd and Sr diffusion rates through diamond are assumed to be negligible. The difference in isotopic signature between the two types of sub-calcic garnet is then simply a function of exposure time in a common host chemical environment, which is similar but not identical from place to place. Since garnet and host diamond are syngenetic, the nature and timing of diamond formation can be derived from garnet Sm-Nd and Rb-Sr isotopic systematics.

Overall, sub-calcic garnets are endowed with trace element abundances which belie their residual major element compositions. Concentrations of Nd (3-15 ppm) and Sr (0.6 -12 ppm) range up to significantly higher values than those for peridotite xenolith garnets (1-4 ppm Nd, 0.5 -1 ppm Sr; see Chapter 2), and appear to be positively correlated (Figure 3-3). Moreover, extremely low garnet Sm/Nd ratios suggest strongly LREE enriched patterns which are the opposite of those observed in peridotite xenolith garnets (Shimizu, 1975b). Garnets in Finsch diamonds have higher Sr and Nd concentrations than those in Kimberley diamonds, as is also the case, on average, for respective concentrate garnets. While inclusion garnet values are averages for composites of many individual specimens, consistent values for both main and pilot study samples, including a Nd concentration for a single diamond inclusion garnet (Table 3-3), suggest reasonably restricted ranges for each locality. In contrast, individual concentrate garnet values show great scatter (Figure 3-3).

FIGURE 3-3

Distribution of Nd and Sr concentrations in sub-calcic garnets from Kimberley and Finsch. Concentrate garnets are single grains from Bultfontein (Kimberley cluster) and Finsch kimberlite heavy mineral concentrates (Table 3-2), while inclusion garnets are composites of many individual specimens from Kimberley Pool and Finsch diamonds (Tables 3-3 & 3-4). Garnets in Finsch diamonds have higher Sr and Nd concentrations than those in Kimberley Pool diamonds, as is also the case, on average, for respective concentrate garnets, but with much greater scatter of individual values.

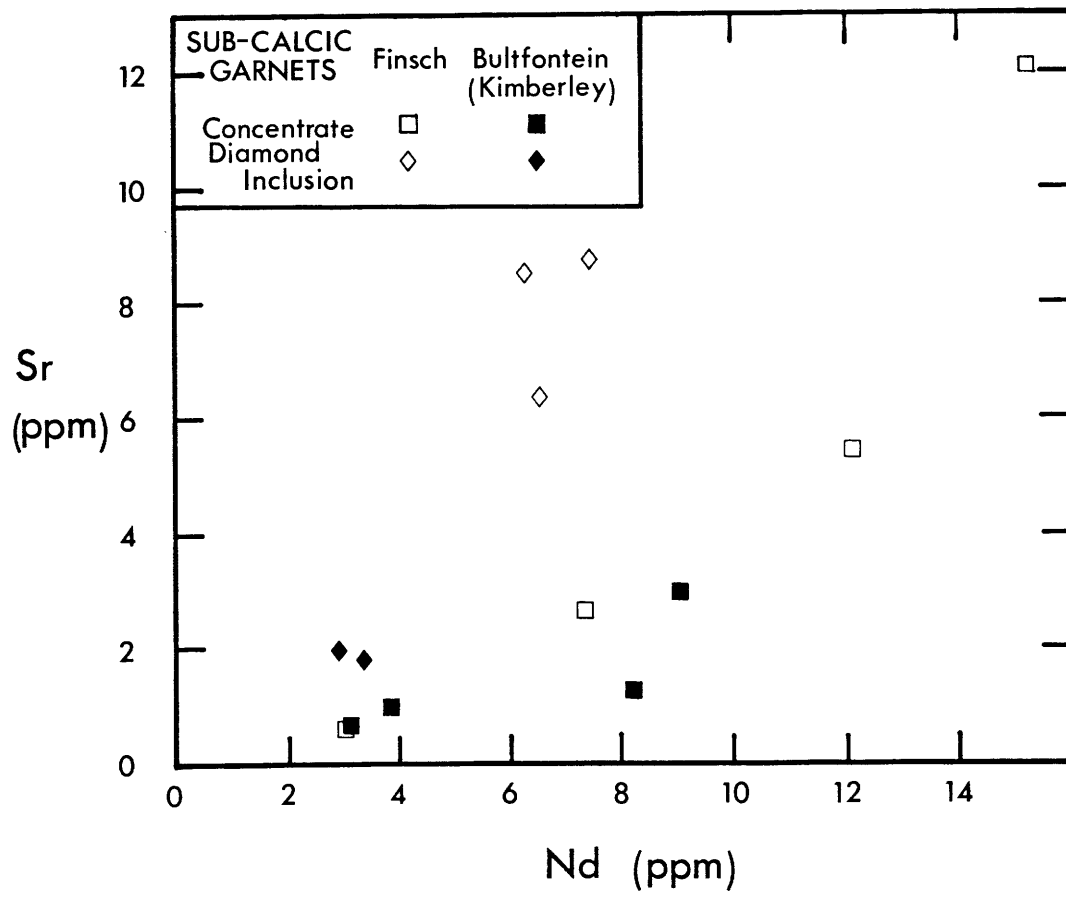


FIGURE 3-4

Sm-Nd isochron diagram, constructed at 90 Ma (time of kimberlite emplacement), illustrating data for sub-calcic garnets from Kimberley and Finsch.

Concentrate garnets are single grains from Bultfontein (Kimberley cluster) and Finsch Kimberlite heavy mineral concentrates (Table 3-2), while inclusion garnets are composites of many individual specimens from Kimberley Pool and Finsch diamonds (Table 3-4). Analytical precision is better than the size of plotted points except where otherwise indicated. A bulk earth (CHUR) value at 90 Ma, based on the average present-day chondritic value (Jacobsen & Wasserburg, 1980), and host kimberlite values (Table 2-1) are shown for reference. Concentrate garnets show a substantial range of $^{143}\text{Nd}/^{144}\text{Nd}$ ratios (Bultfontein: 0.5113-0.5124; Finsch: 0.5112-0.5119) and great scatter of points, with only the crudest of positive correlations observable by averaging data for each of the two localities. In contrast, diamond inclusion garnets show much more restricted variation and a coherent, even if poorly constrained, positive correlation. First order correspondence of this correlation with a 3.3 Ga reference isochron drawn through CHUR suggests crudely contemporaneous isolation of inclusion garnets by diamond formation in a mantle reservoir with Nd isotopic characteristics not radically different from those of the bulk earth at the time. Such Sm-Nd model age relationships are better illustrated in a $^{143}\text{Nd}/^{144}\text{Nd}$ evolution diagram (Figure 3-6).

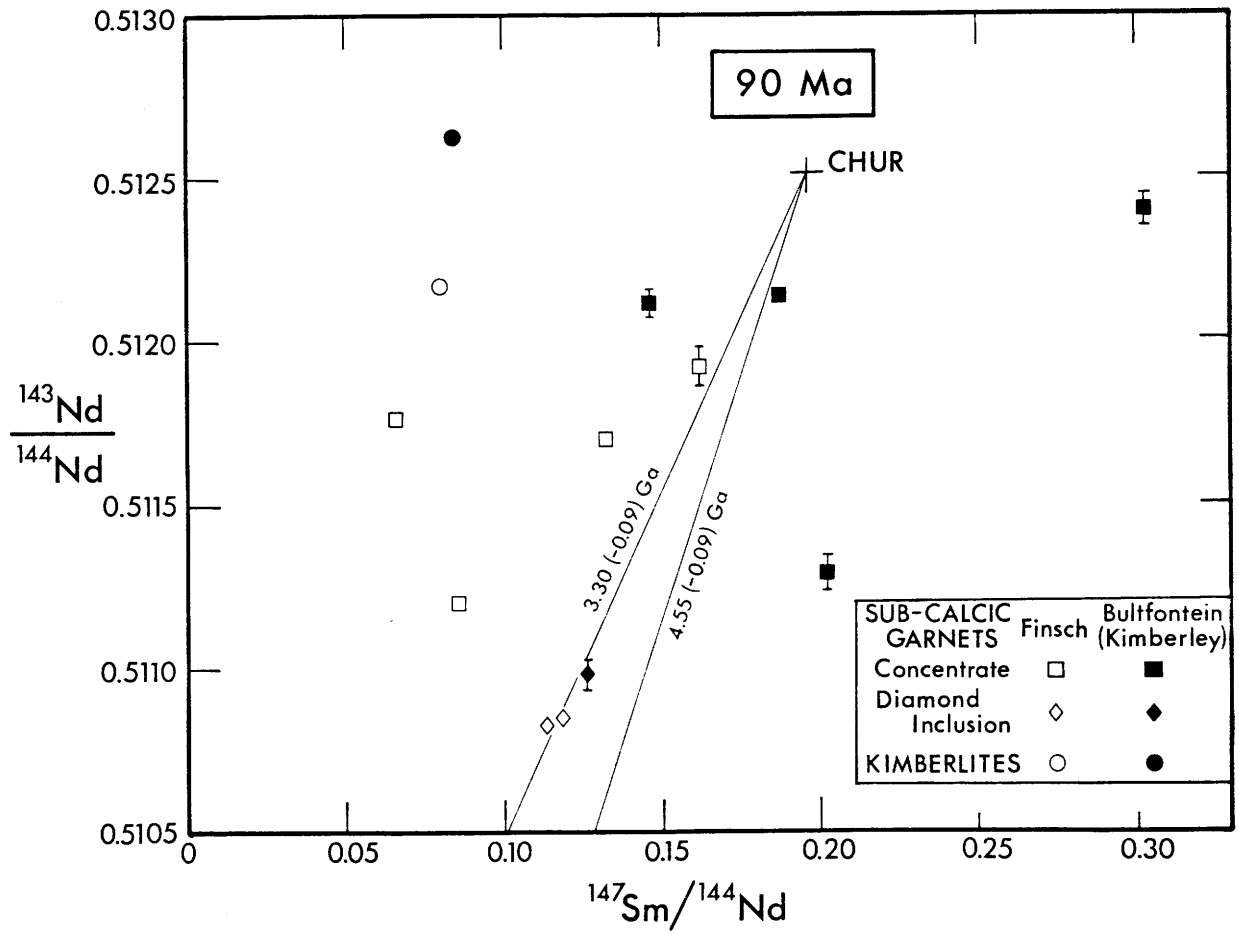
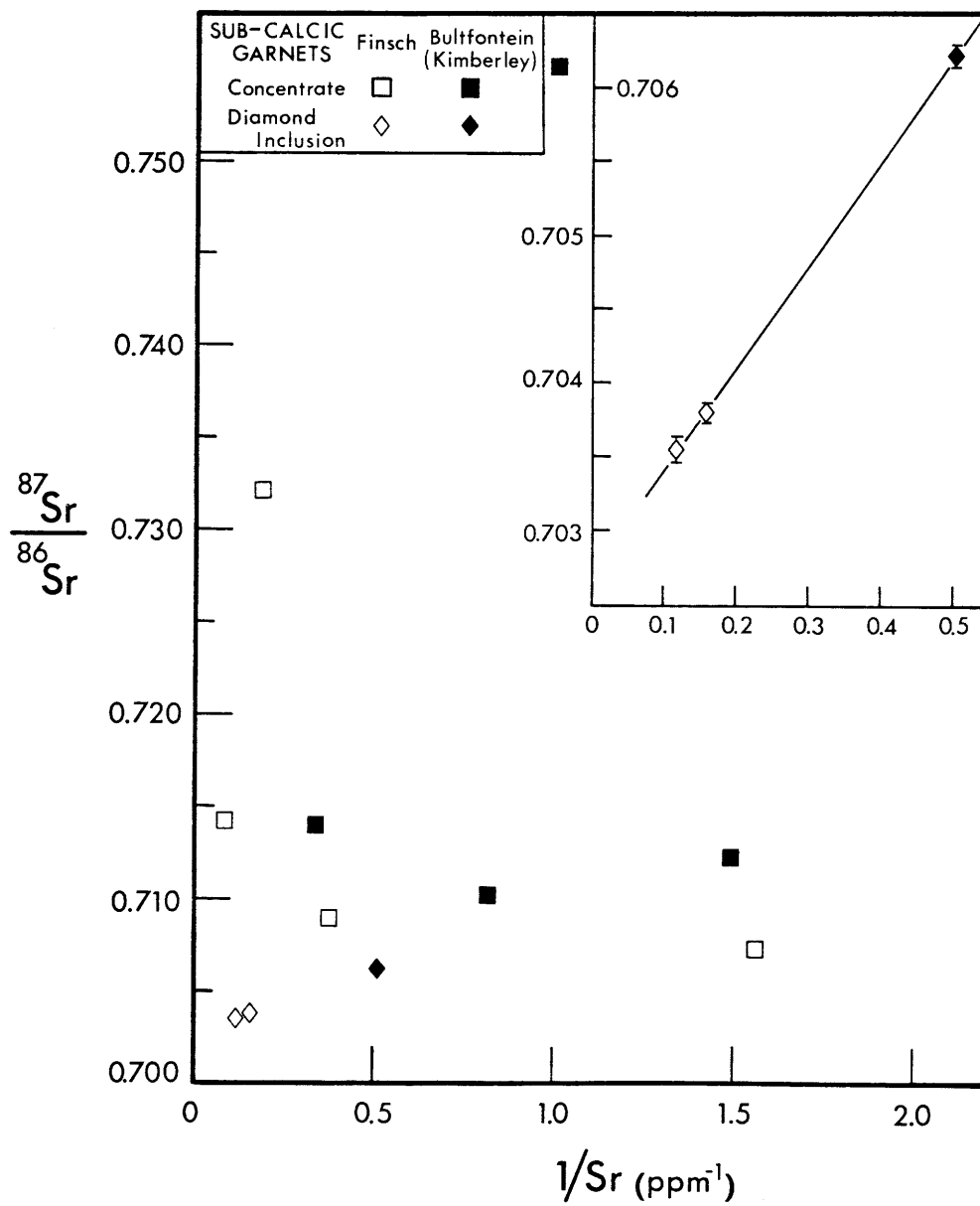


FIGURE 3-5

Variation of $^{87}\text{Sr}/^{86}\text{Sr}$ ratio with reciprocal Sr concentrations in sub-calcic garnets from Kimberley and Finsch. Concentrate garnets are single grains from Bultfontein (Kimberley cluster) and Finsch kimberlite heavy mineral concentrates (Table 3-2), while inclusion garnets are composites of many individual specimens from Kimberley Pool and Finsch diamonds (Table 3-4). Present day and initial $^{87}\text{Sr}/^{86}\text{Sr}$ ratios (at 90 Ma, the time of kimberlite emplacement) are essentially identical, because of very low intrinsic Rb/Sr ratios. Analytical precision is better than the size of plotted points except for the larger scale inset where $^{87}\text{Sr}/^{86}\text{Sr}$ error bars are indicated. Concentrate garnets show an extreme range of $^{87}\text{Sr}/^{86}\text{Sr}$ ratios (Bultfontein: 0.710-0.755; Finsch: 0.707-0.732) and great scatter of points. In contrast, diamond inclusion garnets show an apparent positive correlation (inset) for a limited range of $^{87}\text{Sr}/^{86}\text{Sr}$ ratios (Kimberley Pool: 0.7062; Finsch: 0.7036-0.7038). A corresponding inverse correlation between inclusion garnet Sr concentration and precursor host Rb/Sr ratio is suggested, such that the inset correlation has age rather than mixing significance (see Figure 3-7 and text).



Analogous relationships are also apparent between isotope ratio and parent/daughter ratio, as illustrated on a Sm-Nd isochron diagram (Figure 3-4), constructed at 90 Ma, the time of kimberlite emplacement. Diamond inclusion garnets show restricted variation in $^{143}\text{Nd}/^{144}\text{Nd}$ ratio (0.5108 - 0.5110) and a coherent, even if poorly constrained, positive correlation. First order correspondence with a 3.3 Ga reference isochron drawn through the bulk earth value suggest crudely contemporaneous diamond formation in a mantle reservoir with Nd isotopic characteristics not radically different from those of the bulk earth at the time. In contrast, concentrate garnets show a substantial range of $^{143}\text{Nd}/^{144}\text{Nd}$ ratios (Bultfontein: 0.5113 - 0.5124; Finsch: 0.5112 - 0.5119) and great scatter of points with only the crudest of positive correlations observable by averaging data for each locality (Figure 3-4).

Representation of garnet Rb-Sr data on a Rb-Sr isochron diagram is not particularly useful since Rb/Sr ratios are all extremely low (0.0001 - 0.01) and absolute values are imprecise because of uncertainties in vanishingly small Rb contents (see section 3.4 for cautionary notes on Rb concentration measurements). However, this allows for a more meaningful look at the Rb-Sr systematics of garnet host assemblages. Diamond inclusion garnets show an apparent positive correlation between $^{87}\text{Sr}/^{86}\text{Sr}$ ratio (0.7036-0.7062) and reciprocal Sr concentration (Figure 3-5). A corresponding inverse correlation between Sr concentration and precursor host Rb/Sr ratio is inferred, such that the former correlation has age rather than mixing significance. In contrast, concentrate garnets show an extreme range of $^{87}\text{Sr}/^{86}\text{Sr}$ ratios (Bultfontein: 0.710 - 0.755; Finsch: 0.707 - 0.732) and great scatter of points (Figure 3-5).

By all accounts, Sm-Nd and Rb-Sr concentrations in diamond inclusion garnets show consistent relationships with isotope ratios, whereas in concentrate garnets they do not. Therefore, only diamond inclusion garnet Sm/Nd ratios may be used to derive Sm-Nd model ages for diamond formation. Inferred precursor Rb/Sr ratios, equal to or greater than the minimum time-integrated Rb/Sr ratios required by the highest concentrate garnet $^{87}\text{Sr}/^{86}\text{Sr}$ ratios, may then be used to calculate differential Rb-Sr model ages for precursor formation.

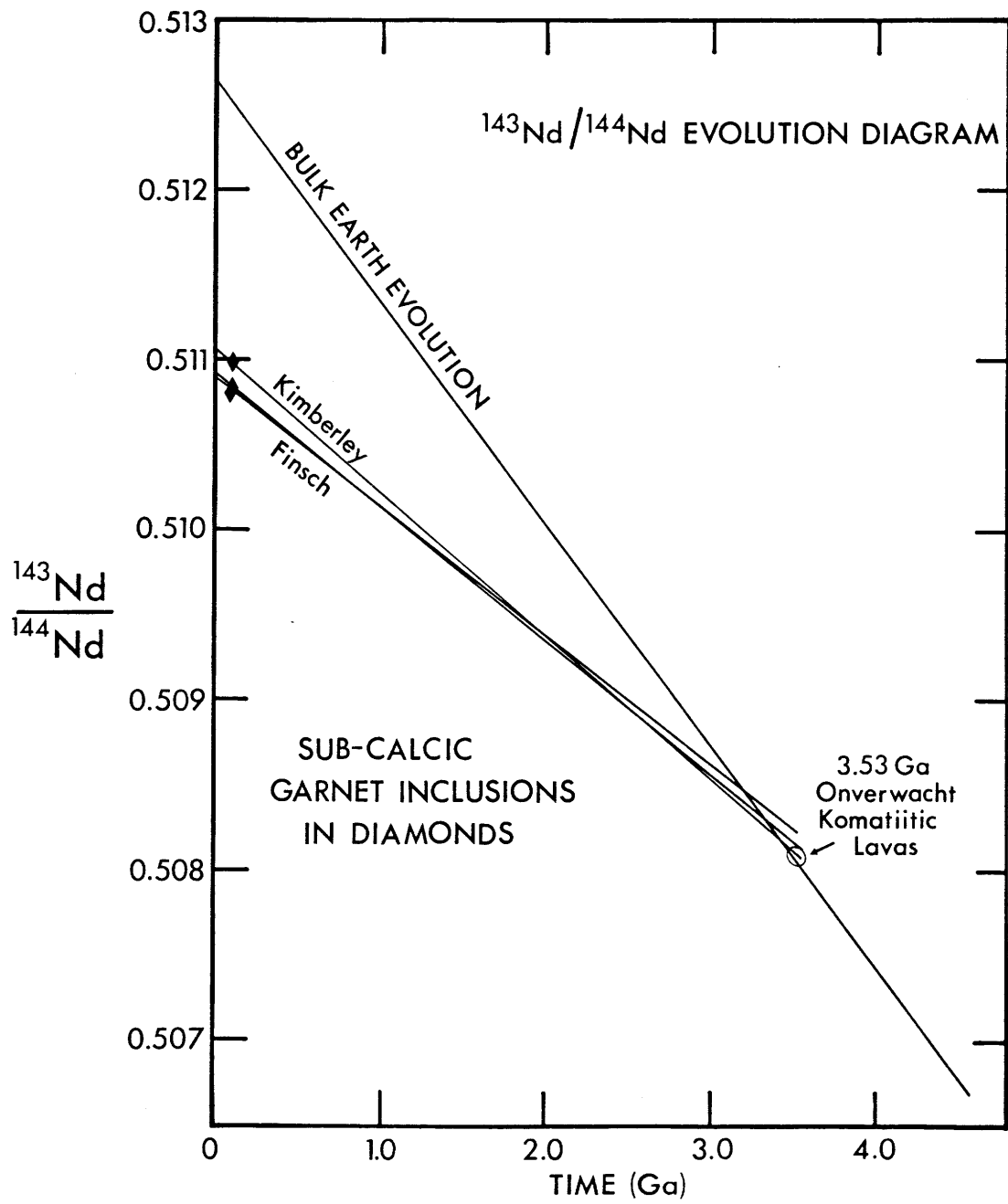
3.6 Model Age Constraints on Diamond Formation

Sm-Nd model age relationships are best illustrated in a $^{143}\text{Nd}/^{144}\text{Nd}$ evolution diagram (Figure 3-6). The bulk earth reference curve is constructed using average present-day chondritic values ($^{143}\text{Nd}/^{144}\text{Nd} = 0.512638$, $^{147}\text{Sm}/^{144}\text{Nd} = 0.1966$ from Jacobsen & Wasserburg, 1980, with appropriate normalizations and minor adjustments from Wasserburg et al, 1981 and Hamilton et al, 1983) and the commonly adopted ^{147}Sm decay constant, $\lambda_{\text{Sm}} = 6.54 \times 10^{-12} \text{a}^{-1}$ (cf Lugmair and Marti, 1978). Evolution curves for sub-calcic garnets in Kimberley and Finsch diamonds are constructed using measured $^{143}\text{Nd}/^{144}\text{Nd}$ and $^{147}\text{Sm}/^{144}\text{Nd}$ ratios (Table 3-4). Intersections with the reference curve yield Sm-Nd model ages for syngenetic garnet and diamond derivation from the hypothetical bulk earth reservoir.

Ages thus obtained are 3.41 ± 0.08 Ga for the Kimberley composite and 3.32 ± 0.03 and 3.19 ± 0.05 Ga for the two Finsch composites. Uncertainties are as propagated from those for both $^{143}\text{Nd}/^{144}\text{Nd}$ ($2\sigma_{\text{mean}}$) and $^{147}\text{Sm}/^{144}\text{Nd}$ ($< 0.1\%$) measurements (Table 3-4) but effectively dominated by the former. In principle, results for the two Finsch composites (P & C) were meant to represent a first order duplicate

FIGURE 3-6

$^{143}\text{Nd}/^{144}\text{Nd}$ evolution diagram showing evolution curves for sub-calcic garnets in Kimberley Pool and Finsch diamonds. Curves are constructed from measured $^{143}\text{Nd}/^{144}\text{Nd}$ and $^{147}\text{Sm}/^{144}\text{Nd}$ ratios, using $\lambda_{\text{Sm}} = 6.54 \times 10^{-12} \text{a}^{-1}$, and arbitrarily terminated at 3.53 Ga. Diamond symbols at 90 Ma mark the time of diamond transport to surface by kimberlite. The bulk earth reference curve is constructed using average present-day chondritic values ($^{143}\text{Nd}/^{144}\text{Nd}=0.512638$, $^{147}\text{Sm}/^{144}\text{Nd} = 0.1966$ from Jacobsen & Wasserburg, 1980, with appropriate normalizations and minor adjustments in Wasserburg et al, 1981 and Hamilton et al, 1983) and terminated at 4.55 Ga. The Onverwacht komatiite age and initial $^{143}\text{Nd}/^{144}\text{Nd}$ ratio is from Hamilton et al (1979) with minor amendment (Hamilton et al, 1983) and error ellipse representation (Minster et al, 1979). Intersections of garnet and bulk earth curves give Sm-Nd model ages for garnet encapsulation by diamond. Using a simple combination of analytical and model uncertainties (see text), a conservative overall estimate of diamond formation age is 3.3 ± 0.2 Ga. Temporal, spatial and major element compositional relationships suggest diamond formation occurred subsequent to komatiite generation in Archean mantle beneath the Kaapvaal craton. Trace element and Sr isotopic relationships (Figure 3-7) require introduction of an enriched component (high Rb/Sr and low Sm/Nd) following komatiite generation as a precursor to diamond formation.



determination, and in this sense the ages obtained are very similar, if not exactly within nominal errors. In practice, the second composite (C) consisted of a lesser grade of garnet and included a minor proportion enclosing minute chromite grains, residual after dissolution (see section 3.2 and Table 3-4). The marginally younger age could therefore be due to sample character, imperfect screening, minor contamination or simply underestimated analytical errors. In effect, the ages of Kimberley and Finsch garnets are not resolved within reasonable errors and approximately synchronous diamond formation is implied.

Further systematic model age uncertainties arise from the assumption of a bulk earth reference curve, since neither an exactly chondritic initial Earth nor a subsequent undifferentiated mantle source for garnet and diamond can be presumed. The Nd isotopic character of real temporally and spatially associated mantle may usefully be represented by that of 3.53 Ga Onverwacht Group volcanics (Hamilton et al, 1979, 1983) from the Barberton Mountainland in southern Africa. These komatiitic volcanics are merely the best preserved remnant of such magmas which appear to have been emplaced across the entire Archean Kaapvaal craton (Viljoen et al, 1982). For a mantle evolution curve passing through the Onverwacht datum (Figure 3-6) and either slightly steeper (depleted mantle with higher Sm/Nd) or shallower (enriched mantle with lower Sm/Nd) than the reference curve, garnet model ages would be respectively increased or decreased by approximately 0.1 Ga. With simple combination of analytical and model uncertainties, a conservative overall estimate of sub-calcic garnet bearing diamond formation age is 3.3 ± 0.2 Ga.

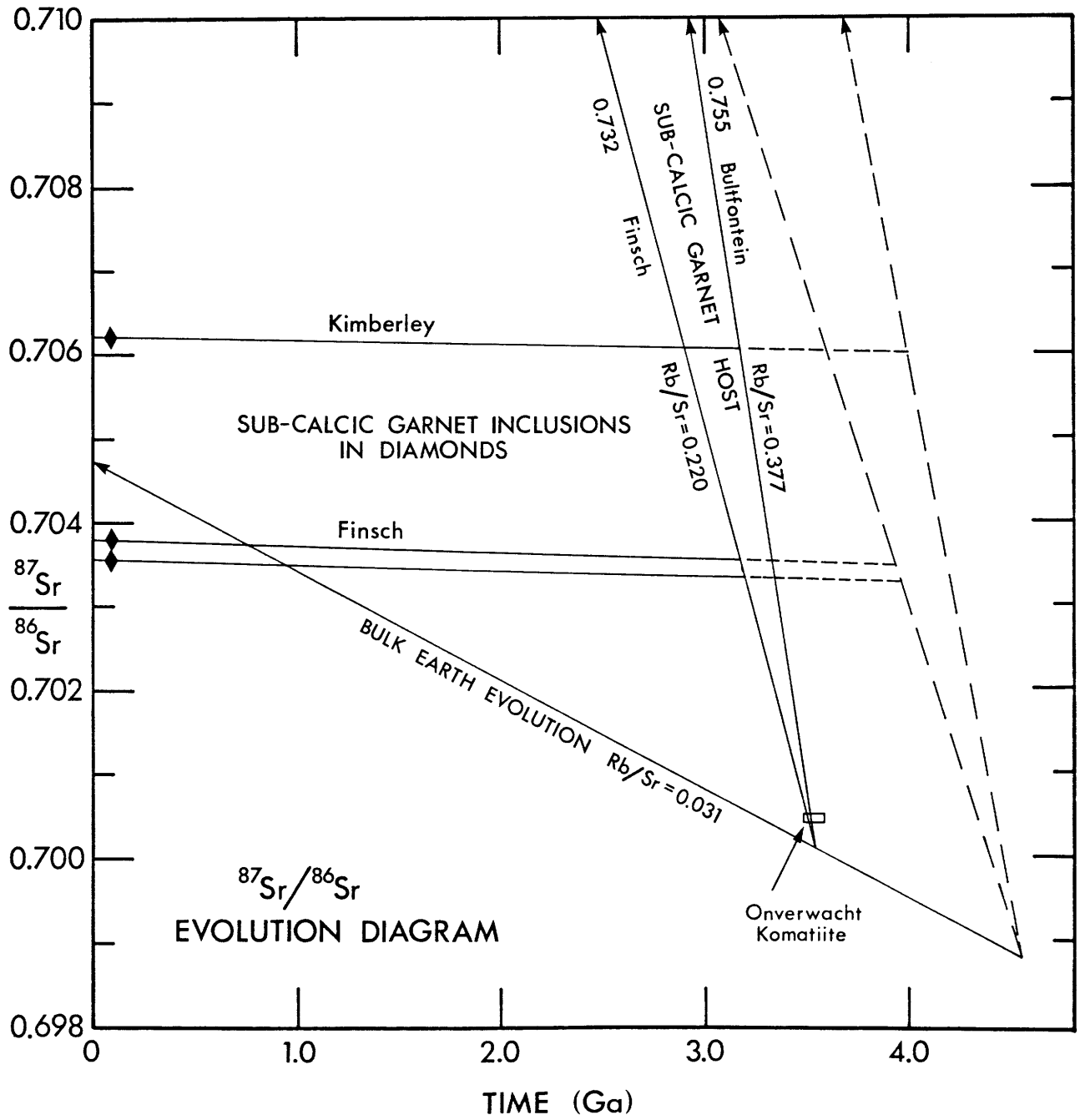
The striking association between diamond and komatiite genesis is not only temporal and spatial, but also compositional. For example,

diamond inclusion olivine $Mg/(Mg+Fe)$ ratios are essentially identical to those for liquidus olivines in peridotitic komatiites (Green et al, 1975). While the mineralogy of residual mantle or high pressure cumulates remaining after komatiite generation is controversial (cf Arndt & Nisbet, 1982), highly magnesian major element compositions are not disputed. Nd/Sm and Rb/Sr ratios equal to or less than bulk earth values may also be inferred for such depleted residual mantle. Such trace element characteristics are the opposite of those now seen in sub-calcic garnet Sm-Nd and Rb-Sr systematics. Therefore, trace element enrichment of such residua is required after komatiite generation and before sub-calcic garnet and diamond crystallization.

A suitable time differential between komatiite and diamond formation is also required to explain dramatic radiogenic growth of ^{87}Sr in the enriched (high Rb/Sr and low Sm/Nd) precursor, evident in diamond inclusion garnet $^{87}Sr/^{86}Sr$ ratios (Figure 3-5). In contrast, differential radiogenic growth of ^{143}Nd is far less pronounced, because relative differences in low Sm/Nd ratio are small by comparison with those in Rb/Sr ratio. The magnitude of this time differential can be derived from Rb-Sr model age relationships as illustrated in a $^{87}Sr/^{86}Sr$ evolution diagram (Figure 3-7). The bulk earth reference curve is drawn between a chondritic initial $^{87}Sr/^{86}Sr$ ratio of 0.69880 (Minster et al, 1979) at 4.55 Ga and a present-day bulk earth $^{87}Sr/^{86}Sr$ ratio of 0.70475, derived from the mantle Nd-Sr correlation (cf regression and review in Allegre et al, 1983). This evolution curve is by definition partially dependent on and less well constrained than its Nd counterpart. However, the Rb-Sr model age relationships to be discussed are insensitive to such uncertainty. A gross indication of regional mantle Sr isotopic character

FIGURE 3-7

$^{87}\text{Sr}/^{86}\text{Sr}$ evolution diagram showing evolution curves for sub-calcic garnets in Kimberley Pool and Finsch diamonds. Curves are constructed from measured $^{87}\text{Sr}/^{86}\text{Sr}$ and $^{87}\text{Rb}/^{86}\text{Sr}$ ratios, using $\lambda_{\text{Rb}} = 1.42 \times 10^{-11} \text{a}^{-1}$. Intrinsic garnet Rb/Sr ratios are so low that corresponding evolution curves are virtually flat. Diamond symbols at 90 Ma mark the time of diamond transport to surface by kimberlite. The bulk earth reference curve is drawn using a chondritic meteorite initial $^{87}\text{Sr}/^{86}\text{Sr}$ ratio of 0.69880 (Minster et al, 1979) and a present-day silicate earth $^{87}\text{Sr}/^{86}\text{Sr}$ ratio of 0.70475 derived from the mantle Nd-Sr correlation (cf regression and review in Allegre et al, 1983). The Onverwacht datum is a combination of the initial $^{87}\text{Sr}/^{86}\text{Sr}$ ratio for density separates of an altered komatiite (Jahn & Shih, 1974) and a 3.53 Ga multiple whole rock Sm-Nd isochron age (Hamilton et al, 1979, 1983). Hypothetical sub-calcic garnet host (diamond precursor) evolution curves have been drawn between the bulk earth curve and extreme $^{87}\text{Sr}/^{86}\text{Sr}$ ratios measured in sub-calcic garnets from kimberlite heavy mineral concentrates. Solid curves are drawn between the bulk earth at 3.53 Ga and the highest concentrate garnet $^{87}\text{Sr}/^{86}\text{Sr}$ ratios (at 90 Ma) for Bultfontein (0.755) and Finsch (0.732). Corresponding time-integrated Rb/Sr ratios are indicated. Dashed curves emanating from the bulk earth at 4.55 Ga are shown for comparison. Intersections of respective diamond and solid sub-calcic garnet host curves give a common model age for garnet encapsulation by diamond of 3.2 Ga, predicated on an approximate 300 Ma time differential between precursor enrichment (following komatiite generation) and diamond crystallization.



at the time of interest (3.5 Ga) is afforded by the initial $^{87}\text{Sr}/^{86}\text{Sr}$ ratio for density separates of an altered Onverwacht komatiite (Jahn & Shih, 1974). While the precise value is suspect because of perturbation of the Rb-Sr system during greenschist facies metamorphism (cf Hamilton et al, 1979; Smith & Erlank, 1978), and thus cannot be used to constrain the mantle evolution curve (Hart & Brooks, 1977; Zindler, 1980, 1982), order of magnitude consistency is apparent (Figure 3-7).

Evolution curves for sub-calcic garnets in Kimberley and Finsch diamonds are constructed from measured $^{87}\text{Sr}/^{86}\text{Sr}$ and $^{87}\text{Rb}/^{86}\text{Sr}$ ratios (Table 3-4). Intrinsic garnet Rb/Sr ratios are so low (see section 3.5) that corresponding evolution curves are virtually flat. Hypothetical sub-calcic garnet host (diamond precursor) evolution curves are shown diverging from the bulk earth curve towards the high present day $^{87}\text{Sr}/^{86}\text{Sr}$ ratios measured in unencapsulated concentrate garnets. A pair of such curves is drawn between the bulk earth at 3.53 Ga (Onverwacht komatiite Sm-Nd isochron age from Hamilton et al, 1979, 1983) and extreme sub-calcic concentrate garnet $^{87}\text{Sr}/^{86}\text{Sr}$ ratios (at 90 Ma, the host kimberlite emplacement age) for Bultfontein (Kimberley cluster) and Finsch. Corresponding time-integrated Rb/Sr ratios are indicated. Intersections of the respective diamond inclusion garnet and precursor curves give a common Rb-Sr model age for diamond formation of approximately 3.2 Ga. This is entirely consistent with the Sm-Nd model age of 3.3 ± 0.2 Ga but specifically predicated on an approximate 300 Ma time differential between precursor formation (enrichment of komatiite residua) and diamond crystallization.

This treatment can be extended to rule out an origin of such diamonds soon after formation of the earth, as proposed by Ozima & Zashu (1983). Intersections of extrapolated diamond curves with precursor

curves diverging from the bulk earth at 4.55 Ga give model ages of less than 4.0 Ga (Figure 3-7). Thus, even with precursor enrichment dating back to original accretion of the earth, formation of such diamonds prior to 4 Ga is effectively precluded.

As previously indicated, concentrate garnets show a range of major element compositions (Figure 3-1) and $^{87}\text{Sr}/^{86}\text{Sr}$ and $^{143}\text{Nd}/^{144}\text{Nd}$ ratios (Figure 3-2) that extend towards those characteristic of periodotite xenolith garnets (cf section 3.3 and Chapter 2). This suggests either that original enriched material in sub-calcic garnet host assemblages has variably dispersed over time through open system behavior or that diamond crystallization was more restricted than sub-calcic garnet crystallization and confined to the zones of greatest enrichment. In either case, more extreme concentrate garnets may remain to be analyzed. Thus, precursor evolution curves may possibly have been even steeper than indicated, with a proportionately smaller time differential between enrichment of komatiite residua and diamond crystallization.

3.7 Nature of Enriched Precursor

The overall consistency of Sm-Nd and Rb-Sr model age relationships is taken as strong support for a 3.2-3.3 Ga origin of diamonds following enrichment of residua or high pressure cumulates from 3.5 Ga komatiites. Given the restriction of sub-calcic concentrate garnets, diamonds and komatiites to the Archean cratons in southern Africa, the most likely site of sub-calcic garnet and diamond crystallization is in harzburgitic assemblages in craton root zones (Boyd & Gurney, 1982). Equilibration temperatures below 1150°C (but with a total range of 900° -1300° C and potential systematic uncertainties; Boyd & Gurney, 1980; Shee et al, 1982) derived from olivine and garnet inclusion pairs, have been used to infer sub-solidus crystallization of diamond

(Boyd & Finnerty, 1980). In addition, the striking absence of corresponding xenoliths has been attributed to the presence of disseminated magnesite which would cause disruption by decomposition during eruption (Boyd & Gurney, 1982; Wyllie et al, 1983). Furthermore, an alkali rich phase is apparently needed to account for sub-calcic garnet Rb-Sr systematics. However, neither magnesite nor an alkali host phase such as phlogopite is an obvious member of the peridotitic inclusion suite. Therefore, the mechanism of enrichment is suggested to be introduction of asthenosphere-derived alkali, LREE, CO₂ and H₂O enriched interstitial melt, which remained liquid until the time of diamond crystallization (Harte et al, 1980). Furthermore, residual interstitial melt may have persisted through time, allowing for easy diffusive exchange with unencapsulated garnet, and finally providing the means of disaggregation during sampling by kimberlite (Harte et al, 1980).

3.8 Implications for Kimberlite Compositions

The chemical and isotopic compositions of two classic types of kimberlite (basaltic and micaceous) found in southern Africa are usefully represented by those for Bultfontein and Finsch (Table 2-1; Figure 3-2; Smith, 1983). The most obvious chemical distinction between the two is alkali content. Notwithstanding alteration problems, it seems clear that the micaceous variety, known for its abundant primary groundmass phlogopite, has on average higher K and Rb concentrations and higher Rb/Sr ratios than the basaltic variety (Table 2-1; Barrett & Berg, 1975; Smith, 1983). In addition, the former apparently has higher Nb, Ta, Zr, Hf, Sc, P, Sr, REE, Th and U concentrations than the latter (Kable et al, 1975).

The inferred trace element and isotopic characteristics of sub-calcic concentrate garnet host assemblages make them attractive

candidates for the enriched component, most obviously apparent in micaceous kimberlites (Smith, 1983). While kimberlites are widely distributed in southern Africa, it is only those erupted within the boundaries of the Archean cratons which carry sub-calcic garnets and diamonds (Figure 2-1; Gurney & Harte, 1980; Boyd & Gurney, 1982). Therefore, if incorporation of sub-calcic garnet host material is involved in modifying isotopic signatures of kimberlites, it must be more significant for micaceous than for basaltic kimberlites on the cratons, and essentially absent for kimberlites off the cratons. In fact, there do not appear to be any obvious occurrences of the micaceous variety among kimberlites erupted well off the Archean cratons in southern Africa. The isotopic signatures of such non-diamondiferous kimberlites have not been determined. However, if megacrysts are derived from kimberlite at depth, their isotopic compositions require that kimberlites originate with distinctly depleted Sr and Nd isotopic characteristics analogous to those of ocean islands (Kramers et al, 1981), rather than those of a bulk earth reservoir (Basu & Tatsumoto, 1979, 1980).

Ironically, recently discovered diamond bearing kimberlites and lamproites from the Kimberley region of Western Australia (Atkinson et al, 1982; Jaques et al, 1982) appear to have even more enriched isotopic signatures (McCulloch et al, 1983) and potentially higher diamond abundances (Atkinson et al, 1982) than micaceous kimberlites from southern Africa. In addition, these intrusions occur marginal rather than interior to the broadly defined Kimberley craton (Atkinson et al, 1982). McCulloch et al (1983) propose a mixing model involving hypothetical enriched and depleted end members to account for the isotopic data. The relationships, if any, between diamonds and sub-calcic garnets for these novel

occurrences are still obscure. Nevertheless, the chemical and isotopic character of sub-calcic garnet and diamond host assemblages, linked with 3.5 Ga komatiites in southern Africa, seem appropriate for the required enriched component. Significantly, similar komatiites dated at 3.5 Ga (Hamilton et al, 1980, 1983), are preserved on the adjacent better defined Pilbara craton in Western Australia.

3.9 Conclusions

Sub-calcic garnets encapsulated by diamonds from relatively young (0.09 Ga) kimberlites in southern Africa, yield ancient Sm-Nd model ages of 3.3 ± 0.2 Ga. Associated sub-calcic garnets from kimberlite concentrate require long-term storage in enriched (high Rb/Sr, low Sm/Nd) harzburgitic assemblages that are efficiently disrupted on sampling by kimberlite. The chemistry and distribution of sub-calcic garnets indicate that diamonds formed following enrichment of residual Archean mantle such as that remaining after widespread extraction of 3.5 Ga komatiitic lavas. Assuming precursor enrichment at 3.5 Ga, sub-calcic garnets yield Rb-Sr model ages for diamond crystallization of approximately 3.2 Ga. These consistent model age relationships obviously preclude a genetic connection between diamonds and host kimberlites. Nevertheless, observed isotopic signatures of diamond-bearing kimberlites may reflect incorporation of variable proportions of the enriched component present in sub-calcic garnet and diamond host assemblages.

REFERENCES

- Ahrens L.H., Dawson J.B., Duncan A.R. and Erlank A.J. (1975) Proceedings 1st International Kimberlite Conference. Phys. Chem. Earth 9.
- Allegre C.J. (1982) Chemical geodynamics. Tectonophysics 81, 109-132.
- Allegre C.J., Brevart O., Dupre B. and Minster J.-F. (1980) Isotopic and chemical effects produced in a continuously differentiating convecting Earth mantle. Phil. Trans. R. Soc. London A 297, 447-477.
- Allegre C.J., Shimizu N. and Rousseau D. (1982) History of the continental lithosphere recorded by ultramafic xenoliths. Nature 296, 732-735.
- Allegre C.J., Hart S.R. and Minster J.-F. (1983) Chemical structure and evolution of the mantle and continents determined by inversion of Nd and Sr isotopic data. Part II. Numerical experiments and discussion. Earth Planet. Sci. Lett. in press.
- Allsopp H.L. and Barrett D.R. (1975) Rb-Sr age determinations on South African kimberlite pipes. Phys. Chem. Earth 9, 605-617.
- Allsopp H.L. and Kramers J.D. (1977) Rb-Sr and U-Pb age determinations on southern African kimberlite pipes. Extended abstracts, 2nd International Kimberlite Conference, Santa Fe, New Mexico.
- Aoki K. (1975) Origin of phlogopite and potassic richterite bearing peridotite xenoliths from South Africa. Contrib. Mineral. Petrol. 53, 145-156.
- Armstrong R.L. (1968) A model for the evolution of strontium and lead isotopes in a dynamic Earth. Rev. Geophys. Space Phys. 6, 175-199.
- Arndt N.T. and Nisbet E.G. (1982) Komatiites. 526 pp. Allen & Unwin, London.
- Atkinson W.J., Hughes F.E. and Smith C.B. (1982) A review of the kimberlitic rocks of Western Australia. Terra cognita 2, 204.
- Barrett D.R. (1975) The genesis of kimberlite and associated rocks: strontium isotope evidence. Phys. Chem. Earth 9, 637-653.
- Barrett D.R. and Berg G.W. (1975) Complementary petrographic and strontium-isotope ratio studies of South African kimberlite. Phys. Chem. Earth 9, 619-635.
- Basaltic Volcanism Study Project (1981) Basaltic volcanism on the Terrestrial Planets. 1286 pp. Pergamon, New York.
- Basu A.R. and Tatsumoto M. (1979) Samarium-neodymium systematics in kimberlites and in the minerals of garnet lherzolite inclusions. Science 205, 398-401.
- Basu A.R. and Tatsumoto M. (1980) Nd-isotopes in selected mantle-derived rocks and minerals and their implications for mantle evolution. Contrib. Mineral. Petrol. 75, 43-54.

- Beaudry B.J. and Gschneidner K.A., Jr. (1978) Preparation and basic properties of the rare earth metals. In Handbook on the Physics and Chemistry of Rare Earths (eds Gschneidner K.A., Jr. and Eyring L.) v 1 pp. 173-232. North Holland.
- Boyd F.R. (1973) A pyroxene geotherm. *Geochim. Cosmochim. Acta* 37, 2533-2546.
- Boyd F.R. and Nixon P.H. (1972) Ultramafic nodules from the Thaba Putsoa kimberlite pipe. *Carnegie Inst. Washington Yearb.* 71, 362-373.
- Boyd F.R. and Nixon P.H. (1973) Structure of the upper mantle beneath Lesotho. *Carnegie Inst. Washington Yearb.* 72, 431-445.
- Boyd F.R. and Nixon P.H. (1975) Origins of the ultramafic nodules from some kimberlites of northern Lesotho and the Monastery Mine, South Africa. *Phys. Chem. Earth* 9, 431-454.
- Boyd F.R. and Nixon P.H. (1978) Ultramafic nodules from the Kimberley pipes, South Africa. *Geochim. Cosmochim. Acta* 42, 1367-1382.
- Boyd F.R. and Meyer H.O.A. (1979a) Kimberlites, diatremes and diamonds: their geology, petrology and geochemistry. Proceedings 2nd International Kimberlite Conference. AGU, Washington, D.C.
- Boyd F.R. and Meyer H.O.A. (1979b) The mantle sample: inclusions in kimberlites and other volcanics. Proceedings 2nd International Kimberlite Conference. AGU, Washington, D.C.
- Boyd F.R. and Finnerty A.A. (1980) Conditions of origin of natural diamonds of peridotite affinity. *J. Geophys. Res.* 85, 6911-6918.
- Boyd F.R. and Gurney J.J. (1982) Low-calcium garnets: keys to craton structure and diamond crystallization. *Carnegie Inst. Washington Yearb.* 81, 261-267.
- Brooks C., Hart S.R., Hofmann A. and James D.E. (1976a) Rb-Sr mantle isochrons from oceanic regions. *Earth Planet. Sci. Lett.* 32, 51-61.
- Brooks C. James D.E. and Hart S.R. (1976b) The role of ancient lithosphere in young continental volcanism. *Science* 193, 1086-1094.
- Brooks C. and Hart S.R. (1978) Rb-Sr mantle isochrons and variations in the chemistry of Gondwanaland's lithosphere. *Nature* 271, 220-223.
- Burke K.C. and Wilson J.T. (1976) Hot spots on the Earth's surface. *Sci. Am* 235, 46-57.
- Carter S.R. Evensen N.M., Hamilton P.J. and O'Nions R.K. (1978) Neodymium and strontium isotope evidence for crustal contamination of continental volcanics. *Science* 202, 743-747.
- Cerrai E. and Testa C. (1963) Separation of rare earths by means of small columns of Kel-F supporting di (2-ethylhexyl) orthophosphoric acid. *J. Inorg. Nucl. Chem.* 25, 1045-1050.

- Chase C.G. (1981) Oceanic island Pb: two stage histories and mantle evolution. *Earth Planet Sci. Lett.* 52, 277-284.
- Chave A.D. (1979) Lithospheric structure of the Walvis Ridge from Rayleigh wave dispersion. *J. Geophys. Res.* 84, 6840-6848.
- Chen J. (1971) Petrology and chemistry of garnet lherzolite nodules in kimberlite from South Africa. *Am. Mineralogist* 56, 2098-2110.
- Davis G.L., Krogh T.E. and Erlank A.J. (1976) The ages of zircons from kimberlites from South Africa. *Carnegie Inst. Washington Yearb.* 75, 821-824.
- Davis, G.L. (1977) The ages and uranium contents of zircons from kimberlites and associated rocks. *Carnegie Inst. Washington Yearb.* 76, 631-635.
- Dawson J.B. and Stephens W.E. (1975) Statistical classification of garnets from kimberlite and associated xenoliths. *J. Geology* 83, 589-607.
- Dawson J.B., Gurney J.J. and Lawless P.J. (1975) Paleogeothermal gradients derived from xenoliths in kimberlite. *Nature* 257, 299-300.
- Dawson J.B. and Smith J.V. (1977) The MARID (mica-amphibole-rutile-ilmenite-diopside) suite of xenoliths in kimberlite. *Geochim. Cosmochim. Acta* 41, 309-323.
- DePaolo D.J. (1980) Crustal growth and mantle evolution: inferences from models of element transport and Nd and Sr isotopes. *Geochim. Cosmochim. Acta* 44, 1185-1196.
- DePaolo D.J. and Wasserburg G.J. (1976a) Nd isotopic variations and petrogenetic models. *Geophys. Res. Lett.* 3, 249-252.
- DePaolo D.J. and Wasserburg G.J. (1976b) Inferences about magma sources and mantle structure from variations in $^{143}\text{Nd}/^{144}\text{Nd}$. *Geophys. Res. Lett.* 3, 743-746.
- Detrick R.S. and Watts A.B. (1979) An analysis of isostasy in the world's oceans: part 3 - aseismic ridges. *J. Geophys Res.* 84, 3637-3653.
- Dingle R.V. and Simpson E.S.W. (1976) The Walvis Ridge; a review. In: *Geodynamics: Progress and prospects* (ed. Drake C.L.) 160-176. AGU, Washington, D.C.
- Dosso L., Vidal P., Cantagrel J.M., Lameyre, J., Marot A. and Zimine S. (1979) Kerguelen: continental fragment or oceanic island?: petrology and isotopic geochemistry evidence. *Earth Planet. Sci. Lett.* 43, 46-60.
- Dosso L. and Murthy V.R. (1980) A Nd isotopic study of the Kerguelen islands: inferences on enriched oceanic mantle sources. *Earth Planet. Sci. Lett.* 48, 268-276.

- Dupre B. and Allegre C.J. (1980) Pb-Sr-Nd isotopic correlation and the chemistry of the North Atlantic mantle. *Nature* 286, 17-22.
- Dupre B. and Allegre C.J. (1983) Pb-Sr isotope variation in Indian Ocean basalts and mixing phenomena. *Nature* 303, 142-146.
- Erlank A.J. (1973) Kimberlite potassic richterite and the distribution of potassium in the mantle. Extended abstracts, 1st International Kimberlite Conference, Cape Town, 103-106.
- Erlank A.J. and Reid D.L. (1974) Geochemistry, mineralogy and petrology of basalts, Leg 25, DSDP. In: Simpson E.S.W., Schlich R. et al., Initial Reports of the Deep Sea Drilling Project 25, 543-551. U.S. Government Printing Office, Washington, D.C.
- Erlank A.J. and Kable E.J.D. (1976) The significance of incompatible elements in mid-Atlantic ridge basalts from 45°N with particular reference to Zr/Nb. *Contrib. Mineral. Petrol.* 54, 281-291.
- Erlank A.J. and Rickard R.S. (1977) Potassic richterite-bearing peridotites from kimberlite and the evidence they provide for upper mantle metasomatism. Extended abstracts, 2nd International Kimberlite Conference, Santa Fe, N.M.
- Erlank A.J. and Shimizu N. (1977) Strontium and strontium isotope distributions in some kimberlite nodules and minerals. Extended abstracts, 2nd International Kimberlite Conference, Santa Fe, N.M.
- Erlank A.J., Allsopp H.L., Duncan A.R. and Bristow J.W. (1980) Mantle heterogeneity beneath southern Africa: evidence from the volcanic record. *Phil. Trans. R. Soc. London* A297, 295-307.
- Erlank A.J., Allsopp H.L., Hawkesworth C.J. and Menzies M.A. (1982) Chemical and isotopic characterization of upper mantle metasomatism in peridotite nodules from the Bultfontein kimberlite. *Terra cognita* 2, 261-263.
- Gast P.W. (1968) Trace element fractionation and the origin of tholeiitic and alkaline magma types. *Geochim. Cosmochim. Acta* 32, 1057-1086.
- Goetze C. (1975) Sheared lherzolites: from the point of view of rock mechanics. *Geology* 3, 172-173.
- Goslin J. and Sibuet J.-C. (1975) Geophysical study of the easternmost Walvis Ridge, South Atlantic: deep structure. *Geol. Soc. Amer. Bull.* 86, 1713-1724.
- Green D.H., Nicholls I.A., Viljoen M. and Viljoen R. (1975) Experimental demonstration of the existence of peridotitic liquids in earliest Archean magmatism. *Geology* 2, 11-14.
- Gurney J.J. and Switzer G.S. (1973) The discovery of garnets closely related to diamonds in the Finsch pipe, South Africa. *Contrib. Mineral. Petrol.* 39, 103-116.

- Gurney J.J., Harris J.W. and Rickard R.S. (1979) Silicate and oxide inclusions in diamonds from the Finsch kimberlite pipe. In: Kimberlites, diatremes and diamonds: their geology, petrology and geochemistry. (eds. Boyd F.R. and Meyer H.O.A.), 1-15. AGU, Washington, D.C.
- Gurney J.J. and Harte B. (1980) Chemical variations in upper mantle nodules from southern African kimberlites. Phil. Trans. R. Soc. London A297, 273-293.
- Haggerty S.E., Smyth J.R., Erlank A.J., Rickard R.S. and Danchin R.V. (1983a) Lindsleyite (Ba) and mathiasite (K): two new chromium-titanates in the crichtonite series from the upper mantle. Am. Mineralogist 68, 494-505.
- Haggerty S.E., Raber E. and Naeser C.W. (1983b) Fission track dating of kimberlitic zircons. Earth Planet. Sci. Lett. 63, 41-50.
- Hamilton P.J., Evenson N.M., O'Nions R.K., Smith H.S. and Erlank A.J. (1979) Sm-Nd dating of Onverwacht Group volcanics, southern Africa. Nature 279, 298-300.
- Hamilton P.J., Evenson N.M., O'Nions R.K., Glikson A.Y. and Hickman A.H. (1980) Sm-Nd dating of Warrawoona Group volcanics, Pilbara Block, Western Australia. Abstract, 2nd International Archaean Symposium, Perth, 11.
- Hamilton P.J., O'Nions R.K., Bridgwater D. and Nutman A. (1983) Sm-Nd studies of Archaean metasediments and metavolcanics from West Greenland and their implications for the Earth's early history. Earth Planet. Sci. Lett. 62, 263-272.
- Hanson G.N. (1977) Geochemical evolution of the sub-oceanic mantle. J. Geol. Soc. Lond. 134, 235-253.
- Harris J.W. and Gurney J.J. (1979) Inclusions in diamond. In: The properties of diamond (ed. Field J.E.), 555-591. Academic, London.
- Harris J.W., Hawthorne J.B. and Oosterveld M.M. (1979) Regional and local variations in the characteristics of diamonds from some southern African kimberlites. In: Kimberlites, diatremes and diamonds: their geology, petrology and geochemistry (eds. Boyd F.R. and Meyer H.O.A.), 27-41. AGU, Washington, D.C.
- Harris J.W., Hawthorne J.B. and Oosterveld M.M. (1982) Diamond characteristics of the De Beers Pool mines, Kimberley, South Africa. Terra cognita 2, 200.
- Hart S.R. (1969) K, Rb, Cs contents and K/Rb, K/Cs ratios of fresh and altered submarine basalts. Earth Planet. Sci. Lett. 6, 295-303.
- Hart S.R. (1971) K, Rb, Cs, Sr and Ba contents and Sr isotopic ratios of ocean floor basalts. Phil. Trans. R. Soc. London A268, 573-587.

- Hart S.R. (1976) LIL-element geochemistry, Leg 34 basalts. In Yeats R.S., Hart S.R. et al., Initial Report of the Deep Sea Drilling Project 34, 283-288. U.S. Government printing Office, Washington, D.C.
- Hart, S.R. (1984) The DUPALL anomaly: a large-scale isotopic mantle anomaly in the southern hemisphere. *Nature*, submitted.
- Hart S.R., Erlank A.J. and Kable E.J.D. (1974) Sea floor basalt alteration: some chemical and Sr isotopic effects. *Contrib. Mineral. Petrol.* 44, 219-230.
- Hart S.R. and Brooks C. (1977) Geochemistry and evolution of early Precambrian mantle. *Contrib. Mineral. Petrol.* 61, 109-128.
- Hart S.R. and Staudigel H. (1978) Oceanic crust: age of hydrothermal alteration. *Geophys. Res. Lett.* 5, 1009-1012.
- Harte B. (1977) Rock nomenclature with particular reference to deformation and recrystallization textures in olivine-bearing xenoliths. *J. Geology* 85, 279-288.
- Harte B. (1978) Kimberlite nodules, upper mantle petrology, and geotherms. *Phil. Trans. R. Soc. London* A288, 487-500.
- Harte B. (1983) Mantle peridotites and processes -the kimberlite sample In: Continental basalts and mantle xenoliths (eds. Hawkesworth C.J. and Norry M.J.), 46-91. Shiva, U.K.
- Harte B., Cox K.G. and Gurney J.J. (1975) Petrography and geological history of upper mantle xenoliths from the Matsoku kimberlite pipe. *Phys. Chem. Earth* 9, 477-506.
- Harte B., Gurney J.J. and Harris J.W. (1980) The formation of peridotitic suite inclusions in diamonds. *Contrib. Mineral. Petrol.* 72, 181-190.
- Hawkesworth C.J., Kramers J.D. and Miller R. McG. (1981) Old model Nd ages in Namibian Pan-African rocks. *Nature* 289, 278-282.
- Hawkesworth C.J. and Norry M.J. (1983) Continental basalts and mantle xenoliths. Shiva, U.K.
- Hawkesworth C.J., Erlank A.J., Marsh J.S., Menzies M.A. and van Calsteren P. (1983) Evolution of the continental lithosphere: evidence from volcanics and xenoliths in southern Africa. In: Continental basalts and mantle xenoliths (eds. Hawkesworth C.J. and Norry M.J.) 111-138. Shiva, U.K.
- Hekinian R. (1972) Volcanics from the Walvis Ridge. *Nature* 239, 91-93.
- Hofmann A.W. and Hart S.R. (1978) An assessment of local and regional isotopic equilibrium in the mantle. *Earth Planet. Sci. Lett.* 38, 44-62.
- Hofmann A.W. and White W.M. (1982) The role of subducted oceanic crust in mantle evolution. *Earth Planet. Sci. Lett.* 57, 421-436.

- Humphris S.E. and Thompson G. (1982) A geochemical study of rocks from the Walvis Ridge, South Atlantic. *Chem. Geol.* 36, 253-274.
- Jacobsen S.B. and Wasserburg G.J. (1979) The mean age of mantle and crustal reservoirs. *J. Geophys. Res.* 84, 7411-7427.
- Jacobsen S.B. and Wasserburg G.J. (1980) Sm-Nd isotopic evolution of chondrites. *Earth Planet. Sci. Lett.* 50, 139-155.
- Jahn B.-M. and Shih C.-Y. (1974) On the age of the Onverwacht Group, Swaziland Sequence, South Africa. *Geochim. Cosmochim. Acta* 38, 873-885.
- Jaques A.L., Gregory G.P., Lewis J.D. and Ferguson J. (1982) The ultrapotassic rocks of the West Kimberley region, Western Australia, and a new class of diamondiferous kimberlite. *Terra cognita* 2, 251-252.
- Jones A.P., Smith J.V. and Dawson J.B. (1982) Mantle metasomatism in 14 veined peridotites from Bultfontein mine, South Africa. *J. Geology* 90, 435-453.
- Kable E.J.D. (1972) Some aspects of the geochemistry of selected elements in basalts and associated lavas. Ph.D. thesis. University of Cape Town.
- Kable E.J.D., Fesq H.W. and Gurney J.J. (1975) The significance of the interelement relationships of some minor and trace elements in South African kimberlites. *Phys. Chem. Earth* 9, 709-734.
- Kramers J.D. (1977) Lead and strontium isotopes in Cretaceous kimberlites and mantle-derived xenoliths from southern Africa. *Earth Planet. Sci. Lett.* 34, 419-431.
- Kramers J.D. (1979) Lead, uranium, strontium, potassium and rubidium in inclusion-bearing diamonds and mantle-derived xenoliths from Southern Africa. *Earth Planet. Sci. Lett.* 42, 58-70.
- Kramers J.D., Smith C.B., Lock N.P., Harmon R.S. and Boyd F.R. (1981) Can kimberlites be generated from an ordinary mantle? *Nature* 291, 53-56.
- Kramers J.D. and Smith C.B. (1983) A feasibility study of U-Pb and Pb-Pb dating of kimberlites using groundmass mineral fractions and whole-rock samples. *Isotope Geoscience* 1, 23-38.
- Kramers J.D., Roddick J.C.M. and Dawson J.B. (1983) Trace element and isotope studies on veined, metasomatic and "MARID" xenoliths from Bultfontein, South Africa. *Earth Planet. Sci. Lett.* 65, 90-106.
- Langmuir C.H., Vocke R.D., Hanson G.N. and Hart S.R. (1978) A general mixing equation with applications to Icelandic basalts. *Earth Planet. Sci. Lett.* 37, 380-392.
- Lawless P.J. (1978) Some aspects of the mineral chemistry of the peridotite xenolith suite from the Bultfontein diamond mine, Kimberley, South Africa. Ph.D. thesis. University of Cape Town.

- le Roex A.P., Erlank A.J. and Needham H.D. (1981) Geochemical and mineralogical evidence for the occurrence of at least three distinct magma types in the Famous region. *Contrib. Mineral. Petrol.* 77, 24-37.
- Lloyd F.E. and Bailey D.K. (1975) Light element metasomatism of the continental mantle: the evidence and the consequences. *Phys. Chem. Earth* 9, 389-446.
- Lugmair G.W. and Marti K. (1978) Lunar initial $^{143}\text{Nd}/^{144}\text{Nd}$: differential evolution of the lunar crust and mantle. *Earth Planet. Sci. Lett.* 39, 349-357.
- MacGregor I.D. (1975) Petrologic and thermal structure of the upper mantle beneath South Africa in the Cretaceous. *Phys. Chem. Earth* 9, 455-466.
- Manhes G., Minster J.-F. and Allegre C.J. (1978) Comparative uranium-thorium-lead and rubidium-strontium of St. Severin amphoterite: consequences for early solar system chronology. *Earth Planet. Sci. Lett.* 39, 14-24.
- McCulloch M.T., Jaques A.L., Nelson D.R. and Lewis J.D. (1983) Nd and Sr isotopes in kimberlites and lamproites from Western Australia: an enriched mantle origin. *Nature* 302, 400-403.
- McWilliams M.O. and Kroner A. (1981) Paleomagnetism and tectonic evolution of the Pan-African Damara belt, southern Africa. *J. Geophys. Res.* 86, 5147-5162.
- Mercier J.C. (1979) Peridotite xenoliths and the dynamics of kimberlite intrusion. In: *The mantle sample: inclusions in kimberlites and other volcanics* (eds. Boyd F.R. and Meyer H.O.A.), 197-212. AGU, Washington, D.C.
- Menzies M. and Murthy V.R. (1980) Enriched mantle: Nd and Sr isotopes in diopsides from kimberlite nodules. *Nature* 283, 634-636.
- Meyer H.O.A. and Tsai H.-M. (1976) The nature and significance of mineral inclusions in natural diamond: a review. *Miner. Sci. Eng.* 8, 242-261.
- Milledge H.J., Mendelssohn M.J., Seal M., Rouse J.E., Swart P.K. and Pillinger C.T. (1983) Carbon isotopic variation in spectral type II diamonds. *Nature* 303, 791-792.
- Minster J.-F., Ricard L.-P. and Allegre C.J. (1979) ^{87}Rb - ^{87}Sr chronology of enstatite meteorites. *Earth Planet. Sci. Lett.* 44, 420-440.
- Moore T.C., Rabinowitz P.D., Boersma A., Borella P.E., Chave A.D., Duee G., Futterer D.K., Jiang M.-J., Kleinert K., Lever A., Manivit H., O'Connell S., Richardson S.H. and Shackleton N.J. (1983) The Walvis Ridge transect, Deep Sea Drilling Project Leg 74: the geological evolution of an oceanic plateau in the South Atlantic Ocean. *Geol. Soc. Am. Bull.* 94, 907-925.
- Morgan J. (1971) Convection plumes in the lower mantle. *Nature* 230,

- Morgan J. (1972) Plate motions and deep mantle convection. *Geol. Soc. Am. Memoir* 132, 7-22.
- Nixon P.H. (1973) Lesotho kimberlites. 350 pp. Lesotho National Development Corporation, Maseru.
- Nixon P.H. (1973) The geology of Mothae, Solane, Thaba Putsoa and Blow 13. In: *Lesotho kimberlites* (ed. Nixon P.H.), 39-56. Lesotho National Development Corporation, Maseru.
- Nixon P.H. and Boyd F.R. (1973) Petrogenesis of the granular and sheared ultrabasic nodule suite in kimberlites. In: *Lesotho kimberlites* (ed. Nixon P.H.), 48-56. Lesotho National Development Corporation, Maseru.
- Nixon P.H., Rogers N.W., Gibson I.L. and Grey A. (1981) Depleted and fertile mantle xenoliths from southern African kimberlites. *Ann. Rev. Earth Planet. Sci.* 9, 285-309.
- O'Nions R.K., Hamilton P.J. and Evensen N.M. (1977) Variations in $^{143}\text{Nd}/^{144}\text{Nd}$ and $^{87}\text{Sr}/^{86}\text{Sr}$ ratios in oceanic basalts. *Earth Planet. Sci. Lett.* 34, 13-22.
- O'Nions R.K., Carter S.R., Cohen R.S. Evensen N.M. and Hamilton P.J. (1978) Pb, Nd and Sr isotopes in oceanic ferromanganese deposits and ocean floor basalts. *Nature* 273, 435-438.
- O'Nions R.K., Carter S.R., Evensen N.M. and Hamilton P.J. (1978) Sr-and Nd-isotope study of ultramafic xenoliths: evolution of sub-cratonic mantle. Abstract, EOS 59, 399.
- O'Nions R.K., Evensen N.M. and Hamilton P.J. (1979) Geochemical modelling of mantle differentiation and crustal growth. *J. Geophys. Res.* 84, 6091-6101.
- Ozima M. and Zashu S. (1983) Primitive helium in diamonds. *Science* 219, 1067-1068.
- Ozima M., Zashu S. and Nitoh O. (1983) $^3\text{He}/^4\text{He}$ ratio, noble gas abundance and K-Ar dating of diamonds - an attempt to search for the records of early terrestrial history. *Geochim. Cosmochim. Acta* 47, 2217-2224.
- Powell J.E. (1978) Separation chemistry. In: *Handbook on the Physics and Chemistry of Rare Earths* (eds. Gschneidner K.A., Jr. and Eyring L.) V. 3 pp. 81-109. North Holland.
- Rabinowitz P.D. (1984) In: Moore T.C., Rabinowitz P.D. et al, *Initial Reports of the Deep Sea Drilling Project 74*, in press. U.S. Government Printing Office, Washington, D.C.
- Rabinowitz P.D. and LaBrecque J. (1979) The Mesozoic South Atlantic Ocean and evolution of its continental margins. *J. Geophys. Res.* 84, 5973-6002.

- Rabinowitz P.D. and Simpson E.S.W. (1979) Results of IPOD site surveys aboard R/V Thomas B. Davies: Walvis Ridge survey: Lamont-Doherty Geological Observatory Technical Report. 40 pp. JOI Inc.
- Richard P., Shimizu N. and Allegre C.J. (1976) $^{143}\text{Nd}/^{144}\text{Nd}$, A natural tracer: an application to oceanic basalts. *Earth Planet. Sci. Lett.* 31, 269-278.
- Richardson S.H., Hart S.R. and Staudigel H. (1980) Vein mineral ages of old oceanic crust. *J. Geophys. Res.* 85, 7195-7200.
- Richardson S.H., Erlank A.J. and Shimizu N. (1982) Nd isotopic disequilibrium in garnet peridotites from the Bultfontein kimberlite and implications for mantle metasomatic component addition. *Terra cognita* 2, 231.
- Richardson S.H., Erlank A.J., Reid D.L. and Duncan A.R. (1984) Major and trace element and Nd and Sr isotope geochemistry of basalts from the DSDP Leg 74 Walvis Ridge transect. In: Moore T.C., Rabinowitz P.D. et al., Initial Reports of the Deep Sea Drilling Project 74, in press. U.S. Government Printing Office, Washington, D.C.
- Ringwood A.E. (1977) Synthesis of pyrope-knorringite solid solution series. *Earth Planet. Sci. Lett.* 36, 443-448.
- Russel R.D. (1972) Evolutionary model for lead isotopes in conformable ores and in oceanic volcanics. *Rev. Geophys. Space Phys.* 10, 529.
- Schilling J.G. (1971) Sea-floor evolution: rare-earth evidence. *Phil. Trans. R. Soc. London* A268, 663-706.
- Schoonover R.M. and Jones F.E. (1981) Air buoyancy correction in high-accuracy weighing on analytical balances. *Anal. Chem.* 53, 900-902.
- Shee S.R., Gurney J.J. and Robinson D.N. (1982) Two diamond-bearing peridotite xenoliths from the Finsch kimberlite, South Africa. *Contrib. Mineral. Petrol.* 81, 79-87.
- Shimizu N. (1975a) Geochemistry of ultramafic inclusions from Salt Lake crater, Hawaii and from southern African kimberlites. *Phys. Chem. Earth* 9, 655-669.
- Shimizu N. (1975b) Rare earth elements in garnets and clinopyroxenes from garnet lherzolite nodules in kimberlites. *Earth Planet. Sci. Lett.* 25, 26-32.
- Shimizu N. (1981) Trace element incorporation into growing augite phenocryst. *Nature* 289, 575-577
- Shimizu N. and Allegre C.J. (1978) Geochemistry of transition elements in garnet lherzolite nodules in kimberlites. *Contrib. Mineral. Petrol.* 67, 41-50.

- Skinner E.M.W. and Clement C.R. (1979) Mineralogical classification of southern African kimberlites. In: Kimberlites, diatremes and diamonds: their geology, petrology and geochemistry (eds. Boyd F.R. and Meyer H.O.A.), 129-139. AGU, Washington, D.C.
- Smith C.B. (1983) Pb, Sr and Nd isotopic evidence for sources of southern African Cretaceous kimberlites. *Nature* 304, 51-54.
- Smith H.S. and Erlank A.J. (1978) Proceedings 1978 Archaean Geochemistry Conference (eds. Smith I.E.M. and Williams J.G.). University of Toronto Press.
- Sobolev N.V. (1977) Deep-seated inclusions in kimberlites and the problem of the composition of the upper mantle (english transl. by Brown D.A.) 279 pp. AGU, Washington, D.C.
- Sobolev N.V., Lavrent'ev Y.G., Pokhilenko N.P. and Usova L.V. (1973) Chrome-rich garnets from the kimberlites of Yakutia and their parageneses. *Contrib. Mineral. Petrol.* 40, 39-52.
- Sobolev N.V., Galimov E.M., Ivanovskaya N.N. and Yefimova E.S. (1979) Isotopic composition of carbon from diamonds containing crystalline inclusions (Russian). *Dokl. Akad. Nauk. SSSR* 249, 1217-1220.
- Staudigel H., Hart S.R. and Richardson S.H. (1981) Alteration of the oceanic crust: processes and timing. *Earth Planet. Sci. Lett.* 52, 311-327.
- Steiger R.H. and Jager E. (1977) IUGS Subcommittee on Geochronology: convention on the use of decay constants in geochronology and cosmochronology. *Earth Planet. Sci. Lett.* 36, 359.
- Strelow F.W.E. and Toerien F. von S. (1966) Separation of lead (II) from bismuth (III), thallium (III), cadmium (II), mercury (II), gold (III), platinum (IV), palladium (II), and other elements by anion exchange chromatography. *Anal. Chem.* 38, 545-548.
- Sun S.-S. (1980) Lead isotopic study of young volcanic rocks from mid-ocean ridges, ocean islands and island arcs. *Phil. Trans. R. Soc. London* A297, 409-445.
- Tatsumoto M., Hedge C.E. and Engel A.E.J. (1965) Potassium, rubidium, strontium, thorium, uranium and the ratio of Sr-87 to Sr-86 in oceanic tholeiitic basalt. *Science* 150, 886-888.
- Tatsumoto M. (1966) Genetic relations of oceanic basalts as indicated by lead isotopes. *Science* 153, 1094-1101.
- Tatsumoto M., Knight R.J. and Allegre C.J. (1973) Time differences in the formation of meteorites as determined by the ratio of lead-207 to lead-206. *Science* 180, 1279-1283.
- Tatsumoto M. (1978) Isotopic composition of lead in oceanic basalt and its implication to mantle evolution. *Earth Planet. Sci. Lett.* 38, 63-87.

- van der Linden W.J.M. (1980) Walvis Ridge, a piece of Africa? *Geology* 8, 417-421.
- Viljoen M.J., Viljoen R.P. and Pearton T.N. (1982) The nature and distribution of Archaean komatiite volcanics in South Africa. In: *Komatiites* (eds. Arndt N.T. and Nisbet E.G.), 53-79. Allen and Unwin, London.
- Wapstra A.H. and Bos K. (1977) The 1977 atomic mass evaluation in four parts: Part 1. Atomic mass table. *At. Data Nucl. Data Tables* 191, 177-214.
- Wasserburg G.J. and DePaolo (1979) Models of earth structure inferred from neodymium and strontium isotopic abundances. *Proc. Nat. Acad. Sci.* 76, 3594-3598.
- Wasserburg G.J., Jacobsen S.B., DePaolo D.J., McCulloch M.T. and Wen T. (1981) Precise determination of Sm/Nd ratios, Sm and Nd isotopic abundances in standard solutions. *Geochim. Cosmochim. Acta* 45, 2311-2323.
- Wilson J.T. (1963) Evidence from islands on the spreading of ocean floors. *Nature* 197, 536-538.
- White W.M. (1979) Pb isotope geochemistry of the Galapagos Islands. *Carnegie Inst. Washington Yearb.* 78, 331-335.
- White W.M. and Hofmann A.W. (1978) Geochemistry of the Galapagos Islands: implications for mantle geodynamics and evolution. *Carnegie Inst. Washington Yearb.* 77, 596-606.
- Wood D.A. (1979) A variably veined sub-oceanic upper mantle - genetic significance for mid-ocean ridge basalts from geochemical evidence. *Geology* 7, 499-503.
- Wyllie P.J., Huang W.-L., Otto J. and Byrnes A.P. (1983) Carbonation of peridotites and decarbonation of siliceous dolomites represented in the system CaO-MgO-SiO₂-CO₂ to 30 k bar. *Tectonophysics*, submitted.
- York D. (1966) Least-squares fitting of a straight line. *Can J. Phys.* 44, 1079-1086.
- York D. (1969) Least-squares fitting of a straight line with correlated errors. *Earth Planet. Sci. Lett.* 5, 320-324.
- Zindler A., Hart S.R., Frey F.A. and Jakobsson S.P. (1979) Nd and Sr isotope ratios and rare earth element abundances in Reykjanes Peninsula basalts: evidence for mantle heterogeneity beneath Iceland. *Earth Planet. Sci. Lett.* 45, 249-262.
- Zindler A. (1980) Geochemical processes in the Earth's mantle and the nature of crust-mantle interactions: evidence from studies of Nd and Sr isotope ratios in mantle-derived igneous rocks and lherzolite nodules. Ph.D. thesis, M.I.T.
- Zindler A. (1982) Nd and Sr isotopic studies of komatiites and related rocks. In: *Komatiites* (eds. Arndt N.T. and Nisbet E.G.), 399-420. Allen & Unwin, London.

APPENDIX

PRECISE CALIBRATION OF MIXED Sm-Nd SPIKE SOLUTIONS FOR DETERMINATION
OF Sm/Nd AND Nd ISOTOPE RATIOS ON TOTALLY SPIKED SAMPLES

Contents

1. Introduction
2. Normal Nd and Sm isotopic compositions
3. Spike solution design and genealogy
4. Spike Nd and Sm isotopic compositions
5. Normal standard solution design and construction
 - 5.1 Specifications
 - 5.2 Metal gravimetry
 - 5.3 Dissolution
 - 5.4 Solution gravimetry
 - 5.5 Buoyancy corrections
6. Standard solution dilution
 - 6.1 Specifications
 - 6.2 Solution gravimetry
7. Spike solution concentration calibration
 - 7.1 Specifications
 - 7.2 Solution gravimetry
 - 7.3 Separation chemistry and mass spectrometry
 - 7.4 Calibration results
8. Sample spiking

1. Introduction

The rationale for determining elemental and isotopic ratios for geochronologically significant systems on totally spiked samples, as opposed to separate powder or liquid aliquots, has long been established. Aliquoting can result in errors in absolute concentrations and concentration ratios in instances where samples or derivative solutions are inhomogeneous at the splitting stage. Total spiking of samples effectively eliminates such errors (provided complete dissolution is attained) while allowing for a greater economy of effort in chemistry and mass spectrometry. However, the accuracy of measured concentrations and now also natural isotope ratios still depends on the calibre of the spike (mixed tracer) solution used. Precise calibration of the spike solution must be performed using absolute gravimetric standards whose purity is the ultimate determinant of accuracy. The fundamental aim of such an exercise is the systematic refinement of isochron age and related evolutionary parameter determinations on natural systems.

The following account documents the characterization and precise calibration of two mixed Sm-Nd spike solutions in current use at both LDGO and MIT for the determination of Sm/Nd and $^{143}\text{Nd}/^{144}\text{Nd}$ ratios on totally spiked samples. The emphasis is on the excruciating detail of laboratory procedures for controlled preparation of a mixed Sm-Nd normal standard solution from ultrapure Sm and Nd metals and subsequent use for precise calibration of mixed Sm-Nd spike solutions. This follows similar efforts in a few other laboratories as documented, for example, by Wasserburg et al. (1981). The major points of departure from procedures in the latter comprehensive account are the initial combination of Sm and Nd metals in a primary mixed Sm-Nd normal solution and the final application of buoyancy corrections which are not negligible as claimed.

The overall effort was motivated by both supply and the demands of analytical progress. Supply was interrupted by the 1982 demise of a previous Sm-Nd spike which required aliquoting. Progress demanded total spiking of ever smaller mantle samples with no room for error and no nanograms to spare.

2. Normal Nd and Sm isotopic compositions

No systematic determination of the abundances of all seven isotopes of normal Nd and normal Sm has been undertaken at MIT. Instead, the compositions used at LDGO (Table A-1) have been adopted. Nd isotopic compositions are corrected for mass discrimination with $^{146}\text{Nd}/^{144}\text{Nd}=0.7219$, the average for triple filament runs of the metal species Nd^+ (O'Nions et al, 1977). Single filament runs of Nd as the oxide species NdO^+ are consistently more fractionated (relative to the above value), resulting in an average $^{146}\text{Nd}/^{144}\text{Nd}$ close to 0.7241 (Wasserburg et al, 1981). Regardless of the absolute value, nominal differences in equivalent data obtained using alternate reference values become transparent after an appropriate normalization. After such a normalization only minor discrepancies are apparent in a comparison (Table A-1) of the normal Nd and Sm compositions in use here and at CIT (Wasserburg et al, 1981). At MIT Nd and Sm are both run on double filaments as Nd^+ and Sm^+ . The absence of major NIMA-B mass spectrometer measurement artifacts was established by measurements of reference isotope ratios (used in concentration determinations), which are within in-run errors ($2\sigma_{\text{mean}}$) of those adopted (BCR-1 Nd: $^{150}\text{Nd}/^{146}\text{Nd} = 0.32745 \pm 2$ for $^{146}\text{Nd}/^{144}\text{Nd} = 0.7219$; SPEX Sm_2O_3 : $^{149}\text{Sm}/^{152}\text{Sm} = 0.51687 \pm 2$ for $^{147}\text{Sm}/^{152}\text{Sm} = 0.56081$). The average $^{143}\text{Nd}/^{144}\text{Nd}$ for normal Nd from the USGS standard rock BCR-1 measured on NIMA-B is 0.512622 ± 30 (2σ , $N=9$; see also section 8). To facilitate comparison

TABLE A-1 Normal Nd and Sm isotopic compositions

| Nd* | $\frac{142}{146}$ | $\frac{143}{146}$ | $\frac{144}{146}$ | $\frac{145}{146}$ | $\frac{148}{146}$ | $\frac{150}{146}$ |
|--------|-------------------|-------------------|-----------------------|-----------------------|-------------------|-------------------|
| | LDGO/MIT | 1.581565 | (0.710126)** | $\cong 1.385233\dots$ | 0.482601 | 0.334645 |
| CIT*** | 1.581697 | (0.710126)** | $\cong 1.385233\dots$ | 0.482639 | 0.334642 | 0.327494 |
| Sm | $\frac{144}{147}$ | $\frac{148}{147}$ | $\frac{149}{147}$ | $\frac{150}{147}$ | $\frac{152}{147}$ | $\frac{154}{147}$ |
| | LDGO/MIT | 0.20510 | 0.74972 | 0.92158 | 0.49218 | $\cong 1.78314$ |
| CIT*** | 0.20504 | 0.74970 | 0.92160 | 0.49213 | 1.78308 | 1.51704 |

*Corrected for mass discrimination with $^{146}\text{Nd}/^{144}\text{Nd} = 0.7219$
(O'Nion's et al, 1977)

**Equivalent to $^{143}\text{Nd}/^{144}\text{Nd} = 0.51264$ for BCR-1 (Dosso and Murthy,
1980; Wasserburg et al, 1981)

***Recalculated from Wasserburg et al (1981)

with data from other labs, sample $^{143}\text{Nd}/^{144}\text{Nd}$ ratios are now routinely normalized to a BCR-1 reference value of 0.51264. This follows the practice initiated by Dosso and Murthy (1980), and rationalized by Wasserburg et al (1981), with measured BCR-1 values indistinguishable from the adopted present-day average chondritic value (0.512638 using $^{146}\text{Nd}/^{144}\text{Nd} = 0.7219$).

For convenience, adopted isotopic compositions are also given in fractional atomic abundance form in Table A-3 along with elemental atomic weights, calculated using individual isotope atomic masses from the 1977 Atomic Mass Evaluation (Wapstra and Bos, 1977). For a natural Sm-Nd system with a present day $^{143}\text{Nd}/^{144}\text{Nd}$ ratio of 0.51264, the parent-daughter ratio, $^{147}\text{Sm}/^{144}\text{Nd}$, is related to the Sm/Nd atomic and weight ratios by

$$\begin{aligned} \left(\frac{^{147}\text{Sm}}{^{144}\text{Nd}} \right)_{\text{atomic}} &= 0.630188 \left(\frac{\text{Sm}}{\text{Nd}} \right)_{\text{atomic}} \\ &= 0.604514 \left(\frac{\text{Sm}}{\text{Nd}} \right)_{\text{weight}} \end{aligned}$$

These factors are respectively 0.059 and 0.064% lower than the corresponding values at CIT (Wasserburg et al, 1981) with differences largely attributable to the alternative normalization procedures used (see also Hamilton et al, 1983).

For simplicity, a linear law has been used to correct for instrumental mass fractionation in all mass spectrometer measurements in this laboratory. Systematic discrepancies introduced by the use of this law as compared to the exponential law, for example, are barely significant for Nd (less than 0.003% per AMU) at the extremes of fractionation observed (cf. extensive discussion in Wasserburg et al, 1981). An exact description of instrumental mass fractionation has yet to be formulated and may well be unattainable (Hart and Zindler, in prep).

3. Spike solution design and genealogy

For Nd, a 96% pure ^{150}Nd tracer was chosen because ^{150}Nd is the least abundant natural isotope as well as being the furthest removed in mass from ^{143}Nd and ^{144}Nd . This affects tracer purity since tracer stocks are produced at Oak Ridge National Laboratory by a bucket mass spectrographic method. The ^{150}Nd tracer contains lower proportions of ^{143}Nd , ^{144}Nd , and ^{146}Nd than all the other Nd tracers. This reduces the magnitude of corrections for these isotopes and makes it the best available tracer for combined determination of $^{143}\text{Nd}/^{144}\text{Nd}$ ratios and Nd concentrations by total spiking.

For Sm, a 98% pure ^{149}Sm tracer was chosen because ^{149}Sm is the least abundant natural isotope not isobaric with a Nd isotope. Use with extraterrestrial materials, in which ^{149}Sm and ^{150}Sm abundances are variable due to neutron capture effects, is not anticipated. The ratio $^{147}\text{Sm}/^{152}\text{Sm}$, neither isotope of which is isobaric with a Nd isotope, is used to correct for mass discrimination.

Mixed Sm-Nd spike solutions allow the most precise determination of natural Sm/Nd ratios in that measured concentration ratios are independent of spike-sample gravimetry. Those in current use at MIT are splits of two mixed spikes prepared in 1982 at LDGO by A Zindler using $^{150}\text{Nd}_2\text{O}_3$ and $^{149}\text{Sm}_2\text{O}_3$ tracers procured from Oak Ridge. Tracer Sm and Nd concentrations in the two spike solutions, designated SMND1 and SMND2, differ by factors of 5 and 10 respectively. The spike with the higher concentrations has the lower Sm/Nd ratio in line with the general geochemical coherence between concentration and LREE enrichment. However, given desired underspiking for Nd (compromise between reducing the concentration error magnification at the expense of increasing the $^{143}\text{Nd}/^{144}\text{Nd}$ correction) and the breadth of the error magnification

minimum for Sm concentration measurement (see section 7.1), both spikes can effectively be used for a wide range of natural Sm/Nd ratios from strongly LREE depleted compositions (high Sm/Nd) to the limit of LREE enrichment (lowest natural Sm/Nd ≈ 0.1).

4. Spike Nd and Sm isotopic compositions

The ^{150}Nd tracer potentially contained a finite amount of ^{150}Sm , as opposed to the ^{149}Sm tracer for which there is no isobaric Nd isotope. Thus, isotopic abundances of spike Nd and Sm were measured after mixing. This involved separation of Nd and Sm from aliquots of the two mixed spikes, SMND1 and SMND2, by liquid-liquid cation exchange chromatography with a spike to blank ratio of greater than 10^6 . Isotopic composition runs were made on 1 microgram double filament loads in the NIMA-B mass spectrometer with ^{150}Nd and ^{149}Sm ion beam currents of 10^{-10} to 10^{-9} A. The large stable Nd ion beams allowed for improved precision of minor isotope abundance determination including measurement of $^{143}\text{Nd}/^{144}\text{Nd}$ and $^{144}\text{Nd}/^{146}\text{Nd}$ ratios at close to the normal intensities for standard and sample runs (3×10^{-12} A for ^{144}Nd). Runs followed a normal mass fractionation sequence and were continued to exhaustion. Data for an entire run were then integrated over the product of intensity and time (ion count) to arrive at the best estimate of overall isotopic composition (Table A-2). The isotope ratio closest to unity ($^{144}\text{Nd}/^{146}\text{Nd}$) was used as the reference ratio for integration to minimize electrometer non-linearity effects between ranges. Mass fractionation related uncertainties in the Nd tracer isotopic composition do not contribute significantly to uncertainties in spiked sample $^{143}\text{Nd}/^{144}\text{Nd}$ ratios. For a doubling of the ^{150}Nd content of a sample by spike addition ($^{150}\text{Nd}/^{146}\text{Nd}_{\text{mixture}} = 0.65304$), the $^{143}\text{Nd}/^{144}\text{Nd}$ of the mixture decreases by

TABLE A-2 Spike Nd and Sm isotopic compositions

| Nd | $\frac{142}{146}$ | $\frac{143}{146}$ | $\frac{144}{146}$ | $\frac{145}{146}$ | $\frac{148}{146}$ | $\frac{150}{146}$ |
|-----------|-------------------|-------------------|-------------------|-------------------|-------------------|-------------------|
| | SMND1 | 0.90958 | 0.45972 | 1.04802 | 0.40784 | 0.77829 |
| SMND2 | 0.90959 | 0.45972 | 1.04749 | 0.40815 | 0.77910 | 114.281 |
| AVERAGE | 0.909585 | 0.459720 | 1.047755 | 0.407995 | 0.778695 | 114.334 |
| Sm | $\frac{144}{147}$ | $\frac{148}{147}$ | $\frac{149}{147}$ | $\frac{150}{147}$ | $\frac{152}{147}$ | $\frac{154}{147}$ |
| | SMND1 | 0.07434 | 2.1004 | 266.356 | 1.54578 | 1.06013 |
| SMND2 | 0.07467 | 2.1013 | 266.381 | 1.53608 | 1.05960 | 0.46939 |
| AVERAGE | 0.074505 | 2.10085 | 266.3685 | 1.54093 | 1.059865 | 0.469485 |
| ADJUSTED* | 0.07406 | 2.10505 | 267.434 | 1.55018 | 1.07046 | 0.47606 |

*Approximately 0.2% per AMU more fractionated than average measured composition (cf. sections 4 and 7.4)

0.000160 with an uncertainty of less than 0.000002 using an arbitrary uncertainty in the tracer isotopic composition of 0.2% per AMU.

Tracer Sm runs were less satisfactory since data acquisition had to be terminated before exhaustion due to irreversible degradation of signal stability. Available data were integrated as above using the $^{152}\text{Sm}/^{147}\text{Sm}$ ratio for reference. The resulting Nd and Sm compositions for the two spikes (Table A-2) were found to be well within expected differential fractionation errors of each other except perhaps for the ^{150}Sm content, potentially attributable to a differential contribution from the Nd tracer (0.6% higher $^{150}\text{Sm}/^{147}\text{Sm}$ in the spike with lower Sm/Nd). The ^{150}Sm isotope is not used directly for Sm concentration determination and the effect on other relevant isotopic abundances is insignificant. For simplicity, Nd and Sm compositions were then averaged (Table A-2) for use in subsequent spike concentration calibration. In the course of this calibration, a bias in the measured tracer Sm isotopic composition in the direction of less fractionated compositions was confirmed. A more accurate composition which gave consistent results for the calibrations using three different reference isotope pairs, was obtained by mass fractionation dependent adjustment of the measured composition. The details of the refinement are given in section 7.5. This adjusted composition, which is approximately 0.2% per AMU more fractionated than the measured composition, appears in atomic ratio form in Table A-2 and fractional atomic abundance form in Table A-3.

TABLE A-3 Normal and spike Nd and Sm fractional atomic abundances and atomic weights

| Nd | ISOTOPE | NORMAL AB* | SPIKE AB** | ATOMIC MASS*** |
|----|------------|------------|------------|----------------|
| | 142 | 0.2716707 | 0.0076476 | 141.907731 |
| | 143 | 0.1219807 | 0.0038652 | 142.909823 |
| | 144 | 0.2379462 | 0.0088093 | 143.910096 |
| | 145 | 0.0828980 | 0.0034303 | 144.912582 |
| | 146 | 0.1717733 | 0.0084078 | 145.913126 |
| | 148 | 0.0574831 | 0.0065471 | 147.916901 |
| | 150 | 0.0562480 | 0.9612928 | 149.920900 |
| | ATOMIC WT: | 144.2397 | 149.7156 | |
| Sm | ISOTOPE | NORMAL AB | SPIKE AB** | ATOMIC MASS*** |
| | 144 | 0.0307549 | 0.0002706 | 143.912009 |
| | 147 | 0.1499509 | 0.0036535 | 146.914907 |
| | 148 | 0.1124212 | 0.0076908 | 147.914832 |
| | 149 | 0.1381917 | 0.9770713 | 148.917193 |
| | 150 | 0.0738028 | 0.0056636 | 149.917285 |
| | 152 | 0.2673834 | 0.0039109 | 151.919741 |
| | 154 | 0.2274950 | 0.0017393 | 153.922218 |
| | ATOMIC WT: | 150.3656 | 148.9269 | |

*Calculated using $^{143}\text{Nd}/^{144}\text{Nd} = 0.51264$ and $^{146}\text{Nd}/^{144}\text{Nd} = 0.7219$
(cf. Table 1)

**Average Nd and adjusted average Sm isotopic abundances for SMND1
and SMND2 spikes (cf. Table 2)

***Atomic masses from the 1977 Atomic Mass Evaluation (Wapstra and Bos, 1977)

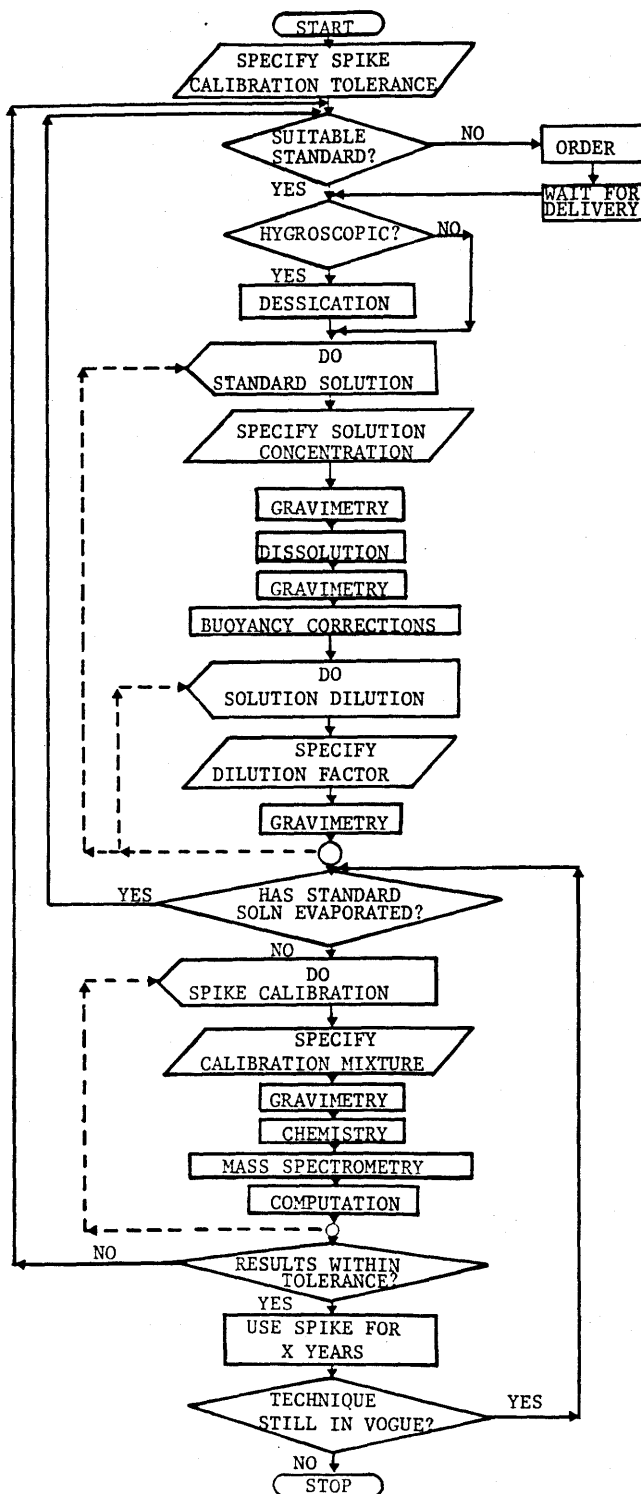
5. Normal standard solution design and construction

For the lost and confused, a streamlined flowchart of standard solution preparation and spike calibration procedures appears in Figure A-1. This serves to illustrate the overall organization of the remaining commentary.

5.1 Specifications

Normal standard solution design specifications are controlled primarily by desired precision and accuracy of spike calibration and secondarily by logistical considerations. If spike concentrations need only be known to within 1-10%, a normal standard solution is not even required since spikes should be constructed gravimetrically and concentrations thus known to within tracer and solution weighing errors. Calibration precision and accuracy of 0.1-1% requires some planning and several person days of effort. The precision and accuracy of 0.01-0.1% aimed for in this report required extensive planning with attention to every detail and several person weeks of effort. The limit is ultimately determined by the quality of the absolute gravimetric standards used in the preparation of normal standard solutions. For Nd and Sm, previous problems with oxide non-stoichiometry prompted the use of 99.99% pure Nd and Sm metals prepared at the Ames Laboratory (Beaudry and Gschneidner, 1978). Ironically, these were derived by reduction of 99.999% pure oxides also prepared at Ames (Powell, 1978). However, the slight decrease in purity is more than compensated for by the ease of metal gravimetry. The cation impurities detected in Ames analyses of the metals are primarily non-rare-earth elements. The metals are shipped as approximately one gram pre-weighed slugs sealed, along with glass wool padding, in evacuated pyrex vials. Those obtained and used here in 1982 bore 1979 fabrication dates (Table A-4).

FIGURE A-1 Flowchart of standard solution preparation and spike calibration procedures.



Due to oversights in spike construction gravimetry, nominal spike concentrations were only known to within about 25%. A normal standard solution with approximately 1 ppm concentrations of both Nd and Sm was considered appropriate for calibration of the two spikes since minimum concentration error magnification could be attained within a reasonable range of calibration mixture spike-to-standard ratios. This would require roughly 1000 μ l of solution for a gram of metal. Two final standard solutions, designated MIT#2 and MIT#3, were thus prepared by roughly 400 fold dilution of aliquots of an initial 2.3 μ l concentrated solution, designated MIT#1. In order to minimize propagation of gravimetric errors, both Sm and Nd metals were combined during construction of MIT#1. The common Sm/Nd ratio of MIT#2 and MIT#3 thus depends on the weights of the metal slugs alone and is independent of solution and dilution gravimetry.

5.2 Metal gravimetry

Nd and Sm metal slugs were liberated from the evacuated vials by breaking the sealed ends with a hammer. Slugs were removed with plastic tweezers, flushed with argon to remove any adhering glass wool fibers and stored in an argon-filled dessicator prior to weighing on a Perkin-Elmer AD-2 electronic microbalance. The balance is supplied with a better-than-Class M 100 mg weight (± 0.005 mg accuracy) for calibration prior to use. A substitution weighing technique using a 1 g Class S substitution weight was employed (readability 1 μ g). As an independent check slugs were then weighed on a less precise (± 0.05 mg) Mettler H16 mechanical semi-microbalance checked with Class S weights calibrated against NBS weights. For reference, the tolerance limits of these classes of calibration weights are described in ASTM Standard E617-78, which

TABLE A-4 Weights of Sm and Nd metals

| | AMES | MIT | |
|----------------|---------|---------------|------------|
| | | P-E AD-2 g | M H16 g |
| Sm (#2, 32379) | 0.99338 | 0.99313 | 0.99320 |
| Nd (#2, 42479) | 1.02699 | 1.02679 | 1.02681 |

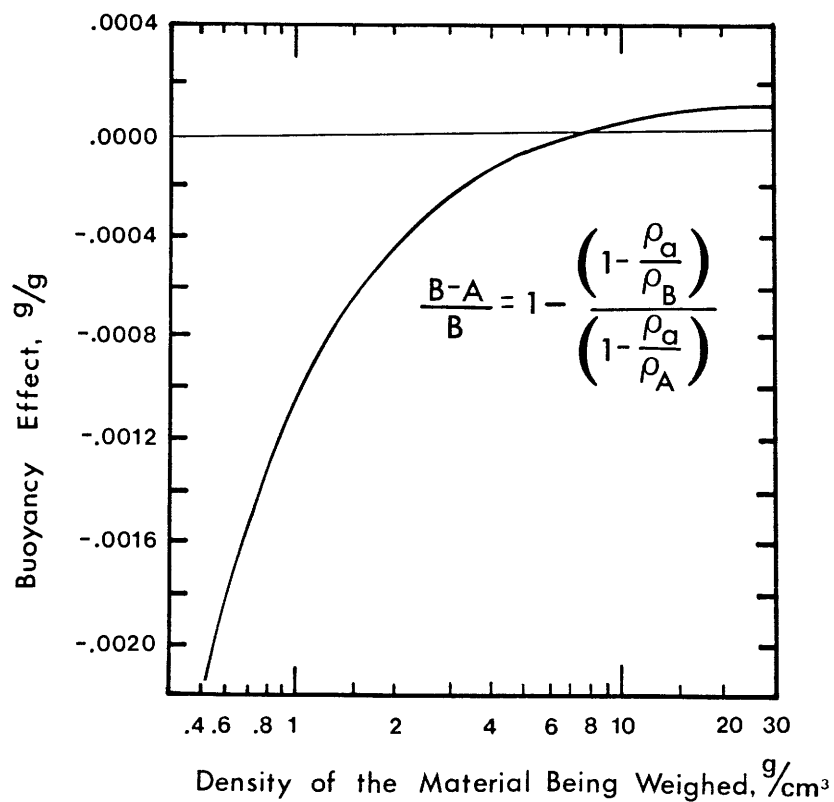
supersedes NBS Circular 547 (with Classes 1 and 2 in the former replacing Classes M and S in the latter). In the future, an electronic top-loading semi-microbalance such as the more recently available Mettler AE163 (precision ± 0.005 mg) could prove to be a more suitable balance for the above task.

The resulting weights of the Nd and Sm metal slugs are compared to those supplied by Ames Laboratory in Table A-4. The weights determined here are both approximately 0.02% lower than the Ames values, outside weighing precision of perhaps $\pm 0.005\%$. The discrepancy cannot be explained by uptake of anion impurities (through oxidation), subsequent to fabrication and weighing at Ames, since this would tend to increase the weights. Rather, a minor systematic weighing error is indicated. It should be noted, however, that the discrepancy in Sm/Nd weight ratio is only 0.005%. In addition, concentration errors due to impurities in the metals ($<0.01\%$) will cancel out to the extent of the smaller of the two. Therefore, the Sm/Nd weight ratio of the resultant mixed normal standard solutions, MIT#1, 2 and 3 is considered to be known to within 0.01%.

5.3 Dissolution

The Nd and Sm metals were transferred into a 2 l glass Erlenmeyer flask with a cap containing a conical polyethylene polyseal insert. 1320 ml water and 8 ml 6.2N HCl were added and the flask mouth covered with a perched conical cap insert. The dissolution reaction (with evolution of H₂ gas) was allowed to proceed in a controlled manner over several hours. When the reaction was complete, a further 883 ml of 6.2N HCl were added to give approximately 2210 ml of 2.5N HCl solution. The flask was then sealed and the solution thoroughly agitated to assure homogeneity.

FIGURE A-2 Relative magnitude of the buoyancy effect, $(B-A)/B$, as a function of the density of the material being weighed, ρ_A , for an air density, ρ_a , of 0.0012 g/cm^3 and a standard weight density, ρ_B , of 8.0 g/cm^3 (figure from Schoonover and Jones, 1981).



5.4 Solution gravimetry

The capped flask was weighed empty (490.9 g) and full (2793.6 g) on a Mettler PC4400 electronic top-loading balance (readability 0.1 g; precision 0.05 g) calibrated with a combination of Class S weights and checked with in-house weights before each use. Solution weights are considered precise to within 0.005%. After withdrawal of solution aliquots for preparation of dilute standard solutions, the flask was resealed and its weight monitored periodically. After a year's storage at room temperature no evaporative loss in weight could be detected within the readability of the balance.

5.5 Buoyancy corrections

The application of air buoyancy corrections in high accuracy weighing on analytical balances is discussed in detail by Schoonover and Jones (1981). The basic equation relating the mass of a material, A, to that of corresponding standard weights, B, taking into account the buoyant forces, is

$$A = B \frac{[1 - (\rho_{\text{air}}/\rho_B)]}{[1 - (\rho_{\text{air}}/\rho_A)]}$$

where ρ_A and ρ_B are the densities of the material and the standard weights respectively. The relative magnitude of the buoyancy effect increases with increasing density difference between standard weights and material being weighed, as illustrated in Figure A-2 (from Schoonover and Jones, 1981).

For Sm and Nd metals with densities of 7.520 and 7.007 g/cm³ respectively (CRC Handbook of Chemistry and Physics) and Class S steel standard weights with a density of 7.8 g/cm³ the buoyancy effects are

TABLE A-5 Concentrations of Sm and Nd and $^{143}\text{Nd}/^{144}\text{Nd}$ ratios in normal standard solutions

| | Dilution factor | Sm $\mu\text{g/g}$ | Nd $\mu\text{g/g}$ | Sm/Nd weight | $^{147}\text{Sm}/^{144}\text{Nd}$ atomic | $^{143}\text{Nd}/^{144}\text{Nd}^*$ |
|-------|--------------------|-----------------------|-----------------------|-----------------|---------------------------------------------|-------------------------------------|
| MIT#1 | | 430.858 | 445.461 | 0.967218 | | |
| MIT#2 | 0.00230621 | 0.993648 | 1.027326 | 0.967218 | 0.58462 | 0.512060 \pm 14 |
| MIT#3 | 0.00260771 | 1.123553 | 1.161634 | 0.967218 | 0.58462 | 0.512053 \pm 12 |

*Normalized to $^{146}\text{Nd}/^{144}\text{Nd} = 0.7219$

small (0.0006% and 0.0017% respectively). However, for aqueous solutions with a density close to 1 g/cm³ the buoyancy effects are significant (0.1%) at the desired level of overall accuracy (0.01%-0.1%). The mass of a liquid weighed in a bottle on an electronic top-loading balance, taking into account buoyant forces, is given by

$$\text{Mass}_{\text{liq}} = (\text{Wt}_{\text{bottle+liq}} - \text{Wt}_{\text{bottle}}) \frac{(\text{Mass}_{\text{std wt}})}{(\text{Wt}_{\text{std wt}})} \frac{[1 - (\rho_{\text{air}}/\rho_{\text{std wt}})]}{[1 - (\rho_{\text{air}}/\rho_{\text{liq}})]}$$

where Wt represents the electronic readout of the balance. The scale calibration factor (Mass_{std wt})/(Wt_{std wt}) is generally made to equal unity by the act of calibration. For a 2.5N HCl solution with a density of 1.041 g/cm³, steel standard weights with a density of 7.8 g/cm³ and an approximate air density of 0.0012 g/cm³ the required buoyancy correction factor is 1.00100. Calculated Sm and Nd concentrations for the resultant concentrated standard solution, MIT#1, are given in Table A-5. Overall concentrations are considered accurate to within 0.02%.

6. Standard solution dilution

6.1 Specifications

A 400 fold dilution of the concentrated standard solution, MIT#1, is required to yield dilute solutions with approximately 1 ppm concentrations of Sm and Nd. This can be achieved by diluting a 5.5 ml aliquot of the concentrated solution with 2200 ml of 2.5N HCl in a 2 l glass Erlenmeyer flask with polyseal cap. Thorough agitation of the resultant solution is necessary to assure homogeneity.

6.2 Solution gravimetry

The major problems in precise weighing of the aliquot of concentrated solution are transfer and evaporation. The 5-6 ml aliquot cannot be weighed with sufficient precision directly inside the approximately 500 g 2 l flask. A much lighter intermediate container with provision for control of evaporation is required. This should preferably be made of non-wetting material for complete delivery of the weighed aliquot into the flask. To this end, a one piece transfer pipet with 10-15 ml capacity integral bulb and long narrow 1-2 mm diameter tip was fabricated out of shrinkable teflon (FEP) tubing. This was weighed empty (<3g) and with each of two 5-6 ml aliquots of MIT#1 on a Mettler H16 mechanical semi-microbalance. In spite of poorer absolute precision due to teflon surface electrostatic charge effects, the relative precision of aliquot weights is still better than 0.005%. After introduction of aliquots of MIT#1 followed by addition of 2200 ml of 2.5N HCl, flasks were sealed and weighed on a Mettler PC4400 electronic top-loading balance as previously described for MIT#1. Since both concentrated and dilute solutions are of the same density, buoyancy corrections cancel out. Sm and Nd concentrations in MIT#2 and MIT#3 are thus related to those in MIT#1 by simple dilution factors (Table 5). The overall accuracy of dilute standard solution concentrations is considered to be better than 0.025%. After withdrawal of solution aliquots for spike calibrations, flasks were resealed and weights monitored periodically. After a year's storage at room temperature no evaporative loss in weight could be detected within the readability of the balance.

7. Spike solution concentration calibration

7.1 Specifications

Spike solution concentrations are calculated from the isotopic composition of a mixture of a measured mass of spike solution and a measured mass of standard solution. Given approximate spike solution concentrations, standard-to-spike weight ratios of calibration mixtures can be specified such that isotopic composition error magnification is minimized. Error magnification is figured in terms of the isotope dilution ratio, R (tracer isotope abundance/reference isotope abundance), of the calibration mixture, and the atomic normal-to-spike ratio, N/S, in the isotope dilution equation

$$\frac{N}{S} = \frac{a - bR}{cR - d}$$

where a, b, c and d are the spike tracer, spike reference, normal reference and normal tracer isotope abundances respectively. By differentiating this equation with respect to R, an explicit expression for error magnification is obtained

$$\frac{(\delta N/S)/(N/S)}{\delta R/R} = -R \left[\frac{b}{(a-bR)} + \frac{c}{(cR-d)} \right]$$

The variation of error magnification with R for Sm-Nd spike-normal mixtures is illustrated in Figures A-3 and A-4. The calibration standard-to-spike weight ratios of approximately 3 for SMND1 and 0.4 for SMND2 used here, yield concentration error magnification values of 1.1 for Sm and 1.5 for Nd.

FIGURE A-3 Variation of Nd concentration error magnification with $^{150}\text{Nd}/^{146}\text{Nd}$ for SMND1 and SMND2 spike-normal mixtures.

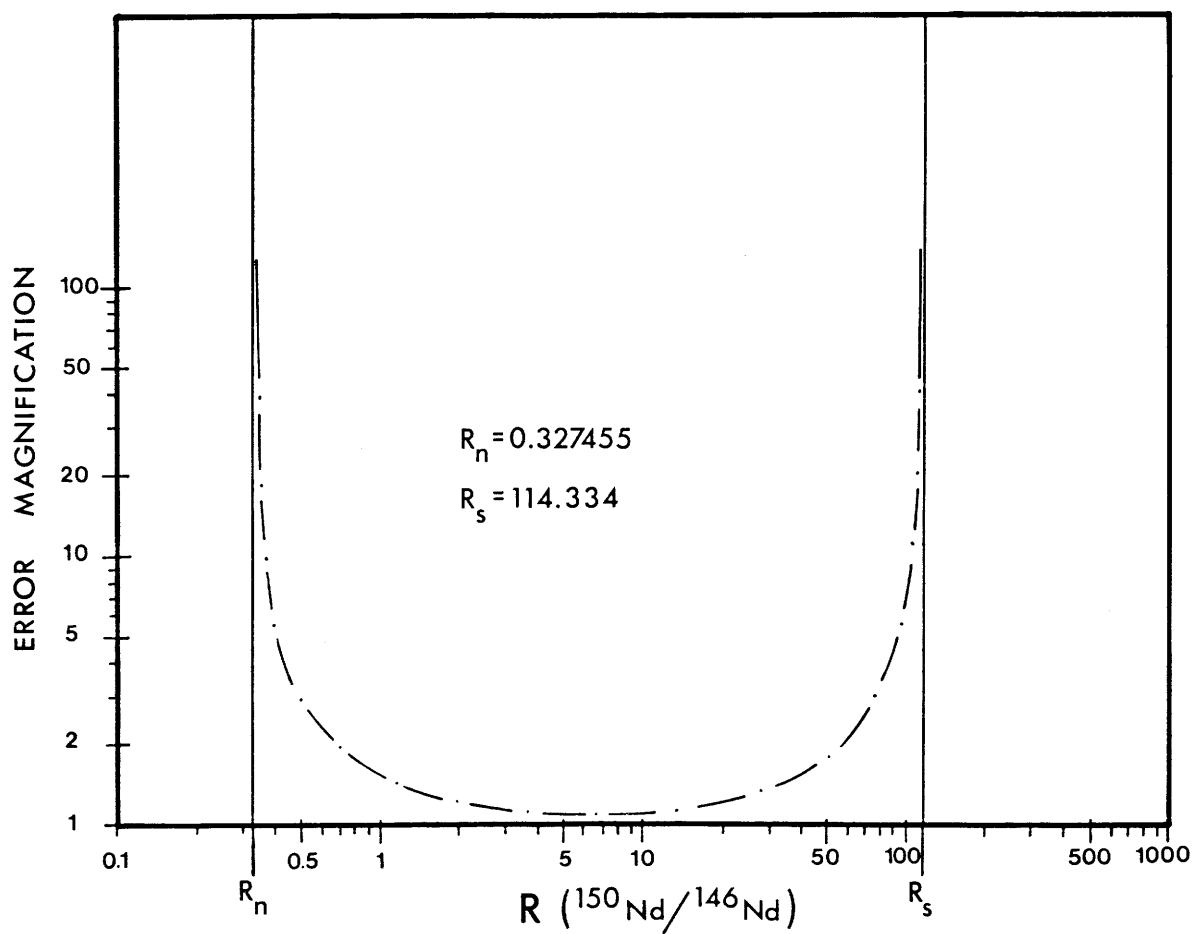


FIGURE A-4 Variation of Sm concentration error magnification with $^{149}\text{Sm}/^{152}\text{Sm}$ for SMND1 and SMND2 spike-normal mixtures.

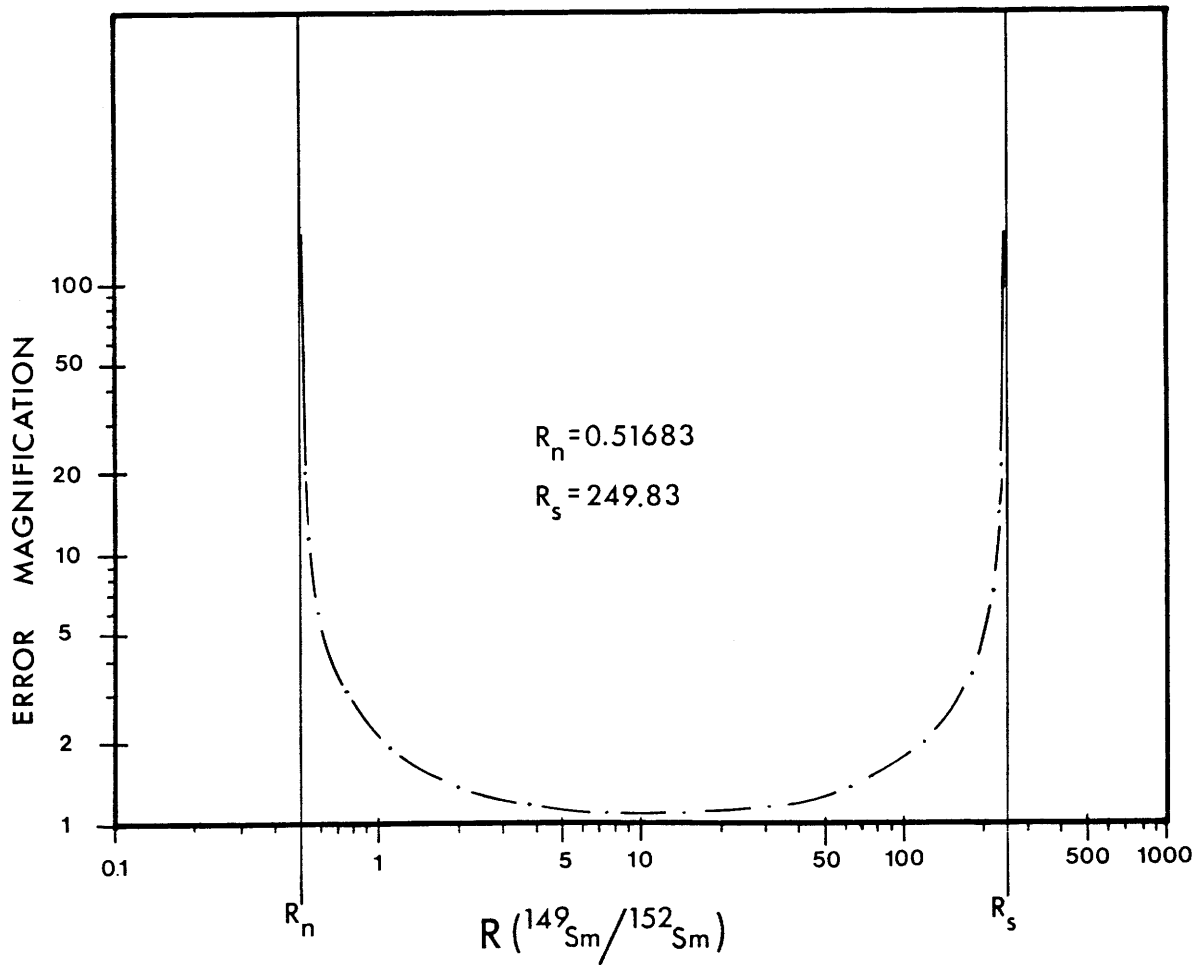


TABLE A-6 Sm and Nd concentrations in mixed Sm-Nd spikes (July 1982)

| SPIKE | STANDARD | Sm μg/g | Nd μg/g | Sm/Nd weight |
|--------------|----------|------------|------------|-----------------|
| <u>SMND1</u> | MIT#2 | 5.07205 | 0.468562 | 10.8247 |
| | MIT#3 | 5.07197 | 0.468603 | 10.8236 |
| | MIT#3 | 5.07223 | 0.468620 | 10.8238 |
| average | | 5.07209 | 0.468595 | 10.8240 |
| <u>SMND2</u> | MIT#2 | 0.909697 | 0.0502476 | 18.1043 |
| | MIT#3 | 0.909624 | 0.0502449 | 18.1038 |
| | average | 0.909661 | 0.0502463 | 18.1040 |

7.2 Solution gravimetry

Aliquots (1-7 ml) of the spike and standard solutions were weighed sequentially into 10 ml teflon (TFE) or glass beakers on a Mettler H16 mechanical semi-micro balance. Evaporation was controlled by sealing beakers with two circular sheets of parafilm weighed with each empty beaker. The spike aliquot was introduced directly into the beaker through a hole in the first sheet of parafilm precut to the diameter of the spike bottle delivery nozzle with a corkcutter. After delivery of the spike aliquot, the hole was sealed with the second sheet of parafilm. The standard solution aliquot was transferred from storage flask to beaker in a teflon (FEP) pipet with narrow tip robust enough to pierce the second sheet of parafilm which self-sealed on spiralled withdrawal of the pipet. Since both spike and standards solutions are of the same density, buoyancy corrections cancel out. Solution weights are considered precise to better than 0.005%.

7.3 Separation chemistry and mass spectrometry

A highly detailed description of routine Sm-Nd chemical and mass spectrometric procedures used in this lab is given by Zindler (1980). Calibration mixture Sm and Nd were separated by liquid-liquid cation exchange chromatography with sample to blank ratios of greater than 10^6 . Isotopic composition runs were made on 200-300 nanogram double filament loads in the NIMA-B mass spectrometer with ^{150}Nd and ^{149}Sm ion beam currents of 10^{-11}A . In-run precision for all measured isotope ratios was better than 0.01%.

7.4 Calibration results

In order to test the measured spike Sm isotopic composition (section 4, Table A-2), Sm concentration data were calculated from three different

TABLE A-7 Sm and Nd concentrations, Sm/Nd and $^{143}\text{Nd}/^{144}\text{Nd}$ ratios for BCR-1

| BCR-1 weight (g) | SPIKE weight (g) | Sm $\mu\text{g/g}$ | Nd $\mu\text{g/g}$ | Sm/Nd weight | $^{147}\text{Sm}/^{144}\text{Nd}$ atomic | $^{143}\text{Nd}/^{144}\text{Nd}$ atomic |
|---------------------|---------------------|-----------------------|-----------------------|-----------------|---------------------------------------------|---------------------------------------------|
| | SMND1 | | | | | |
| 0.09795 \pm 5 | 1.00115 \pm 5 | 6.6091 | 28.874 | 0.22889 | 0.13837 | 0.512624 \pm 13 |
| | SMND2 | | | | | |
| 0.02486 \pm 5 | 1.32477 \pm 5 | 6.5980 | 28.827 | 0.22888 | 0.13836 | 0.512621 \pm 14 |

pairs of isotope dilution and reference ratios: $^{149}\text{Sm}/^{147}\text{Sm}$ normalized to $^{148}\text{Sm}/^{147}\text{Sm}$; $^{149}\text{Sm}/^{152}\text{Sm}$ normalized to $^{147}\text{Sm}/^{152}\text{Sm}$; $^{149}\text{Sm}/^{152}\text{Sm}$ normalized to $^{154}\text{Sm}/^{152}\text{Sm}$. The mass fractionation and isotope dilution mixing lines for the first and third of these pairs have singularities (at $^{149}\text{Sm}/^{147}\text{Sm} = 146.4$ and $^{149}\text{Sm}/^{152}\text{Sm} = 209.3$ respectively) and low angles of divergence in the vicinity of the spike isotopic composition. They are thus sensitive to mass fractionation related errors in spike isotopic composition. Calculated concentrations for these two pairs were found to lie on opposite sides of those for the second pair (which has no singularity and a higher angle of divergence), consistent with a bias in the measured spike Sm isotopic composition towards underfractionated values. By iterative adjustment of the spike composition, a 0.2% per AMU more fractionated composition was found to give the best agreement for all three pairs. Reported Sm concentration data are those calculated from the second pair, $^{149}\text{Sm}/^{152}\text{Sm}$ normalized to $^{147}\text{Sm}/^{152}\text{Sm}$, using the adjusted spike Sm isotopic composition (Table A-2).

Results for calibrations of the two mixed Sm-Nd spikes, SMND1 and SMND2, using the two dilute mixed Sm-Nd standard solutions, MIT#2 and MIT#3, are given in Table A-6. Sm and Nd concentration and Sm/Nd ratio data for each spike agree to within 0.01%.

8. Sample spiking

Field trials of the calibrated mixed Sm-Nd spike solutions, SMND1 and SMND2, were conducted using the USGS standard rock BCR-1. Approximately 100 mg and 25 mg aliquots of undessicated BCR-1 powder were totally spiked with 1 g aliquots of SMND1 and SMND2 in 10 mL teflon (TFE) beakers on a Mettler H16 mechanical semi-micro balance (± 0.05 mg

precision). As a test of sample $^{143}\text{Nd}/^{144}\text{Nd}$ corrections, spike-to-sample ^{150}Nd ratios were purposely made up to twice the one-to-one ratio (a compromise between reducing the Nd concentration error magnification at the expense of increasing the $^{143}\text{Nd}/^{144}\text{Nd}$ correction) normally used. After complete dissolution and separation of Nd and Sm by cation exchange chromatography with sample to blank ratios of 10^5 - 10^6 , isotopic compositions were measured on the NIMA-B mass spectrometer (cf. Zindler, 1980, for detailed account of chemical and mass spectrometric procedures). Calculated Sm and Nd concentrations (with no corrections for either buoyancy effects or adsorbed water content) and $^{143}\text{Nd}/^{144}\text{Nd}$ ratios appear in Table A-7. Concentrations agree to within only 0.17% but this is to be expected given the gravimetric uncertainties (0.05 and 0.2%), for small quantities of BCR-1. However, Sm/Nd ratios, which are independent of the above gravimetry, agree to within 0.01%. The $^{143}\text{Nd}/^{144}\text{Nd}$ ratios of 0.512624 ± 13 and 0.512621 ± 14 (in run $2\sigma_{\text{mean}}$) are essentially identical and well within errors of the average of 0.512622 ± 30 (2σ , $N=9$) for runs of unspiked BCR-1 during the previous year (1981-82). An identical average of 0.512622 ± 14 (2σ , $N=6$) was obtained for runs of spiked BCR-1 during the following year (1982-83). These consistent results illustrate the precision attainable in measurements of Sm/Nd and $^{143}\text{Nd}/^{144}\text{Nd}$ ratios on totally spiked natural rock samples.

BIOGRAPHICAL NOTE

With much love and little fanfare, SHR surfaced in southern Africa on 11 November 1953. After a youth of naked abandon and various misadventures to do with religious truth and conscription, the raw materialist came of age, geochemically speaking, at the University of Cape Town in 1977. The lure of the New World was irresistible and in 1978 said marginal man arrived at the Center for Geoalchemy to delve into the chemical evolution of the earth. After grovelling in green crud from upper oceanic crust and baked mud from lower continental crust, the as yet unenlightened savage set out in search of enriched mantle. An expedition to gut the Walvis Ridge preceded unrestrained kimberlite nodule bashing, and the sought-after chemical signatures were duly found. Finally, being forever intrigued by the De Beers line on the durability of diamonds, the newly converted carbon freak rounded out his development by venturing into diamond smashing - sure enough, this was the most durable enriched mantle yet. Meanwhile, the business of evolution went on in the biosphere at large. Somewhere between 1978 and 1983 the number of people on the planet surpassed the number of years in its history - no mean milestone for such a headstrong species with its origins in clay.